Space Science Reviews (2026) 222:27
https://doi.org/10.1007/s11214-025-01263-6

# Io and the Minor Jovian Moons – Prospects for JUICE

**Tilmann Denk · David A. Williams · Federico Tosi · James F. Bell III · Stefano Mottola · Imke de Pater et al.** ***[full author details at the end of the article]***

Received: 16 May 2024 / Accepted: 18 December 2025 / Published online: 5 March 2026


**Abstract**
The *Jupiter and Icy Moons Explorer* (JUICE) mission of the European Space Agency (ESA) will investigate the Jovian system with multiple instruments over several years, beginning in early 2031. This paper describes the historical context and state of knowledge, as well as JUICE's scientific goals and measurement techniques of the satellites that will not be encountered in close flybys. These include the large volcanically active moon Io, the four small inner moons Metis, Adrastea, Amalthea, and Thebe, and the numerous small Irregular (outer) moons. JUICE will provide multiple opportunities to observe Io from relatively remote distances of hundreds of thousands of kilometers. These observations will enable monitoring of Io's surface for changes, and for the study of its neutral clouds and plasma torus. Io observations will be performed with the four optical remote sensing instruments and with the Particle Environment Package. For the small inner moons it is planned to obtain complete geographic longitude (scales up to 8 km/px), solar-phase and multi-color coverage, oblique polar views, and UV to near-IR spectra. Astrometric measurements will also be performed. The Irregular moons will mostly appear unresolved to the JUICE instruments. Nonetheless, long-duration disk-integrated lightcurves will be acquired to derive rotation periods, object dimensions, pole-axis orientations, and colors for most objects for the first time. From these data, convex-shape models will be generated and phase curves determined. Furthermore, the precision of the orbital elements will be improved via accurate astrometry. UV and near-IR measurements will be attempted for the largest of these objects.

**Keywords** Io · Irregular satellites · Jovian satellites · JUICE · Jupiter system · Small moons

## 1 Introduction

The name of the European Space Agency's *JUpiter and ICy moons Explorer* mission – JUICE[1] – is aptly chosen since it inconspicuously hints at the primary targets of the mission: The icy Galilean satellites (Europa, Ganymede, Callisto) and the planet itself. These planetary objects are of extreme interest to study from various perspectives, however, there is much more to explore in the Jovian system. Besides the three icy Galilean moons, there is also the innermost (but non-icy) Galilean moon Io. Furthermore, the four small inner moons Metis, Adrastea, Amalthea, and Thebe orbit Jupiter in a very narrow space between Io's

[1] https://www.cosmos.esa.int/web/juice.

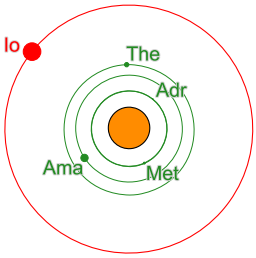


**Fig. 1** The orbits of Jupiter's small inner moons Metis (Met), Adrastea (Adr), Amalthea (Ama), and Thebe (The), and of Io on 01 Jan 2032 (north-pole view). The objects move counterclockwise. Jupiter's size and the orbits are to scale. The mean sizes of the inner moons are shown to scale to each other, but enlarged compared to Jupiter and the orbits. Io's size is not to scale. The semi-major axis of Thebe is ∼3.1 $R_J$, of Io 5.9 $R_J$. The semi-major axis of Metis is ∼1000 km smaller than Adrastea's, which is not not distinguishable in this graph

orbit and the planet's cloud tops (Fig. 1). The numerous outer or Irregular[2] Jovian satellites – 89 discoveries have been announced so far[3] – revolve around the planet outside the orbit of Callisto. Far away from the planet, they occupy a huge volume of space with a diameter reaching the closest opposition distances between Earth and Mars (Fig. 2). Because of their small sizes (mean diameters <170 km) and non-spherical shapes, the Irregulars and the small inner moons are also referred to as the minor moons. Drawing attention to even smaller objects leads to the Jovian dust rings, which are a dynamically highly variable phenomenon produced by micrometeoroid impacts on the small inner moons.

While in this special issue the JUICE observations of the icy Galilean satellites are covered by Witasse et al. (2026), Tosi et al. (2024b), Van Hoolst et al. (2024), and Masters et al. (2025), and the Jupiter observations by Fletcher et al. (2023), Io and the minor moons are the topic of this paper. Because there are no close flybys of these objects in the current reference trajectory[4] (Boutonnet et al. 2024), the potential for JUICE is to obtain new insights while observing these targets from large distances, especially by remote sensing with JANUS (Jovis Amorum ac Natorum Undique Scrutator; camera; 0.34-1.08 µm wavelength range; Palumbo et al. 2025), MAJIS (Moons And Jupiter Imaging Spectrometer; visible/near-IR spectrometer; 0.49-5.56 µm; Poulet et al. 2024), UVS (Ultraviolet Imaging Spectrograph; 50-204 nm; Retherford et al. 2026; Davis et al. 2021), SWI (Submillimetre Wave Instrument; near 530-625 GHz and 1067-1275 GHz;[5] Hartogh et al. 2026), and by the passive fields-and-particles experiment PEP (Particle Environment Package, Barabash et al. 2026).

**Io** is comparable in size to our Earth's Moon. As the most volcanically active object in the Solar System, it is peppered with hundreds of active volcanoes, gently leaking or violently spewing their magmatic materials in horizontal and vertical directions dozens to hundreds of kilometers from their vents, giving this moon its reddish-yellowish white and black colorful "pizza" appearance. In Sect. 2, Io as a planetary body and the envisioned JUICE science for this satellite will be described. The section starts with a brief overview on discovery and early research (Sect. 2.1.1), on volcanism and surface chemistry (2.1.2), and on the tenuous atmosphere and torus (2.1.3). The middle part describes the science objectives

[2] See Sect. 4 about the motivation and justification of writing the term "Irregular moon" with a capital 'I'.

[3] As of December 2025.

[4] CReMA_5_1 (Consolidated Report on Mission Analysis 5.1). The actual orbit tour will be finalized in 2028.

[5] 600 GHz ↔ 500 µm; 1200 GHz ↔ 250 µm.

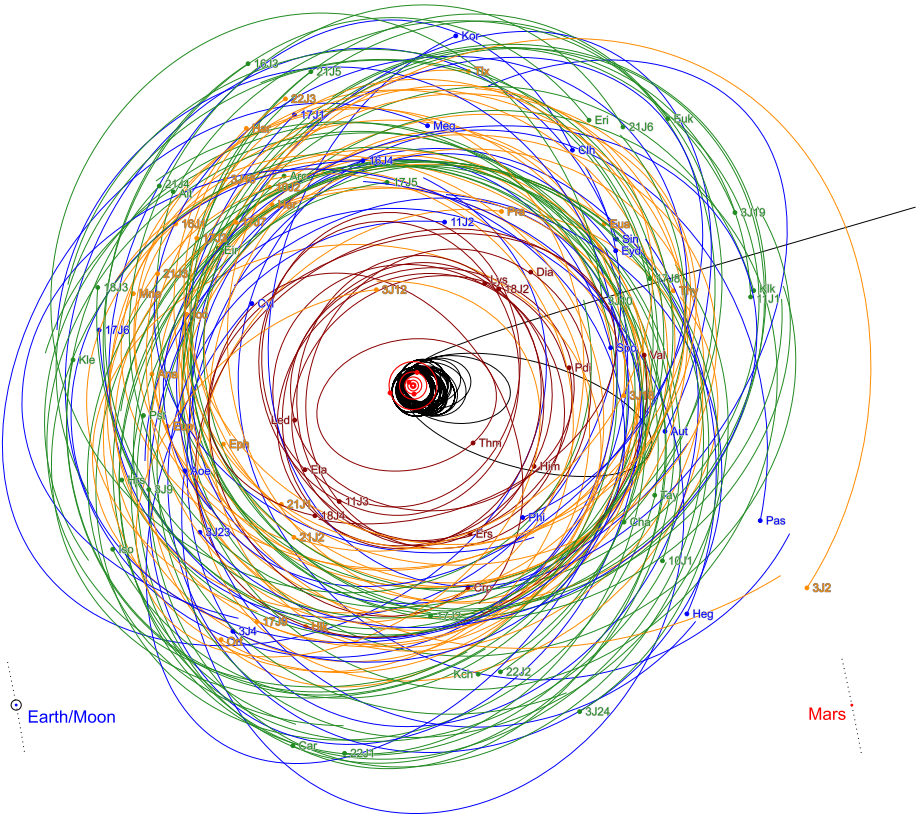


**Fig. 2** 2D-visualisation of the Irregular-moon system of Jupiter, plotted in a reference system co-rotating with the planet and seen from its north pole. Sun direction is ∼11:00. The 3- or 4-character codes point to the individual objects, see Table 6 in Sect. 4 for full names and object properties, and Table 7 for orbit dynamical grouping. The orbits of the Irregular moons are drawn as full orbits for each object, all starting 01 Jan 2032 and ending after one orbit period (the longest orbit at 21 Jul 2034). The symbols depict the end points. The orbits are not closed because of strong solar perturbations.
Color key: dark red = prograde groups; orange = Ananke group; green = Carme group; blue = Pasiphae and Sinope groups; red = Galilean satellites and small inner moons (compare with Fig. 1); black = JUICE spacecraft orbit. The ellipse outside the Galilean moons, labelled 'Thm', is the orbit of innermost Irregular moon Themisto. With a semi-major axis of ∼100 $R_J$, it marks the known inner boundary of the Jovian Irregulars.
The size of the Earth-Moon system as well as the distance between Earth and Mars (on 05 Jul 2033; somewhat arbitrarily chosen date near opposition) are shown to scale for comparison; the distance between these two planets will be 63.3 Gm or 885 $R_J$ on that day

addressable with JUICE (2.2). The section ends with a brief overview of observations with JUICE according to the planned activities of JANUS (2.3.1), MAJIS (2.3.2), UVS (2.3.3), SWI (2.3.4), and PEP (2.3.5).

Compared to the four Galilean satellites, the **inner moons** of Jupiter are much smaller objects. Amalthea, being the largest, just measures 251 km across its long side and 126 km along its pole axis. The orbits of the inner moons all have semi-major axes smaller than Io's. This region in the Jovian system is an extreme environment located deep within the planet's gravity funnel and within the high-energy radiation belts. The small inner moons are the topic of Sect. 3. First, this section revisits the discoveries (3.1.1) and gives an overview of

previous spacecraft observations with relevance to the small inner moons (3.1.2). Then, it reviews in somewhat chronological order the gain of our knowledge of Amalthea in particular (3.2.1) and of the physical and orbital properties of all four objects in general (3.2.2), and summarizes past search efforts for additional objects inside the orbit of Callisto (3.2.3). The next sub-section discusses science objectives JUICE plans to address (3.3). The final part presents unique advantages of the spacecraft compared to ground-based (3.4.1), compares JANUS imaging with *Galileo*'s and *Voyager*'s (3.4.2), gives an overview on the observation approaches and goals by the different remote sensing instruments (3.4.3), discusses JUICE's astrometric observations (3.4.4), and concludes with a short overview on a possible search of additional objects (3.4.5).

Among the **Irregular moons**, only 15% revolve around Jupiter on direct or prograde orbits (in the same direction as the planet spins and orbits the Sun), all others do so on retrograde orbits (opposite direction of the planet spin and orbit). Himalia is largest (∼140 km sized), about nine or ten objects are larger than 10 km. Most are much smaller with the smallest known objects measuring only about 1 km across (Sheppard et al. 2023; Ashton et al. 2020). This size limit is not given by the population's size distribution, but by the current discovery capabilities. The Irregular moons are presented in Sect. 4. Herein, these objects are reviewed with respect to their discovery histories (4.1.1), previous spacecraft observations (4.1.2), and known orbital (4.1.3) and physical properties (4.1.4). This is followed by a brief summary of the research of the Irregular-moons of Saturn by the *Cassini* spacecraft as the role model for the planned JUICE JANUS observations (4.2). The next sub-section describes observation strategies and science objectives of the Jovian Irregular satellites with JUICE (4.3). In detail, it compares spacecraft versus Earth-based observations (4.3.1), presents science objectives addressable with JUICE (4.3.2), gives insight into possible observation details and strategies of JANUS, MAJIS, and UVS (4.3.3), discusses astrometry (4.3.4), describes the potentials of a search campaign (4.3.5), and concludes with a presentation of the potentials of a targeted flyby of object Kallichore (4.3.6) which is currently not in the plan, but under investigation.

Section 5 then recaps the most important aspects of the potential JUICE observations of Io, the small inner moons, and the Jovian Irregulars.

A list of quantities recurring in the different sections is provided in Table 1. With respect to JUICE data acquisition of Io and the minor moons, the most likely epochs for observations will be between 19 Jan 2031 and late 2034. The former date marks the scheduled beginning of the science phase six months before Jupiter Orbit Insertion (JOI; scheduled for 21 Jul 2031) at a Jupiter distance of 100 Gm, the latter the approximate time window for the Ganymede orbit insertion (GOI) (Boutonnet et al. 2024, this collection).

## 2 Io

Io (Fig. 3; Table 2) is the innermost planet-sized moon of Jupiter. Along with the other three large satellites, it was discovered on 7-13 January 1610 by Galileo Galilei in Padova, Italy (Galilei 1610). Io is in an orbit-synchronous rotation state with a period of 1 d 18 h 27.6 min and completes 2450 orbits or day-night cycles during one Jupiter revolution around the Sun. Furthermore, it is in a 4:2:1 Laplace orbital resonance with Europa and Ganymede, which has a very stabilizing effect on the entire system (Laplace 1805). Because its orbit plane lies almost exactly in the Jupiter equatorial plane, with Jupiter's rotation axis being tilted by 3.1° relative to Jupiter's orbit plane around the Sun, Io often moves through Jupiter's shadow and experiences solar eclipses.

**Table 1** General numerical values used in this paper

| | |
|---|---|
| *Length and time units* | |
| Gigameter | 1 Gm $= 10^6$ km $= 13.988\ R_J$ |
| Jupiter equatorial radius | 1 $R_J = 71{,}492$ km |
| Jupiter Hill radius | 1 $R_{H,J} = 53.1$ Gm $= 743\ R_J$ |
| Astronomical Unit | 1 au $= 149.5978707$ Gm |
| Julian year | 1 yr $= 365.25$ d |
| *Jupiter orbit* | |
| Semi-major axis | $a_J = 5.20285044$ au |
| Period | $P_J = 4334.7d$ |

*Notes:*

- $R_J$ — Jupiter equatorial radius; from IAU resolution B3 (2015).[¶] See also Mamajek et al. (2015).
- $R_{H,J} = a_J \cdot \sqrt[3]{Gm_J / 3(Gm_\odot + Gm_J)}$ — Jupiter Hill radius; e.g., de Pater and Lissauer (2015). Herein, $m_J$ and $m_\odot$ are the masses of Jupiter and the Sun, respectively, derived from Gravitational parameters.[♯] Jupiter: $Gm_J = 126{,}712{,}761.8$ km$^3$/s$^2$; Sun: $Gm_\odot = 132{,}712{,}440{,}041$ km$^3$/s$^2$; Newtonian constant of gravitation $G = (6.67430 \pm 0.00015) \times 10^{-11}$ m$^3$/kgs$^2$.[§]
- Astronomical Unit: From IAU resolution B2 (2012).[$]
- Julian year: IAU recommendation.[†]
- $a_J$ — semi-major axis of Jupiter's orbit around the Sun; estimated for year 2031 from JPL SSD.[‡]
- $P_J$ — sidereal orbit period of Jupiter around the Sun; calculated with 3rd Keplerian law from $a_J$; see also Standish and Williams (2012).

*External sources (URLs):*

[¶] https://web.archive.org/web/20160128180606/https://www.iau.org/static/resolutions/IAU2015_English.pdf

[♯] From NAIF/SPICE kernel jup365: https://naif.jpl.nasa.gov/pub/naif/generic_kernels/spk/satellites/; see also https://web.archive.org/web/20250101184127/https://ssd.jpl.nasa.gov/sats/phys_par/

[§] https://physics.nist.gov/cgi-bin/cuu/Value?bg

[$] https://web.archive.org/web/20120901040303/https://www.iau.org/static/resolutions/IAU2012_English.pdf

[†] From Table 5 in https://web.archive.org/web/20250318075742/https://www.iau.org/publications/proceedings_rules/units/

[‡] https://web.archive.org/web/20250101184053/https://ssd.jpl.nasa.gov/planets/approx_pos.html

Io's diameter and distance to the central planet's "surface" (∼3645 km and ∼350,000 km, respectively) are quite comparable to the respective values for Earth's Moon (∼3475 km and ∼378,000 km). But because of Jupiter's much stronger gravity, Io's orbital speed is 17 times faster and the revolution period 15.5 times shorter. Most intriguing is the tremendous difference of the geologic histories of these satellites. While the surface of the Moon is currently geologically "dead", the Laplace resonance of Io with Europa and Ganymede induces a forced eccentricity in its orbit around Jupiter, which results in periodic tidal flexing of the surface on the order of ∼100 m every 1.8 d (Peale et al. 1979; Schubert et al. 2004; Keane et al. 2023). This intense tidal activity generates heating of Io's interior sufficient to induce partial melting up to ∼20-30 vol.% (Keszthelyi et al. 2007), which results in a mushy subsurface zone that feeds silicate magma to over 400 mapped volcanoes on the surface (Radebaugh et al. 2001; Williams et al. 2011a,b), ranking Io as the most volcanically active world in the Solar System. Recent Juno geophysical measurements during its 2023-2024 close flybys suggest that a shallow global magma ocean is not present (Park et al. 2025).

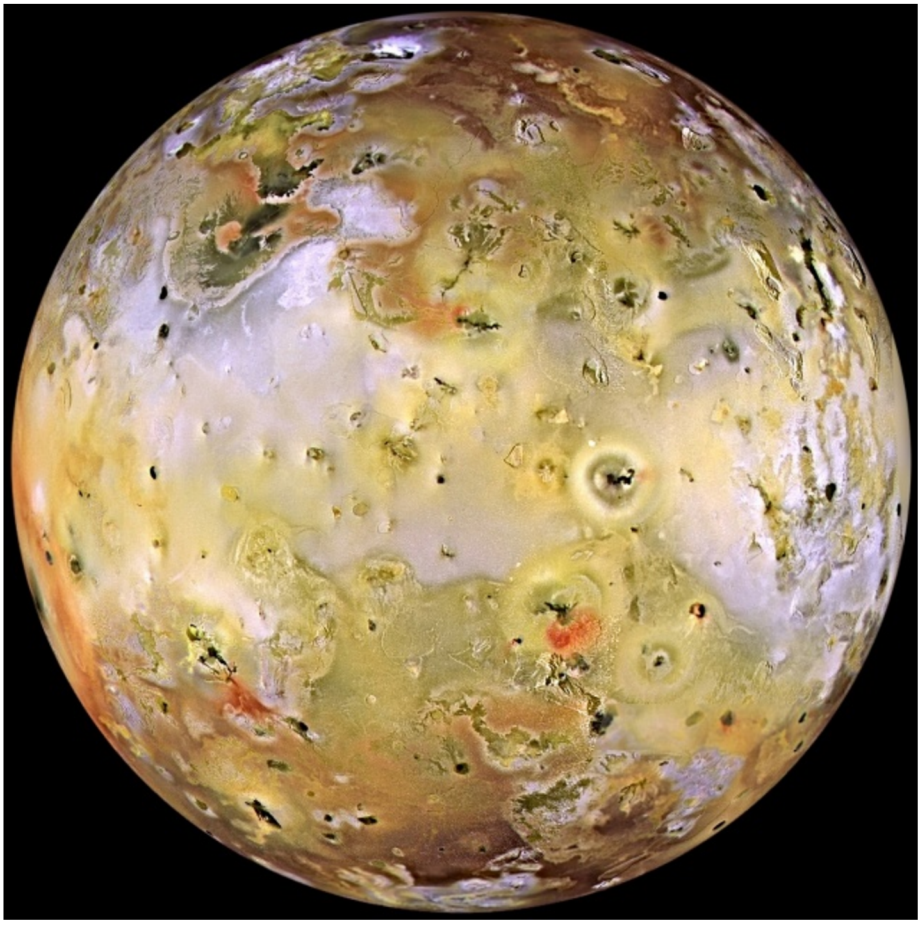

**Fig. 3** Anti-Jovian hemisphere of Io. *Galileo*-SSI image composite, recorded 07 Sep 1996 (color data from near-infrared 756 nm, green 559 nm, violet 404 nm filters) and 06 Nov 1996 (high-resolution clear-filter mosaic). North is up. *Source:* NASA/JPL PIA00583 (slightly modified); https://web.archive.org/web/20250423142133/https://photojournal.jpl.nasa.gov/catalog/PIA00583

## 2.1 Review of Knowledge

Of course, compiling exhaustive information on today's state of knowledge on Io would require more than a complete book – far beyond the scope of this paper. Two such books were published after the *Galileo* mission: The first (Lopes and Spencer 2007) provided a comprehensive overview of Io with emphasis on *Galileo* mission research. One-and-a-half decades later, the second one (Lopes et al. 2023) offered the most recent summary of our knowledge of Io's activity and other facts about Io and related topics, including considerations on tidally heated exoplanets and on future exploration. Other valuable sources of information since the *Galileo* mission are the first review after *Galileo* by Lopes and Williams (2005), a global geologic map of Io published by the U.S. Geological Survey (Williams et al. 2011b),[6] and

[6] http://pubs.usgs.gov/sim/3168/

**Table 2** Io at a glance

| **Io** | | | |
|---|---|---|---|
| IAU designation | J I | | |
| JPL/SPICE ID | 501 | | |
| Discovery | 07 Jan 1610 | | |
| Announced | 13 Mar 1610 | | *Sidereus Nuncius* (Galilei 1610) |
| Distance to Sun | 4.95 to 5.45 au | | |
| **ORBIT** | | | |
| Semi-major axis $a$ | 421,800 | km | JPL SSD[¶] (jup365)[♯] |
| | 5.900 | $R_J$ | |
| Eccentricity $e$ | 0.004 (forced) | | JPL SSD[¶] (jup365)[♯] |
| Inclination $i$ | 0.0 | ° | JPL SSD[¶] (jup365)[♯] |
| Period $P$ | 42.4593 | h | from $\omega$ |
| Angular motion $\omega$ | 203.4890 | °/d | Archinal et al. (2018) |
| Speed $v_{Io}$ | 17.33 | km/s | from $Gm_J$ and $a$ |
| **BODY** | | | |
| Apparent mag. $V$ | +5.02 | mag | from $H$ and $a_J$ |
| Absolute mag. $H$ | −1.85 | mag | Morrison and Morrison (1977) |
| Geometric albedo | 0.72 | | Morrison and Morrison (1977) |
| Angular diameter | 1.20 | ” | from $a_J$ and mean size |
| Mean size | 3645.4 | km | de Pater et al. (2021) |
| Radii $a \times b \times c$ | 1831.1 × 1820.4 × 1816.6 | km | Oberst and Schuster (2004) |
| $a/c$ | 1.008 | | |
| $Gm_{Io}$ | 5959.91547 | $km^3/s^2$ | NAIF SPICE (jup365)[♯] |
| Mass | $8.9296 \times 10^{22}$ | kg | from $Gm_{Io}$ |
| Density | 3520.5 | $kg/m^3$ | from mass and radii $a$, $b$, $c$ |
| Gravity | 1.794 | $m/s^2$ | from $Gm_{Io}$ and mean size |
| Volcanoes | >425 | | Williams et al. (2011a) |

*Notes:*

• Orbital elements $a$, $e$, $i$ are mean orbital elements referred to the local Laplace planes. (Note that the orbital elements are only approximations because there is no definition of $a$, $e$, $i$ for a body in an n-body system perturbed by tides, an oblate central body, the Sun, the other Galilean moons, etc.)

• $P$ is the mean orbit period and the rotation period (synchronous rotation), $\omega$ the mean daily angular motion, $v_{Io}$ the mean orbit velocity around Jupiter, $m_J$ the mass of Jupiter. Note that Io's jovicentric speed is larger than Jupiter's heliocentric speed around the Sun (13.07 km/s); hence in the heliocentric system, Io performs loops.

• The apparent visual magnitude $V$ (0.55 μm peak wavelength) is for ground-based observers near opposition, $H$ is the absolute visual magnitude. The geometric albedo is measured in the $V$ filter of the Johnson UBV filter system.

• The angular diameter (apparent size) is also from Earth at opposition.

• Radii: $a$ – largest axis (radial to Jupiter); $b$ – intermediate axis (parallel to movement direction); $c$ – shortest axis (parallel to spin axis). $a/c$ is the ratio of largest to shortest axis.

• Among the observed volcanoes, many have been active in the last several decades.

*External sources (URLs):*

[¶] JPL Solar System Dynamics: https://ssd.jpl.nasa.gov/sats/elem/sep.html

[♯] From NAIF/SPICE kernel jup365: https://naif.jpl.nasa.gov/pub/naif/generic_kernels/spk/satellites/; see also https://web.archive.org/web/20250101184127/https://ssd.jpl.nasa.gov/sats/phys_par/

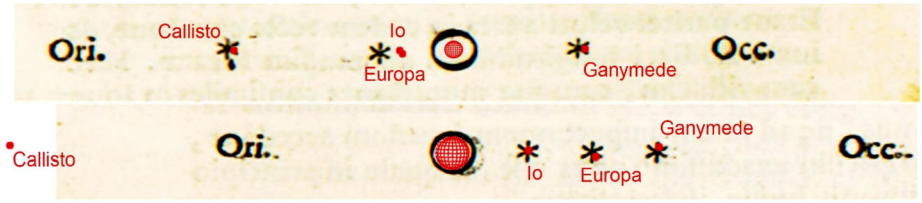


**Fig. 4** First two evenings (07 and 08 Jan 1610) of the Galilean-satellites discovery drawings by Galileo Galilei in the *Sidereus Nuncius* (Galilei 1610; black lettering), overlain by the viewing geometries based on modern ephemerides (red lettering). The geometries for epochs 07 Jan 1610 17:30 UTC and 08 Jan 1610 18:00 UTC were derived from https://pds-rings.seti.org/tools/. While the relative distances of the moons are remarkably accurate in Galileo's sketch drawings, the scales differ almost by a factor of 2 between the two days (as indicated by the different sizes of the Jupiter globe in the modern representation). Io and Europa could not be distinguished on 07 Jan, but were well separated at the next day, and while Callisto had been recognized in the first observation, it escaped Galileo's notice in the second. Ori. = east, Occ. = west. At that time, Galileo was very likely not yet aware that he has observed satellites of Jupiter

more recently a review on observational perspectives of Io by de Pater et al. (2021) and a series of short articles about "Exploring Jupiter's Moon Io" in *Elements* Magazine (Pommier and McEwen 2022).

Io was among the first ever discoveries of moons orbiting another planet. Comprehensive summaries of Io research history are for example given by Cruikshank and Nelson (2007) and by Schneider and Spencer (2023) in chapters of the books mentioned above. This section provides a general overview on historic Io research landmarks as well, but with content that is not always found in Io books or review papers.

### 2.1.1 Discovery and Early Research

Shortly after the invention of the telescope, the discovery of Io and the three other Galilean satellites by Galileo Galilei occurred in the second week of January 1610 (Fig. 4) in Padova (Italy) and probably independently by Simon Mayr (latinized form: Marius) in Ansbach (Franconia, Germany).[7] Likely less than a week after his first perception of "stars" in the vicinity of Jupiter on Thursday, 07 Jan 1610, Galileo recognized the significance of his discovery as a strong support of the Copernican system because it proved to him that not everything in the universe revolves around the Earth (e.g., Gingerich and Van Helden 2003, 2011). He published his findings just two months later, on 13 Mar 1610, in the famous booklet *Sidereus Nuncius* (Galilei 1610). Therein, he described how the "Medicean stars" changed their daily positions in the vicinity of Jupiter between 07 Jan and 02 Mar 1610. He also noticed that the innermost moon had a higher speed than the others. In 1612, Galileo gave approximate revolution periods for the satellites (for Io: "1 day and 18 and almost half an hour") right at the beginning of his 'Discourse on Floating Bodies' (Galilei 1612).[8] Over the subsequent years (until 1619), he further observed the "new planets" to refine the orbit

[7] Although likely, whether Marius could have seen the Galilean moons before the end of 1610 may possibly never be clarified beyond doubt. Among the more skeptical views are, e.g., Pagnini (1931), Van Helden and Zuidervaart (2018), or Zik et al. (2020).

[8] Quoting Galilei (1612): "Dove finalmente m'accertai, che 'l primo, e più vicino a Giove, passa del suo cerchio gradi 8 e m. 29 in circa per ora, faccendo la 'ntera conversione in giorni naturali 1 e ore 18 e quasi mezza."

periods. His measurements of the daily rotation rate of Io settled at 203° 25',[9] which is equivalent to a period of 1 d 18 h 28$\frac{1}{2}$ min and within several seconds to the modern value.[10]

While Galileo published his observations immediately, Marius[11] made first public allusions about his own observations more than 1$\frac{1}{2}$ years later in an astrological almanac series (*Prognosticon Astrologicum*), which he had published annually since the year 1600 in German. Herein, he acknowledged Galileo as the discoverer (Marius 1611)[12] and provided orbit periods (Marius 1612) at virtually the same time as Galileo. In his main work, *Mundus Iovialis* (Marius 1614), he made various insightful statements about the four newly discovered Jovian moons, including recognition of a very subtle orbit inclination, or that their movement can only be explained as uniform if Jupiter orbits the Sun and not the Earth. The orbital periods given by Marius after only a few years of observations were remarkably accurate. For example, his value for Io (1 d 18 h 28 min 30 s) differs from the modern IAU value (Archinal et al. 2018) by just 6 seconds.[13] Marius also made considerations on the possible real size of the Jovian world; however, his estimated radius of Io's orbit (∼22,500 km), of Io's size (∼620 km), and of Io's orbit speed (0.91 km/s) do not match the real values. The part of the *Mundus Iovialis* that has likely the most lasting effect is the part about the names. Among the four different possible naming schemes for the newly found objects that Marius proposed, the mythological designations (Io, Europa, Ganimedes, Calisto) prevailed and provide, partly with slightly different spelling, the official names in use today.

Subsequent research on Io and the other Galilean satellites mainly focused on ephemeris tables. For example, Jean-Dominique Cassini in 1694 published results of his decades-long measurements of Io. His determination of the orbital period (1 d 18 h 28 min 36 s; Cassini 1694) is already identical to the one currently adopted by the IAU. Almost two decades earlier, Io played a crucial role for another fundamental discovery. Danish astronomer Ole Rømer claimed in a talk to the French Academy of Sciences on 22 Nov 1676 that the speed of light is finite.[14] Rømer had recognized that eclipses of Io occurred prematurely or were delayed compared to prediction, depending on the position of the Earth relative to Jupiter. Without knowledge of the value of the Astronomical Unit, he had concluded that the light requires 22 minutes to pass the diameter of Earth's orbit, not very far from the true value of 16 min 38 s.

While the Galilean satellites were used mainly as clocks for longitude position determination on Earth for several centuries after their discovery, there were also some research activities focusing on their physical properties. In the late 18th century, scientists like Jean-Sylvain Bailly, William Herschel and Johann Hieronymus Schroeter claimed to have visually seen brightness variations which they attributed to satellite rotation (Müller 1897).

[9] Value is from tables in Galilei (1931).

[10] The accuracy of the rotation rates given in Galileo's tables is limited to arcminutes, and these are synodic values. The sidereal IAU value of Io's rotation rate (203.4889538°/d; Archinal et al. 2018) converts to a synodic value of 203.4059026°/d, or 203° and 24.35' daily.

[11] In-depth information on Simon Marius is compiled at the Marius portal: https://www.simon-marius.net/.

[12] Quoting Marius (1611): "Von diesem neuen Planeten hat Galilæus Galilæi Patavinus Mathematicus, allbereit ein Tractätlein außgehen lassen/wie auch zu anfang der Practica angezeigt worden/vnd ich es allhier als ein grossen wunder mit fleiß widerholen wollen." – [*Translation:*] "On these new planets has Galileo Galilei, mathematician from Padova, already published a small treatise, as was also indicated at the beginning of this Practica, and I want to repeat it here as a great miracle with diligence."

[13] Marius' given precision is at the second level. The IAU synodic rotation rate is equivalent to a period of 1 d 18 h 28 min 35.9 s.

[14] Published soon after by an anonymous listener in the *Journal des Sçavans*; N.N. (1676; in French); english version: N.N. (1677).

Herschel determined the relative sizes of the Galilean satellites and potential light variations throughout the orbital paths, which he interpreted as synchronous rotations (Herschel 1797). However, another ∼70 years had to pass until brightness measurements of the Galilean moons had been performed with photometers (Engelmann 1871). Measurements by various astronomers still resulted in contradicting interpretations ranging between "no notable light variation" by Pickering and "brightness variations are independent of the rotational phases, but caused instead by weather phenomena on the satellites" by Flammarion (Müller 1897).

Io observations in 1890 and 1893 by Edward Barnard led to the conclusion that this moon has "dusky" polar caps, and that the rotation axis of Jupiter's first satellite is oriented nearly perpendicular to its orbit (Barnard 1894). A comparison of Barnard's sketch figure of Io in front of the Jovian cloud top to spacecraft images centered near the anti-Jovian hemisphere (like the one shown in Fig. 3) confirms this impressive perception – remember that the angular size of Io as seen from Earth is only about one arcsecond. On the other hand, in the same paper, Barnard speculated that "this satellite at least is in a physical condition not vastly different from that of Jupiter itself" – a statement not at all in alignment with more recent research results, and a reminder of how difficult it might be sometimes to distinguish between observation and interpretation based on expectations.

Further research at the turn of the 20th century included attempts to directly measure the diameters of the Galilean moons' tiny disks with micrometers. For example, See (1902) describes in high detail the substantial obstacles of such an effort. Still, his result for Io (3318 km) is only about 10% off (smaller than) today's value (3645 km). The density of Io was calculated to 3.29 of water, again a value close to what is adopted today (3.53).[15] Similar work was performed and published by Michelson (1891) and Barnard (1897); they measured the size of Io to 3844 km and 3946 km, respectively, which is off by 6-10% in the other direction (i.e., larger). A few decades later, results from photoelectric lightcurves included findings that the brightness of Io varies by ∼0.2 mag over one orbit with the leading side being brighter, that Io has a spherical shape, and that the lightcurve variations stem from an irregularly spotted surface (Stebbins 1927; Stebbins and Jacobsen 1928). Harris (1961) emphasizes the unusually reddish color of Io as well as surface color variations. At that time, the name "Io" also has started to migrate into scientific papers, gradually replacing or complementing the term "Jupiter I".

Spectral measurements from 0.3 to 1.1 μm by Johnson and McCord (1970) showed that the Galilean satellites are unlike what is observed in the inner Solar System at the Moon and Mars. For Io, an unusual deep spectral slope between 0.3 and 0.5 μm was found, whose cause could not then be explained. On Europa and Ganymede, Pilcher et al. (1972) identified water frost in the spectra of their surfaces, however $H_2O$ appeared to be absent on Io. Shortly after, Wamsteker et al. (1974) identified sulfur as a surface component on Io in visible and near-IR spectra. In May 1971, Taylor (1972) determined Io's equatorial diameter from a stellar occultation to 3656 ± 5 km. In 1977, the book "Planetary Satellites" (Burns 1977) compiled the knowledge about Io and the other Galilean satellites, in preparation for the *Voyager* spacecraft missions that were launched in the same year.

On 02 Mar 1979, just a few days before Jupiter arrival of *Voyager 1*, Peale et al. (1979) predicted that a major fraction of Io's mass is likely molten due to dissipation of tidal energy, and that this "may be evident" in the *Voyager* images to be returned to Earth, possibly in the form of volcanism. Six days later, two volcanic plumes were discovered over regions afterwards named Pele and Loki. Io images of *Voyager 1*, taken at 124° phase angle from a

[15] For Io's mass used for the density calculation by See (1902), see tables on p. 335 and 336 in his paper. The oldest estimate goes back to Laplace (1805). See also de Sitter (1931).

distance of 4.5 million km for spacecraft navigation purposes, proved that Io is a geologically very active body even today (Morabito et al. 1979; Morabito 2012).

The highest resolved data of the surface of Io have been provided so far by *Voyager-1* (March 1979, ∼1 kilometer per line pair, Smith et al. 1979a) and the *Galileo* orbiter (between October 1999 and October 2001, 10-600 m/px). While *Voyager 1* passed Io at a minimum distance of 20,600 km, *Galileo* performed seven targeted flybys at altitudes between 100 and 900 km (e.g., Keszthelyi et al. 2001; Turtle et al. 2004; Lopes and Williams 2005),[16] in which the images with the highest spatial resolution were sampled at ∼5 m/px. More recently, the *Juno* spacecraft came close to Io as well, conducting two flybys on 30 Dec 2023 (perijove PJ57) and 03 Feb 2024 (PJ58) at just 1500 km altitude (∼1.8 km/px). Because the JIRAM and JunoCam instruments onboard *Juno* are wide-angle devices, the spatial resolutions of the best images are slightly lower than the best-resolved Voyager-1 images despite the lower altitude. However, because *Juno* follows a polar orbit, JunoCam and JIRAM observed Io's north polar region with better resolution than *Voyager*'s or *Galileo*'s. *Juno* was also able to observe the southern hemisphere which has so far been seen rarely and at coarse spatial resolution only. From larger distances, the *Cassini* and *New Horizons* spacecraft have also observed Io during their Jovian system flybys in 2000/01 and 2007, respectively. From the ground, Io has been observed over more than four centuries, and it is also occasionally a target for spaceborne observatories like *HST* (e.g., Spencer et al. 2000) and *JWST* (de Pater et al. 2023b, 2025).

### 2.1.2 Volcanism and Surface Chemistry

Volcanism on Io manifests in both explosive and effusive eruptions from volcano-tectonic depressions akin to terrestrial calderas, called "paterae" (singular: "patera"), which are irregularly shaped craters. On Io, sulfur dioxide ($SO_2$; Smythe et al. 1979) and sulfur ($S_2$; Spencer et al. 2000) act as volatile gases that enable fragmentation of mafic (and possibly ultramafic) magmas, as well as producing plumes and corresponding bright plume deposits. Five different colors (shades of yellow, red, white, black, and green) of diffuse plume deposits have been mapped on Io, representing different combinations of sulfur allotropes[17] ($S_3$-$S_4$) and $SO_2$ molecules and silicate tephra in both irregularly and ring-shaped deposits (Geissler and McMillan 2008; Williams et al. 2011a,b). Because of Io's comparatively lower gravity and lack of a substantial atmosphere, explosive eruptions have been detected reaching up to 500 km above the surface, producing umbrella-shaped plumes (Fig. 5) and ring-shaped deposits >1000 km in diameter (Turtle et al. 2004; Spencer et al. 2007). Effusive volcanism manifests as large fields of lava flows that cover ∼29% of Io's surface, as well as small dome-like structures that cover <0.2% of the surface (Williams et al. 2011a,b). Major lava flows are observed, like the Amirani flow field, which is considered one of the longest known active lava flow in the Solar System, as it spans more than 300 km (Keszthelyi et al. 2001). The lack of stratovolcanoes or steep-sided domes is suggestive of low-viscosity, Mg- and Fe-rich and Si-poor magmas. Most dark lava flows are thought to be silicate in origin, likely something similar to terrestrial high-Mg basalts or lunar mare basalts. However, Io has substantial fields of bright, yellow to white flows, indicative of sulfur flows and even rare $SO_2$ flows (Williams et al. 2001; Turtle et al. 2004). Lava channels have been recognized and lava tubes have been inferred (Keszthelyi et al. 2001; Schenk and Williams 2004).

[16] The flybys were labeled I0, I24, I25, I27, I31, I32, and I33. Imaging data has been recorded in I24 to I32.

[17] Colors and surface materials on Io: yellow: $S_8$; red/brown: $S_3$, $S_4$; white: $SO_2$ frost; black: Si; green: alteration product of hot silicate lava and sulfurous materials (Geissler et al. 1999).

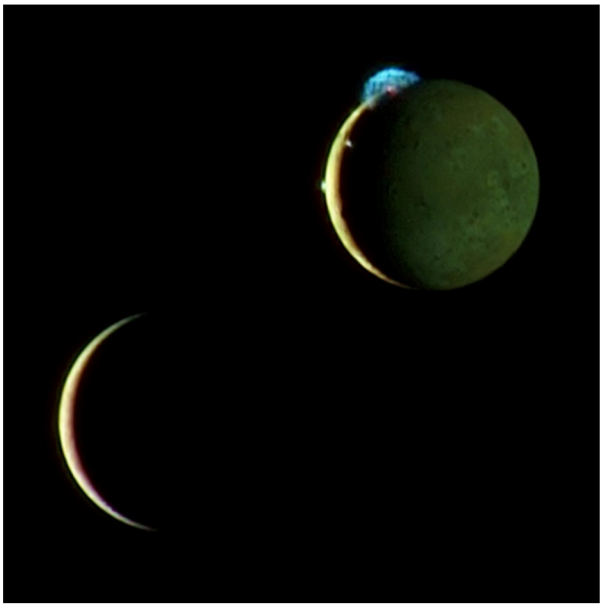

**Fig. 5** Io plumes observed by *New Horizons* from 4.6 Gm distance on 02 Mar 2007 10:23 UTC. 11 o'clock position: Tvashtar, ∼300 km high; 9 o'clock: Prometheus; bright spot at terminator in between: Amirani. For JUICE/JANUS, Io will appear similar from ∼1.8 Gm distance. The other moon is Europa at 3.8 Gm range. *Source:* NASA/JPL PIA10103 (https://web.archive.org/web/20250430025026/https://photojournal.jpl.nasa.gov/catalog/PIA10103)

*Galileo* Solid State Imager (SSI) and Near Infrared Mapping Spectrometer (NIMS) data have shown active eruptions including lava fountains, advancing flows akin to lobate, compound pahoehoe flows, and advancing (possibly overturning) lava lakes (McEwen et al. 1998; Keszthelyi et al. 2001; Turtle et al. 2004; Rathbun et al. 2002; Lopes et al. 2004). The accumulation of explosive and effusive volcanic deposits causes crustal compression, resulting in tectonic fracturing and uplift of crustal blocks to form mountains (Carr et al. 1998; Schenk and Bulmer 1998), which cover ∼3% of Io's surface (Williams et al. 2011a,b). About 35% of mountains are within 25 km of paterae, suggestive of a genetic relationship in which tectonic fractures related to mountain formation often serve as conduits for magma ascent and patera formation (Radebaugh et al. 2001; Jaeger et al. 2003).

Thermal emission from Io's paterae and lava flow fields has been detected both from spacecraft flybys and space-based telescopes, and from Earth-based telescopes using adaptive optics (see review by de Kleer and Rathbun 2023). These observations have enabled scientists to track the eruption styles of specific volcanoes over multiple decades. In 2024, adaptive optics of Io extended to visible wavelengths (Conrad et al. 2024), enabling visual recognition of large-scale (∼80 km) surface changes on Io from Earth's surface. A Geographic Information Systems (GIS) database of published Io data from the NASA *Voyager*, *Galileo*, *New Horizons* missions and telescopic observations and modeling studies was published in 2021 (Williams et al. 2021).[18]

The NASA *Juno* mission (Bolton et al. 2017), primarily aimed at observing Jupiter, also studied the spatial distribution of hot spots on Io, and the temporal variability of the total emitted power. It successfully captured 2-5 μm infrared images and spectra of Io thanks to the JIRAM instrument (Adriani et al. 2017) on more than 25 occasions (Mura et al. 2020; Tosi et al. 2020; Zambon et al. 2023; Davies et al. 2024; Mura et al. 2024; Fig. 6). The natural evolution of *Juno*'s orbit has made it possible to progressively decrease the distance from this satellite at the closest encounter of each orbit, and therefore increase the spatial

[18]GIS database for Io at ASU (Arizona State University): https://rgcps.asu.edu/gis_data/.

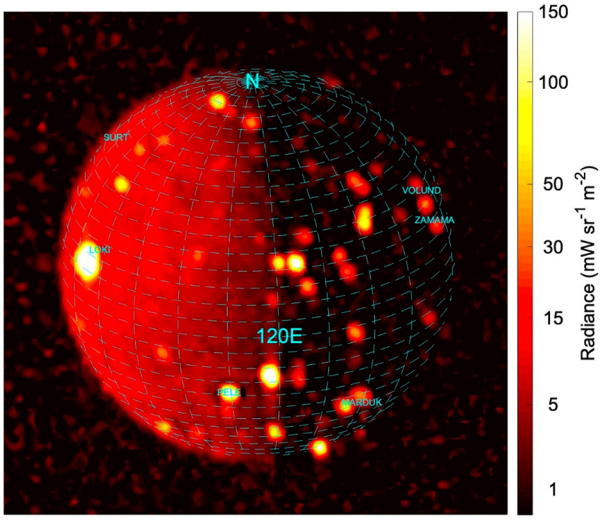


**Fig. 6** Image of Io, showing the infrared M-band integrated radiance (4.5 to 5 μm), taken by *Juno*-JIRAM on 16 Oct 2021 from a distance of 260,000 km; spatial resolution is 60 km/px

sampling of JIRAM images down to about 10 km/px. Spectroscopic data acquired between 2 and 5 μm allowed JIRAM to confirm the widespread presence of $SO_2$ frost and to suggest the presence of minor species such as hydrogen sulfide $H_2S$ (Tosi et al. 2020). The data acquired with the imaging filters (at 3.455 and 4.780 μm) were used to map the distribution of hot spots with particular emphasis on the polar regions, which are practically invisible from Earth- or space-based telescopes and imaged only marginally by previous spacecraft such as *Voyager*, *Galileo*, and *New Horizons*. This investigation ultimately allowed updating the existing catalogs (Mura et al. 2020; Zambon et al. 2023; Davies et al. 2024).

### 2.1.3 Tenuous Atmosphere and Torus

Io's tenuous atmosphere consists primarily of $SO_2$ gas, with a surface pressure of several tens of nanobars at most. At much lower levels SO, O, NaCl and KCl have been detected as well.

ALMA observations of $SO_2$ and NaCl showed that the isotopic ratios $^{34}S/^{32}S$ and $^{37}Cl/^{35}Cl$ are highly enriched compared to average solar system values, which implies that Io has lost 94-99% of its sulfur inventory since it formed (de Kleer et al. 2024).

The atmosphere is thought to collapse when Io is eclipsed by Jupiter or on the nightside of Io, because of the $SO_2$ gas condensing when the surface temperature drops below its condensation temperature. However, the details of this process, and how much of the atmosphere collapses, are far from understood. The atmosphere also plays a most intriguing role in any Io-magnetosphere interactions, since neutrals originating from Io's atmosphere form the main source of plasma in Jupiter's magnetosphere.

While the dominant immediate source of Io's atmosphere is sublimation of $SO_2$ ice from its surface, leading to a collisionally thick atmosphere at low latitudes during the day, volcanoes have a substantial impact on its atmosphere, and can be dominant locally. Sputtering from Io's surface by impact of magnetospheric ions may also be a source at high latitudes, at night, and during an eclipse (see, e.g., review by de Pater et al. 2023a). Although the atmosphere is dominated by $SO_2$ molecules, ~10% is SO, in part formed through photodissociation of $SO_2$, as well as ejected directly from volcanoes. The source of $S_2$ is primarily volcanic, as it has been detected primarily above active volcanoes. $O_2$ might form in the

atmosphere and be abundant at small fractions as well (Roth et al. 2014), but has yet to be observed. Sodium chloride (NaCl) and potassium chloride (KCl) have both been detected in Io's atmosphere (Lellouch et al. 2003; Moullet et al. 2013). Whether NaCl and KCl are volcanically produced or through sputtering off the surface is not clear, because while these molecules are spatially confined (as expected in a "plume"), they appear at locations that differ from volcanically-sourced $SO_2$ (e.g., Redwing et al. 2022; de Pater et al. 2023a). Indications that other salts are also present on Io have been provided by Io's neutral clouds containing Na, K, Cl and the presence of sulfuryl chloride ($SO_2Cl_2$, Schmitt and Rodriguez 2003) and other exotic materials in Io's red surface deposits. Water and water ice, however, are absent in all previous Io observations, in stark contrast to Io's sister Galilean moons.

Although most volcanic plumes are visible through sunlight scattered off dust particles, there is growing evidence that a number of volcanoes produce "stealth" plumes, emitting only gas and no dust (Johnson et al. 1995; see also review by de Pater et al. 2023a and references therein). Red, green, and bluish glows, with intriguing morphologies, were captured in *Galileo* and *HST* images while Io was in eclipse, and were attributed to both atomic (e.g., Na, K, Cl, S) and molecular emissions excited via electron impact (e.g., Geissler et al. 1999; Bouchez et al. 2000; Schmidt et al. 2023).

Some of the neutral species escape Io's gravity to form giant neutral clouds of S and O (several Jupiter radii in size; see e.g., Koga et al. 2018 and Koga et al. 2019 for observations of the oxygen neutral cloud). Those clouds extend along Io's orbit and are continuously passed by the plasma flow of the Io plasma torus at a relative velocity of ∼57 km/s (Kivelson et al. 2004). They experience charge exchange and electron-impact ionization, which supply the Io plasma torus with fresh plasma (see review by Bagenal and Dols 2020). The rate at which neutrals are supplied from Io to the neutral clouds (and also at which these are ionized later and added to the plasma torus) is about 1000 kg/s (Broadfoot et al. 1979; Dessler 1980). About 300 kg/s of material is ionized locally at Io and fed directly into the plasma torus (e.g., Bagenal 1997; Dols et al. 2008). Io is the main source of plasma in Jupiter's magnetosphere and is thereby responsible for driving a wide variety of processes and interactions in this magnetosphere that will be studied by JUICE (Masters et al. 2025, this collection). Figure 7 illustrates the key regions of the space environment that surrounds Io within the Jupiter system.

Large variations of a factor >3 have been suggested to occur in the supply of the plasma torus (e.g., Hikida et al. 2020). Considering that Io's atmosphere is relatively stable (e.g., Giles et al. 2024), it is not clear from where these strong variations originate. Though volcanic activity is often considered as a possible explanation, it has been shown that large eruptions only change the mass loading by a few percent (Blöcker et al. 2018). Therefore, the cause of the variability of the plasma torus and the role of volcanoes therein remains unexplained (Roth et al. 2025), although combined JWST (2023) and HST (2000) observations of sulfur suggest that the entire system is quite stable over decades-long timescales (de Pater et al. 2025).

Since the 1970s, Io has been observed by the *Pioneer*, *Voyager*, *HST*, *Galileo*, *Cassini*, *New Horizons*, and *Juno* spacecraft, as well as by many Earth-based telescopes (see review by Schneider and Spencer 2023). The experience gained from the Jupiter orbiters *Galileo* and *Juno* as well as from large space telescopes like *HST* and *JWST* will inform the design of Io observations by JUICE discussed in the next section.

### 2.2 Science Objectives for Io Addressable with JUICE

The science rationale for the continued exploration of Io was outlined in a white paper by Keane et al. (2021) in preparation for the 2023 *Origins*, *Worlds and Life* US Na-

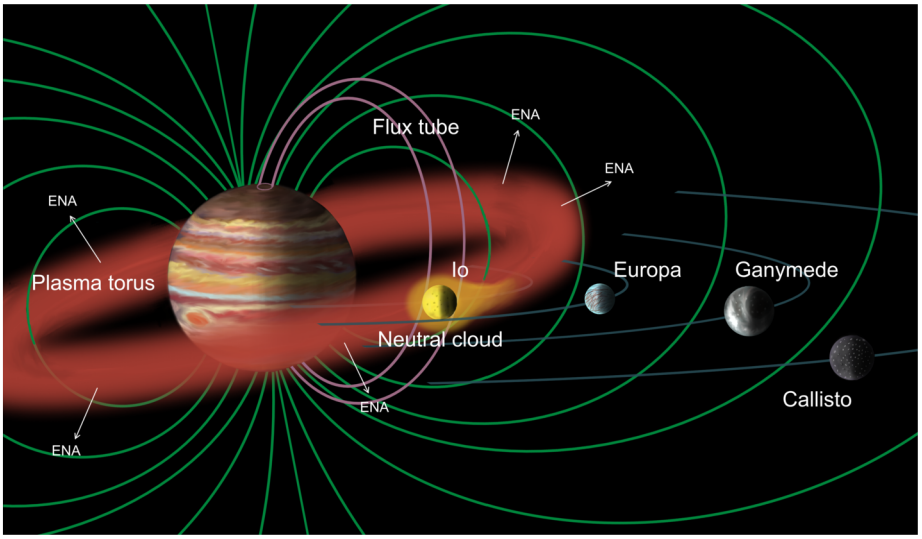


**Fig. 7** Artist's depiction of the space environment surrounding Io within the Jupiter system. It illustrates the neutral clouds and plasma torus originating from Io, as well as the flux tube connecting Io to Jupiter's magnetic poles. Note that the neutral clouds for certain species may form a full torus (e.g., the O torus). The illustration also depicts Energetic Neutral Atoms (ENAs) generating from the charge exchange between the neutral clouds or atmosphere and the magnetospheric plasma. These ENAs, not constrained by the electromagnetic field, follow ballistic trajectories and can be used for remote imaging of the plasma population (Wurz 2000)

tional Academies Astrobiology and Planetary Science Decadal Survey. They highlighted five cross-cutting themes: Tidal heating, heat flow, volcanism, atmospheres, and magnetospheric interactions. Io remains the best place in the Solar System to study tidal heating and how rocky planets respond to extreme heat flow and volcanism, and how Io's dynamic atmosphere interacts with the powerful Jovian magnetosphere (Keane et al. 2021). These concepts have become even more important with the recognition of lava-rich exoplanets from recent Astrophysics missions.

Because Io is so geologically active, it can and should be studied as frequently as possible, by as many types of instruments as possible, from all available platforms from Earth-based telescopes to space-based telescopes to Jupiter-orbiting spacecraft. The science goals that can be addressed will vary based on the platform used to study Io. Here we focus on the science objectives addressable using a Jupiter-orbiting spacecraft that can only do distant ($\geq$500,000 km) observations. As described in the JUICE mission Definition Study Report (ESA 2014), the goal of the JUICE mission at Io is "to monitor the volcanic activity of Io and determine the composition of different materials on the surface at regional scale through remote multi-wavelength imaging spectroscopy".

More specifically, the science objectives for the JUICE mission at Io include the following: (1) Characterize the composition of Io's surface and monitor Io's surface, volcanic and plasma activity (including the plasma torus) at multiple time scales (hours to months); (2) Observe Io and the plasma torus at spatial resolutions of 200 km and 2000 km, respectively; and (3) Monitor radio emissions from 1 kHz to 45 MHz from the Io environment, including the torus and auroral emissions. These objectives require repeated remote observations of Io and the inner Jovian system during the satellite tour prior to Ganymede orbit insertion, from multiple instruments. For example, the JANUS camera will conduct repeated imaging

of sites of active volcanism with pixel scales ∼10 km/px, while MAJIS will monitor thermal hot spots at these sites during Io dayside observations. MAJIS will also obtain spectral mapping at 50 km pixel scale of Io's far side. The UVS spectrometer will conduct searches for $SO_2$ plume activity, while SWI will map temperatures and gas abundances in Io's exosphere, and RPWI will monitor Io's torus and aurorae for radio emissions from 1 kHz to 45 MHz. PEP will monitor energetic particle activity at times of closest approaches to Io.

The JUICE spacecraft is expected to come as close as about half a million kilometers to Io. During the observations, JUICE will focus on: (a) daytime observations for surface change detection from active volcanism, composition, and geologic feature identification; (b) eclipse and nighttime observations to detect active volcanic plumes and to monitor Io's aurora and magnetospheric interactions; and (c) study of Io's sodium cloud for spatial and temporal variations. Detailed measurements of Io by JUICE's instruments are discussed in the next sections.

### 2.3 Io Observations with JUICE

Because the JUICE mission is designed to be a Ganymede orbiter after multiple flybys of the icy Galilean satellites, the spacecraft trajectory will not bring JUICE closer to Io than ∼500,000 km, and most observations will take place from distances $\gtrapprox$800,000 km. In the following sections we highlight Io observations planned with five different JUICE instruments.

#### 2.3.1 Io Imaging with JANUS

A Science and Operations Plan for imaging Io in the visible and near-infrared has been developed, building on past experience obtained by NASA's *Galileo* mission and on experience being gained by NASA's ongoing *Juno* mission. Prior to Ganymede orbit insertion, the JUICE instruments are expected to provide distant monitoring of Io's volcanoes. The JANUS camera (Palumbo et al. 2025, this collection) will have the opportunity to observe Io to (1) characterize the thermal activity providing insights into volcanic processes and their nature, (2) determine the composition, surface changes and geological features to investigate Io's dark deposits and lava composition, (3) detect and monitor plumes, (4) monitor the changes of Io's sodium cloud, and (5) monitor Io's aurora and interactions with Jupiter's magnetosphere.

Such scientific objectives will be addressed with the existing Io observation opportunities during the entire JUICE mission. Indeed, based on the current[19] JUICE trajectory profile, there will be 52 observation opportunities at close range (distances below 800,000 km), resulting in a JANUS pixel scale equal or better than 12 km/px and a full disk angular width equal or larger than 16 arcmin (Fig. 8). In addition, there are 347 eclipse observation opportunities at a distance below 2 Gm (of which just a small fraction might be observed). In particular, during close observations, JANUS will observe with a range of different solar incidence angles, different filters (broadband PAN; color filters from 0.45 μm to 1.02 μm) and, when possible, with high phase angle to acquire bright limb observations to detect surface changes (e.g., at scarps or mountains), plumes and recurrence of known plumes and to map geological features. On the other hand, during night side and eclipse observations, JANUS will perform hot spot detection and temperature measurements. For example, McEwen et al. (1998) used the Clear/1-micron filter ratio in eclipse images of the Galileo

[19] Orbit tour CReMA_5_1; will be revised; final tour release is expected for 2028.

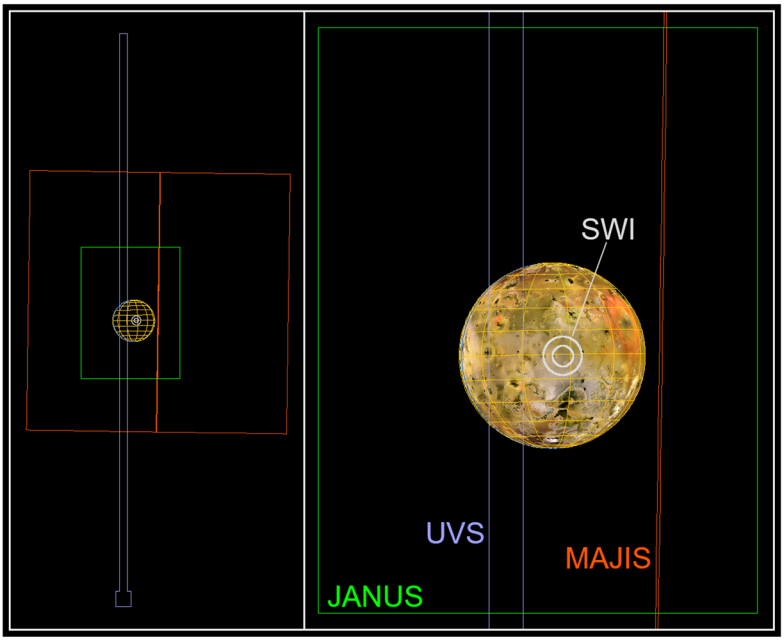


**Fig. 8** Io as will be seen by JUICE on 31 Jul 2032 08:49:45 UTC at a distance of 379,581 km (the closest approach in reference orbit tour CReMA_5_1). JANUS pixel scale: 5.7 km/px; apparent diameter in JANUS images: 639 pixels.
*Left:* JANUS field-of-view (green frame; 30.0×22.5 mrad = 1.72°×1.29°), UVS slit (blue; 1.7×127 mrad + 3.5×3.5 mrad = 0.1°×7.3° + 0.2°×0.2°), SWI circular beam FWHM (white; 1 mrad = 3.4' at 1200 GHz, 2 mrad = 6.9' at 600 GHz), MAJIS slit (red; 60×0.15 mrad = 3.4°×31"), and an example of MAJIS field-of-view envelope (red frame) of 60×60 mrad (3.4°×3.4°) that can be obtained using the MAJIS internal scanning mirror.
*Right:* Enlarged version with Io map (south is up; visible is the anti-Jovian hemisphere). The plots were compiled with the multi-mission planning tool CKVIEW (Matz and Roatsch 2018)

SSI camera[20] to estimate brightness temperatures of hot spots; a similar strategy is possible with JANUS. However, combined JANUS and MAJIS observations might yield more robust measurements. Figure 9 shows examples of *Galileo* spacecraft observations for the detection of plumes, which could be similar to what JANUS will observe.

### 2.3.2 MAJIS Infrared Observations

Io is also an interesting object to be remotely studied by MAJIS (Moons And Jupiter Imaging Spectrometer; Poulet et al. 2024, this collection). Remote sensing measurements will be dedicated to monitoring the volcanic activity in space and time. As obtained from ground-based and space-based measurements and described in Sect. 2.1.2, Io's surface is dominated by sulfur-bearing species, particularly $SO_2$ frost, but also including $S_2$, SO, $SO_2$ gas, NaCl, and KCl. Other compounds such as iron sulphide minerals have been speculated to exist, but not convincingly identified (Carlson et al. 2007).

Achivements of Juno's JIRAM instrument have also briefly been introduced in Sect. 2.1.2. The JUICE mission's MAJIS spectrometer data will not surpass the spatial resolution of JIRAM data, given JUICE's trajectory, but will still have several opportunities

[20] Galileo Solid State Imaging Experiment (Belton et al. 1992).

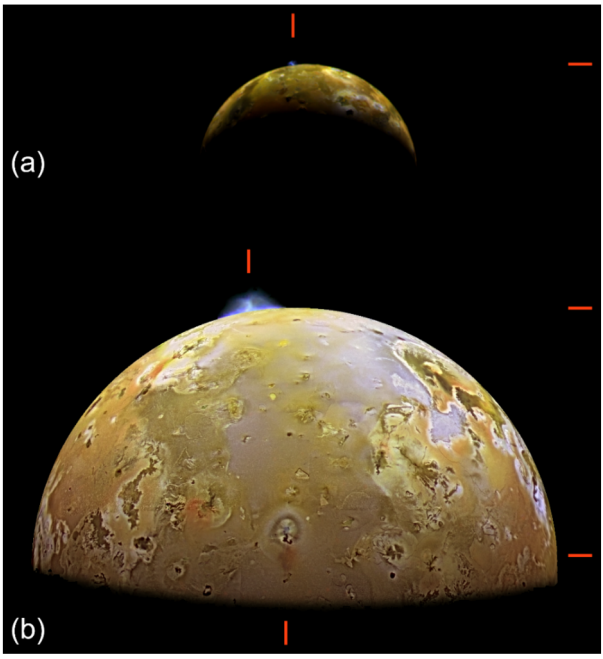


**Fig. 9** *Galileo* observations of Io, similar to what JANUS will acquire. The red bars point to volcanic eruption plumes. North is to the right.
(a) From orbit G1 (28 Jun 1996; observation ID G1ISGLOMON0; pixel scale 20 km/px; range 972,000 km; color filters near-infrared, green, violet). The Ra Patera plume extends ∼100 km into space.
(b) From orbit C9 (28 Jun 1997; C9ISSRFMON02; 6 km/px; range ∼600,000 km; same color filters). The plume of Pillan Patera (at limb) is 140 km high. From the Prometheus eruption (bottom), a reddish shadow is visible. Plumes on Io have a blue color, thus the plume shadow is reddish.
*Sources:* (a) NASA/JPL PIA00293 (https://web.archive.org/web/20250516044603/https://photojournal.jpl.nasa.gov/catalog/PIA00293). (b) NASA/JPL PIA01081 (https://web.archive.org/web/20250320055121/https://photojournal.jpl.nasa.gov/catalog/PIA01081) (slightly modified)

to observe Io from afar. MAJIS was designed primarily for studying the icy Galilean satellites Ganymede, Callisto (Stephan et al. 2021), and Europa, as well as Jupiter's atmosphere, but its overall spectral range of 0.49-5.56 μm also suits the study of Io.

JUICE's current mission profile predicts that MAJIS will have 18 opportunities to observe Io at a spatial sampling <100 km/px during the Jupiter tour, with a minimum value of 57 km/px. This is comparable to what was achieved for example by *Juno*-JIRAM in April 2020 or in October 2021. At this spatial resolution, not even the largest volcanic features on Io, such as Loki Patera, will be resolved. However, MAJIS has augmented performances compared to any other imaging spectrometer carried onboard spacecraft,[21] which should help in investigating low abundance species associated with specific regions on Io's surface. Although none of the 18 observation opportunities (dubbed "segments") occur when Io is in eclipse, the MAJIS sensitivity range extends beyond 5 μm, which enables a better temperature retrieval of cooler volcanic features with respect to JIRAM. The current MAJIS observing plan is to acquire one hyperspectral image ("image cube") every 60 minutes in

[21] Average spectral sampling 3.7 nm in the 0.49-2.36 μm range and 6.5 nm in the 2.27-5.56 μm range (see Poulet et al. 2024, this collection).

those segments where most of the dayside (>60%) will be visible, and acquire one hyperspectral image every 30 minutes when most of the nightside is visible, commanding different exposure times to track also the weakest spots.

Should additional data volume become available for Io observations, MAJIS could also consider additional segments with the satellite in eclipse, although those observations would have coarser spatial resolution (>100 km/px). Eclipses are ideal both for the absence of the reflected solar component, which facilitates the monitoring of hot spots, and for investigating the response of the atmosphere-surface system to a sudden shading condition. Decades of observations conducted both from Earth and from space and in a wide spectral range in search of variations in the abundance of surface $SO_2$ frost (the so-called "post-eclipse brightening") have led to still uncertain and debated conclusions (e.g., Binder and Cruikshank 1964; Bellucci et al. 2004; Cruikshank et al. 2010; Tsang et al. 2016).

Additionally, recent observations with *Juno*-JIRAM in the 2-5 μm spectral band (Tosi et al. 2020) allowed identifying features at 4.07 μm and 4.37 μm caused by the combination of $\nu_1+\nu_3$ and the overtone $2\nu_1$ of $SO_2$, and other weaker spectral features at 2.54, 2.79, 2.92, 3.35, 3.56 and 3.78 μm (Nash and Betts 1995, 1998). Other absorptions at about 3.9 μm and 3.0 μm indicate the presence of $H_2O/SO_2$ and $H_2O/SO_2$ mixtures (Salama et al. 1990; Sandford et al. 1994; Carlson et al. 1997; Carlson et al. 2007) and oxyhydroxides. The IR region also allowed the detection of weak absorptions, which could possibly be explained with hydronium in sulfuric acid tetrahydrate or $S^{16}O^{18}O$ isotope (at 4.47 μm), $CO_2$ in $SO_2$ or $ClSO_2$ (at 4.26 μm) and other unassigned features like the one at 2.65 μm, which deserves further investigation. The spatial resolution of JIRAM at the time of observations was about 100-150 km/px, and the obtained images in the M-band (centred at 4.85 μm) were used to study the distribution of the hot spots on Io's surface, also exploring its polar regions (Mura et al. 2020; Zambon et al. 2023; Davies et al. 2024; Mura et al. 2024).

The spectroscopic capabilities of JUICE, in particular by using MAJIS and JANUS, will be used to study the composition and distribution of the above-listed species with a spatial resolution in the range of 50-200 km/px. Additional observations of Io in eclipse by MAJIS and other JUICE remote sensing instruments such as SWI, albeit at coarser spatial resolution, would allow further investigation of the satellite's thermodynamic response, indirectly constraining the predicted atmospheric condensation process and the contribution of volcanic emissions to sustaining the atmosphere.

### 2.3.3 UVS Observations of Emitted and Reflected Light

The JUICE Ultraviolet spectrograph (UVS) bandpass (50-204 nm; Retherford et al. 2026, this collection) encompasses important emission and absorption features of atomic and molecular species known to exist in Io's atmosphere, facilitating new studies of atmospheric composition, morphology, and variability. UVS will obtain two-dimensional spectral-spatial images of auroral and airglow emissions of S, O, and Cl, observing how their intensities and locations change as a result of the time-variable interaction between Io and Jupiter's tilted magnetic field (e.g., Roesler et al. 1999; Roth et al. 2014). Images of reflected solar Lyman-$\alpha$ at 121.6 nm will be used to map the $SO_2$ atmosphere, which has a large absorption cross section at Lyman-$\alpha$ (e.g., Feldman et al. 2000; Feaga et al. 2009, Giono and Roth 2021). Further constraints on the $SO_2$ density, along with information about the concentration of $O_2$ and other UV-absorbing atmospheric species, will be obtained using transit observations – which map the absorption of Jupiter airglow by atmospheric gases above Io's limb – and during stellar occultations – where characteristic UV absorption features are detected in the spectrum of a star as it passes behind Io's atmosphere from the point of view of the observer (i.e., the UVS boresight). Observations of Io's atmosphere near the terminator and

on the nightside, as well as in Jupiter's shadow during eclipse, are of particular importance for determining the relative importance of sublimation and volcanism for generating the atmosphere. Occultations should target a wide range of local times and latitudes, as well as regions close to known plumes.

At wavelengths that are less affected by atmospheric absorption, UVS will monitor Io's UV surface reflectance and search for large scale variations (e.g., leading compared to trailing hemisphere; low compared to high latitudes) potentially related to differing rates of sublimation, sputtering, and radiation darkening across the globe. Moving away from Io, UVS will perform regular scans of the Io neutral cloud and plasma torus to monitor composition and variability on timescales ranging from hours to months (see Masters et al. 2025, this collection). Combined with observations of the surface and near surface atmosphere, these measurements aim to provide a more complete understanding of how material is transported from Io's surface (via sublimation and sputtering) and subsurface (via volcanism) out through the Jovian magnetosphere.

The main challenge for UVS will be the relatively low spatial resolution due to the large Io-JUICE distance: at most, Io's diameter will fit within ∼5 UVS slit widths. It may be possible to improve the cross-slit resolution using a sub-slit sampling technique similar to that used by Trumbo et al. (2022) in their *HST* Space Telescope Imaging Spectrograph (*HST*/STIS) Io maps. In the along-slit direction, the spatial resolution may be improved by using the UVS High resolution Port (HP mode – see Retherford et al. 2026, this collection), which reduces the aperture size to provide improved spatial resolution at the cost of reduced throughput. Even using these techniques, UVS will not match the resolution of previous *HST*/STIS studies, likely achieving spatial resolution worse than ∼500 km per resolution element. However, *HST* cannot obtain nightside coverage and lacks the EUV sensitivity necessary to detect many of the Io torus emission lines accessible to UVS. For these reasons the UVS stellar occultation measurements, based on a point-source probe of the atmosphere independent of spatial resolution and regardless of distance to target, offer the most uniquely new information and are the priority technique to implement (especially for nightside constraints).

### 2.3.4 SWI Monitoring of Io in the Far-Infrared

Because the Submillimetre Wave Instrument (SWI; Hartogh et al. 2026, this collection) can use its own pointing mechanism (±72° and ±4.3°), the science operation plan includes daily Jovian moon monitoring operations, which will include Io observations. These observations will build on much previous ground-based work (millimeter-wavelength detection of $SO_2$/SO, Lellouch et al. 2003; of NaCl/KCl, Moullet et al. 2013; and of isotopologues, de Kleer et al. 2024), and SWI observations will cover various daytime and nighttime conditions over the course of the three-year Jupiter science phase. Varying with distance, a typical spatial resolution SWI can achieve is on the order of 800 and 1600 km in the 1200 and 600 GHz channels, respectively, allowing it to place several beams across the Io disk, albeit not resolving necessarily individual volcanoes. SWI's science goals for Io include (1) exploring Io's nightside atmosphere for the first time at submillimeter wavelengths (building upon de Pater et al. 2020), (2) investigating Io's atmospheric chemistry with a search for minor species, (3) determining and mapping the mean gas temperature and, if possible, the vertical structure (thermal profile, hydrostatic structure, plumes), and (4) measuring atmospheric dynamics from Doppler shifts (building upon Thelen et al. 2025). Model simulations indicate that daytime observations of Io will allow SWI to detect intrinsically weak $SO_2$ lines, which in combination with strong lines, will permit analyses to disentangle temperature and abundance effects. SWI will also measure and map volcanically-produced NaCl

and KCl, already detected from Earth. It will also yield determinations of the isotopic ratios in oxygen, sulfur and chlorine ($^{16}O/^{18}O$, $^{32}S/^{34}S$, $^{35}Cl/^{37}Cl$), which are diagnostic of the history of Io's volcanism. Depending on Io's atmospheric conditions, SWI may also observe as-yet undetected atmospheric species such as $O_2$, SiO, $S_2O$, CO, $H_2O$, $O_3$ and $H_2O_2$.

### 2.3.5 PEP Observations of the Particle Environment

The JUICE Particle Environment Package (PEP) experiment (Barabash et al. 2026, this collection) consists of six instruments that will investigate plasma ions and electrons, energetic particles, and thermal and energetic neutral particles. The Jupiter Neutrals Analyser (JNA) instrument records Energetic Neutral Atoms (ENAs) in the energy range between 10 eV and 3 keV. JNA measures the energy, the particle's arrival direction, and has mass resolution to distinguish the major species. ENAs are created through charge exchange processes between ions and neutral gas. In the charge exchange process, a plasma ion becomes neutralized forming an ENA, and the neutral gas atoms or molecules becomes ionized. The ENAs travel unhindered by the electromagnetic fields along ballistic trajectories, thus ENAs can be used for remote sensing of plasma populations (Wurz 2000).

Io's neutral clouds are thought to be the main source of plasma for the torus, which becomes ionized and supplies the plasma population in the Io torus. Futaana et al. (2015) have modeled the emission of S and O energetic neutral atoms (10 eV - 3 keV), resulting from the charge exchange of plasma from the plasma torus with Io's neutral clouds. This energy range includes the corotational plasma flow energy. The expected differential ENA flux at Ganymede orbit is in the range of $10^3$ to $10^5$ $cm^{-2}$ $s^{-1}$ $sr^{-1}$ $eV^{-1}$ near the energy of the corotation. It is above the detection level of the JNA instrument with integration times of 0.01 to 1 s. The ENA flux has strong asymmetry with respect to the phase of Io. Because of the wide energy range of JNA, the observations will exhibit periodicities that can be attributed to the Jovian magnetosphere rotation (time scale $\sim$10 h) and to the rotation of Io around Jupiter (time scale $\sim$50 h; considering Io's and the spacecraft's motion around Jupiter). The ENA energy spectra will exhibit dispersion signatures with a typical time scale of several hours, because of the non-negligible flight time of the ENAs from Io to the Ganymede orbit. From the JNA observations, several characteristic quantities of the Io plasma torus will be derived, such as the density, velocity, velocity distribution function, and composition of plasma torus ions. Plasma torus and neutral cloud observations through ENA measurements are discussed further in Masters et al. (2025, this collection).

Furthermore, Huybrighs et al. (2024) suggest that energetic protons with energies exceeding 155 keV will charge-exchange with Io's atmosphere, and produce Energetic Neutral Atoms (ENA) of such energies. These ENA emissions from Io's direct environment could potentially be detected remotely by the Jovian Energetic Neutral and Ions (JENI) detector part of PEP. Variations of keV ENA flux at Io could provide information about variations in the density of the neutral environment of Io, and thereby the production of plasma near Io. While the keV ENA's described in Futaana et al. (2015) will reach JUICE within a few hours, the $\sim$155 keV ENAs could reach JUICE in Ganymede orbit within just a few minutes, thereby providing a more instantaneous assessment of the neutral-ion interaction at Io.

## 3 Small Inner Moons

Four small inner moons of Jupiter are known. Their names, in order of distance from Jupiter, are Metis, Adrastea, Amalthea, and Thebe. Fig. 1 shows the orbits, Fig. 10 displays disk-resolved images from the *Voyager* and *Galileo* spacecraft, and Table 3 provides basic quantities on orbit and body properties. These objects differ significantly in size. Adrastea (mean

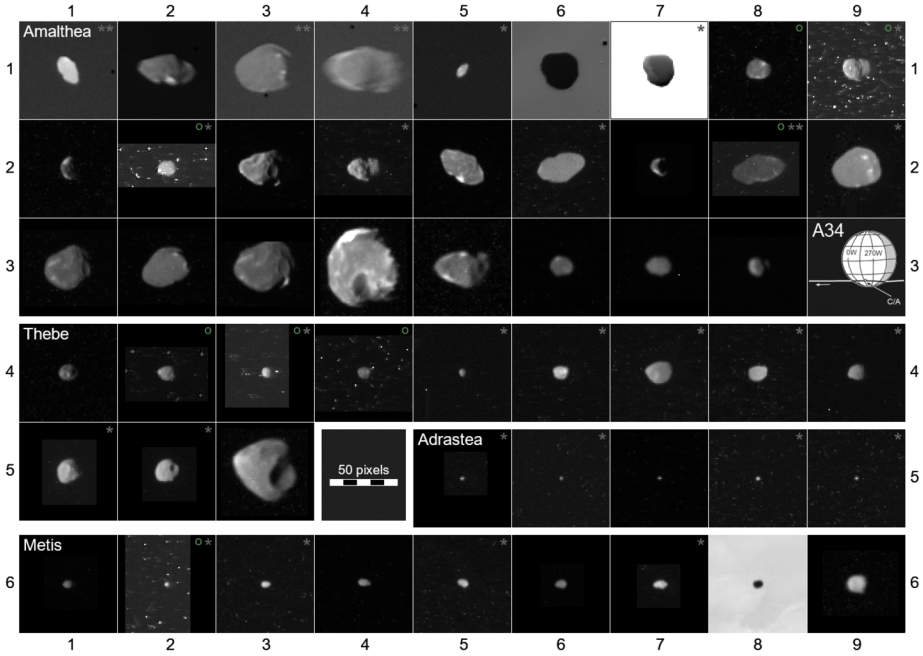


**Fig. 10** Inner Jovian moons disk-resolved image potpourri from *Voyager* (Vgr) and *Galileo* (GLL prime mission and GMM); ordered for each object by observation time. The images were retrieved from https://opus.pds-rings.seti.org.

• *Image content* (numbers in brackets point to rows and columns):
1st row – **Amalthea**: 4 Vgr-1 [1|1-4]; 3 Vgr-2 [1|5-7]; 2 GLL prime [1|8+9]
2nd row – **Amalthea**: 9 GLL prime [2|1-9]
3rd row – **Amalthea**: 8 GMM [3|1-8]; A34 flyby sketch [3|9]
4th row – **Thebe**: 9 GLL prime [4|1-9]
5th row – **Thebe**: 2 GLL prime [5|1+2], 1 GMM [5|3]. **Adrastea**: 5 GLL prime [5|5-9]
6th row – **Metis**: 8 GLL prime [6|1-8], 1 GMM [6|9]
Shown are cutouts of almost all *Galileo* clear and green filter raw images, and selected *Voyager* clear filter raw images. Each box is a 72×72 pixels cutout from the original raw data (800×800 pixels for both cameras), with the original camera orientation retained (i.e., no rotations to align spin axes). The scale bar in panel [5|4] indicates 5×10 pixels. The geometric pixel scale for the *Galileo* SSI and the *Voyager* Narrow Angle Camera (NAC) images is 1 km at a distance of 100,000 km. Black spots in Voyager images are reseau marks.

• *Contrast enhancement and camera filters:* Original image depth was 8 bit (256 gray values). Not enhanced are 25 images (DN values "0-255" preserved), 23 are linearly enhanced by a factor of 2 (marked by a '*'; cut at DN 127), four are enhanced threefold (marked with '**'; cut at DN 85). *Galileo* green-filter images are marked with 'o'; all others are clear filter.

• *Image geometry notes:*
- *Closest distances:* The highest-resolved views of Metis, Amalthea and Thebe from *Galileo* orbit 26 on 04 Jan 2000 show the anti-Jupiter hemispheres of these moons. **Amalthea**: panel [3|4], 237,800 km distance, 2.4 km/px pixel scale, 60° phase, sub-spacecraft longitude 164°W. **Thebe**: panel [5|3], 192,800 km, 1.9 km/px, 59°, 167°W. **Metis**: panel [6|9], 292,600 km, 3 km/px, 54°, 158°W. For these three images, north is approximately down.
- *Solar phase:* Four observations of **Amalthea** have been taken at very low phase: Vgr-1 image at panel [1|1] (0.8°); *Galileo* images in panels [2|6] (4.0°), [2|8] (0.7°), and [2|9] (3.6°). Lowest phase for **Adrastea** was 2.5° [5|7], for **Thebe** 3.0° [4|8], for **Metis** 12° [6|5].
- *Satellite in front of Jupiter:* **Amalthea** from Vgr-2 (panels [1|6] and [1|7]; these images were taken just a few minutes apart with different exp. times); **Metis** from *Galileo* [6|8].
- *Prominent crater on **Thebe**:* The ∼40-km sized crater very well visible in about half of the Thebe images has been named Zethus (https://planetarynames.wr.usgs.gov/Page/THEBE/target).

**Fig. 10** (*Continued*)
• *Image identification* (Column in figure; Image ID; Voyager spacecraft or Galileo orbit):
- 1st row (**Amalthea**): 1: C1636914, Vgr1; 2: C1637736, Vgr1; 3: C1638131, Vgr1; 4: C1638537, Vgr1; 5: C2058954, Vgr2; 6: C2065532, Vgr2; 7: C2065534, Vgr2; 8: C0360025813R, G2; 9: C0368495813R, C3.
- 2nd row (**Amalthea**): 1: C0368603500R, C3; 2: C0374546001R, E4; 3: C0383748201R, E6; 4: C0401703400R, C9; 5: C0401762600R, C9; 6: C0401784900R, C9; 7: C0413581201R, C10; 8: C0420626379R, E11; 9: C0420652501R, E11.
- 3rd row (**Amalthea**): 1: C0512324201R, C22; 2: C0512335101R, C22; 3: C0527365602R, I25; 4: C0532888101R, E26; 5: C0625614501R, I32; 6: C0625709201R, I32; 7: C0639004613R, I33; 8: C0639056513R, I33; 9: A34 flyby geometry sketch.
- 4th row (**Thebe**): 1: C0368591600R, C3; 2: C0374551614R, E4; 3: C0383612834R, E6; 4: C0389705614R, G7; 5: C0401604400R, C9; 6: C0401718500R, C9; 7: C0401759200R, C9; 8: C0401787200R, C9; 9: C0413711201R, C10.
- 5th row (**Thebe** and **Adrastea**): 1: C0420691701R, E11; 2: C0420703301R, E11; 3: C0532888401R, E26; 4: Scale bar; 5: C0374674101R, E4; 6: C0401718000R, C9; 7: C0401749000R, C9; 8: C0401764300R, C9; 9: C0401776900R, C9.
- 6th row (**Metis**): 1: C0394682801R, G8; 2: C0401639113R, C9; 3: C0401751800R, C9; 4: C0401773600R, C9; 5: C0401786800R, C9; 6: C0420681401R, E11; 7: C0420685801R, E11; 8: C0420722500R+501R, E11; 9: C0532890501R, E26

diameter ∼16 km) is smallest, followed by Metis (∼43 km), Thebe (∼99 km), and Amalthea (∼167 km). Amalthea is the largest Jovian moon after the Galilean satellites (of which Europa, with a diameter of 3121 km is the smallest). Interestingly, there are no "mid-sized" moons with diameters of ∼400 to 1700 km orbiting Jupiter, as is the case at Saturn and Uranus.

All four small inner moons rotate synchronously. The distances of innermost moons Metis and Adrastea to the Jovian cloud deck are just 0.8 Jupiter radii. Their orbit periods (∼7 h) are faster than the rotation period of Jupiter (9.9 h); thus, they orbit Jupiter within the "geosynchronous" orbit. During one Jupiter revolution around the Sun, Metis fulfills ∼14,700 orbits around Jupiter. During each orbit, it moves through Jupiter's shadow for about 68 min. Outermost Thebe revolves Jupiter ∼6430 times during one Jupiter year. The inner moons are located deep within the Jovian radiation belts and gravity funnel. The resulting extreme particle bombardements, impact and escape velocities, and fictitious forces potentially acting on the surfaces have significant effects on the surface chemistry and physics. The inner moons are also producing the Jovian rings (e.g., Ockert-Bell et al. 1999).

The *Voyager* ISS cameras (Smith et al. 1977) and the *Galileo* SSI camera (Belton et al. 1992) provided the majority of our knowledge of the small inner moons from distant observations while the objects were just barely spatially resolved (Fig. 10). In the images of Amalthea and Thebe, some impact craters and bright spots could be identified. The *Galileo* spacecraft performed a targeted flyby at Amalthea on 05 Nov 2002 (Bindschadler et al. 2003), allowing for mass and density measurements of this moon (Anderson et al. 2005), but no imaging was possible. Observations from the ground or from space observatories also provided valuable information, especially when observing in the near IR at wavelengths of a methane band at 2.2 μm where Jupiter appears very dark and thus its otherwise severe straylight is limited.

## 3.1 Inner Moons' Discoveries and Spacecraft Observations

### 3.1.1 Discoveries

Amalthea was discovered in the late 19th century, which represented somewhat of a surprise at this time. While smaller and smaller moons had been discovered at Mars (2 moons),

**Table 3** Basic properties of Jupiter's small inner moons

| | Metis | Adrastea | Amalthea | Thebe | |
|---|---|---|---|---|---|
| Provisional desig. | S/1979 J 3 | S/1979 J 1 | — | S/1979 J 2 | |
| IAU designation | J XVI | J XV | J V | J XIV | |
| JPL/SPICE ID | 516 | 515 | 505 | 514 | |
| Announced | 26 Aug 1980 | 23 Nov 1979 | 11 Sep 1892 | 28 Apr 1980 | |
| **ORBIT** | | | | | |
| $a$ | 127,980 | 128,981 | 181,366 | 221,889 | km |
| | 1.790 | 1.804 | 2.537 | 3.104 | $R_J$ |
| $e$ | 0.0002 | 0.0015 | 0.0032 | 0.0175 | |
| $i$ | 0.06 | 0.03 | 0.37 | 1.08 | ° |
| $\omega$ | 1221.2547 | 1206.9987 | 722.6315 | 533.7004 | °/d |
| $P$ | 7.075 | 7.158 | 11.956 | 16.188 | h |
| $v_{Orb}$ | 31.5 | 31.5 | 26.6 | 23.9 | km/s |
| **BODY** | | | | | |
| $V$ (0.55 µm) | 17.5 | 18.7 | 14.1 | 16.0 | mag |
| $K$ (2.2 µm) | 14.3 | 16.4 | 12.2 | 13.3 | mag |
| Geometric albedo | 0.063 | ~0.1 | 0.091 | 0.049 | |
| Abs. magnitude $H$ | 10.5 | ~12.1 | 7.2 | 9.0 | mag |
| Mean size | $43 \pm > 3$ | 16 | $167 \pm$ ~2.5 | $99 \pm$ ~3 | km |
| Radii | 30×20×17 | 10×8×7 | 126×73×63 | 58×49×42 | km |
| $a/c$ | 1.76 | 1.4 | 2.00 | 1.38 | |
| Surface area | 6080 | ~870 | 97,300 | 31,700 | $km^2$ |
| Volume | 41,300 | ~2350 | 2,434,000 | 505,000 | $km^3$ |
| Mass | | | $2.08 \pm 0.15 \times 10^{18}$ | | kg |
| Mean density | | | $0.857 \pm 0.099$ | | $g/cm^3$ |
| Average slope | 9 | | 10 | 7 | ° |
| Escape speed | <0...20 | 0...8 | 5...75 | 30...55 | m/s |
| Abbr. (TD) | Met | Adr | Ama | The | |

*Notes:*

• For details on discoveries, see text. Orbital elements $a$, $e$, $i$ are semi-major axis, eccentricity, and inclination (with respect to Jupiter's equator), from Porco et al. (2003) for Metis and Adrastea and from Cooper et al. (2006) for Amalthea and Thebe. $\omega$ is the mean daily angular motion (Archinal et al. 2018), $P$ is the orbit period and the rotation period (derived from $\omega$), $v_{Orb}$ the mean orbit velocity around Jupiter (derived from $Gm_J$ and $a$).

• Apparent visual magnitudes $V$ (for ground-based observers at opposition) are from Burns (1986); $K$ magnitudes from Neugebauer et al. (1981) for Amalthea, for the other moons from de Pater et al. (1999; for a 2.19-2.35 µm filter); geometric albedo (global average, Galileo SSI clear filter at 0.64 µm) from Thomas et al. (1998); absolute visual magnitudes $H$ are calculated from mean sizes and albedos.

• 'Mean size' is the average diameter (Thomas et al. 1998).

• 'Radii' are the semi-axes of a reference ellipsoid based on the volume of the shape model (Thomas et al. 1998; with minor updates including later Galileo SSI data, reprocessed for this paper); the largest number represents the axis pointing toward Jupiter, the middle number gives the axis in moving direction, and the smallest the pole-axis direction; uncertainties are approximately ±2-3 km. $a/c$ is the ratio of the largest to the shortest axis.

• Surface areas and volumes are from the shape models except for Adrastea where they are calculated from the radii. The mass and bulk density of Amalthea are from Anderson et al. (2005), the others are unknown.

• 'Average Slope' is the average macroscopic slope on the surface. Except for Thebe, the escape speeds might reach zero at some parts of the surfaces (assuming densities of ~0.9 $g/cm^3$).

**Table 3** (*Continued*)

• 'Abbr. (TD)' is a 3-characters abbreviation (T. Denk scheme for outer Solar System moon names: https://tilmanndenk.de/wp-content/uploads/Moons_TDAbbrevs_JPL-ID.txt).
• The "geosynchronous" orbit of Jupiter is located in between Adrastea and Amalthea at a semi-major axis of 2.24 $R_J$ (hypothetical satellite velocity: 28.1 km/s). The Roche limit for fluid satellites is at ∼2.7 $R_J$. For rigid objects, it is at Metis' orbit for an object density of ∼0.46 g/cm$^3$.

Saturn (8), Uranus (4), and Neptune (1) in the 17th, 18th, and 19th centuries (5, 4, and 6 objects, respectively), the four Galilean moons remained the only known Jovian companions for 282 years. Finally, during a dedicated search on the night from 09 to 10 Sep 1892, Edward E. Barnard discovered from Lick Observatory (on Mt. Hamilton in California) a fifth Jovian satellite which he could track for 2.5 h before it got lost in the glare of Jupiter (Barnard 1892; Fig. 11a; see also Cruikshank 1982 or Sheehan 1995 for many details). After the following night, when he recognized the object again on the eastern side of Jupiter, the news was announced to the public. This was the last discovery of a moon with the observer still sitting or standing directly at the telescope and examining the sky through an eyepiece with his naked eye.

The new object received the official designation 'Jupiter V'. Shortly after discovery, French astronomer Camille Flammarion proposed the name Amalthea (Flammarion 1893). Despite refusal by Barnard, this name was in unofficial use for a long time until officially named so in 1975.[22] In 1909, after 16.4 years of observations, Barnard published a value for Amalthea's orbit period (11 h 57 m 22.6708 s; Barnard 1909) that deviates from the modern values of Cooper et al. (2006) or Archinal et al. (2018) by less than 20 ms. In this paper, he also notes a hemispheric variation on the surface by stating his impression that Amalthea "is certainly brighter on the following side of Jupiter than on the preceding side" (meaning: Amalthea's leading hemisphere appears brighter than its trailing side).

The other three discoveries succeeded with imaging data from the *Voyager 1* and *2* spacecraft taken in 1979, although not immediately when the images became available. Adrastea (1979 J 1) was spotted first by astronomers David Jewitt and Edward Danielson in a *Voyager-2* 15-sec exposure Wide Angle Camera (WAC) image as a point source (Fig. 11b right) and in a preceeding 96-sec exposure Narrow Angle Camera (NAC) image as a smeared trail (Fig. 11b left), both taken within 5 minutes on 08 Jul 1979, 23 hours before Jupiter closest approach (Jewitt et al. 1979). This was the first ever discovery of a moon by a spacecraft.[23]

Thebe (1979 J 2), discovered by Stephen Synnott from the *Voyager* Navigation Team, has been announced on 28 Apr 1980.[24] Its ∼10 pixels wide shadow moving over the planet's cloud top was recognized in *Voyager-1* WAC images obtained on 05 Mar 1979 about 4.5 h before closest approach to Jupiter (Fig. 11c). A subsequent detailed search revealed images from both *Voyager* probes of the object itself while transiting Jupiter (Synnott 1980).

Finally, again by Stephen Synnott, Metis (1979 J 3) and its shadow have been identified in *Voyager-1* images (Fig. 11d) as a second object on an orbit very close to Adrastea and

[22] IAU circ. no. 2846 (07 Oct 1975): Satellites of Jupiter (JV - JXIII) naming. http://www.cbat.eps.harvard.edu/iauc/02800/02846.html.

[23] Publication date of Jewitt et al. (1979) (discovery of 1979 J 1, later named Adrastea) in *Science* was 23 Nov 1979.

[24] IAU circ. no. 3470 (28 Apr 1980): Satellites of Jupiter. (Discovery of 1979 J 2, later named Thebe.) http://www.cbat.eps.harvard.edu/iauc/03400/03470.html.

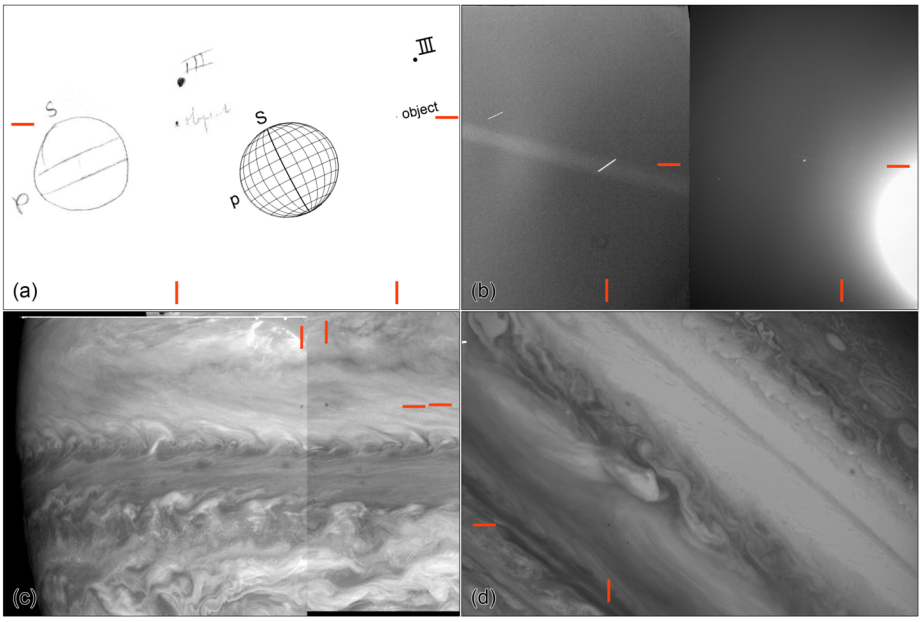


**Fig. 11** Discovery images of the small inner Jovian moons. The red bars on the edges of each panel point to the objects.
(a) **Amalthea** — the sketch drawing (at left) by E. Barnard in the discovery night shows Jupiter, Ganymede (III), and the new object; the plot (at right) shows the geometry 13 minutes past midnight, based on modern ephemerides.[¶]
(b) **Adrastea** (1979 J 1) — *Right: Voyager 2* WAC frame FDS 20630.53; 15.36 s exposure; 08 Jul 1979 23:36:31 UTC. The very faint Jovian ring is also visible as a thin, not exactly horizontal line. Jupiter's limb is less than 1° off the right image edge, Ganymede is less than 3° away from the left edge. The brighter dot in the image center is a background star ($\rho$ Leo; $V \sim 3.9$). *Left: Voyager 2* NAC frame FDS 20630.48; 96 s exposure, taken 5 minutes earlier, strongly contrast enhanced. The ring, Adrastea, and the stars appear smeared due to spacecraft motion. Note the different length and direction of the Adrastea trail compared to the star trails.
(c) **Thebe** (1979 J 2) — the mosaic of *Voyager 1* WAC frames FDS 16383.50 (in front; 05 Mar 1979 07:36:36 UTC) and 16383.54 (taken 3:12 minutes later) shows the motion of Thebe's shadow on the Jovian cloud deck.
(d) **Metis** (1979 J 3) — this *Voyager 1* WAC frame (FDS 16364.13; 04 Mar 1979 15:55:48 UTC) is the last in a row of seven images showing Metis and its shadow moving in front of Jupiter's cloud surface.
The *Voyager* images are calibrated versions retrieved from the Planetary Data System (PDS).[♯] The Adrastea and Metis images are slightly cropped from their originally squared format.[§]
*Notes:*
[¶] Generated with https://pds-rings.seti.org/tools/ for epoch 10 Sep 1892 08:13 UTC.
[♯] https://opus.pds-rings.seti.org/
[§] Field of Views (FOV) of the Voyager cameras: WAC 3.2°; NAC 25.8' (Smith et al. 1977)

announced on 26 Aug 1980.[25] Originally, it had been mis-identified in IAU circ. 3470 as being 1979 J 1, but since it was later found in an image at a time where 1979 J 1 should have been occulted by Jupiter, it was recognized to be another moon with a very similar orbit (Synnott 1981).

[25] IAU circ. no. 3507 (26 Aug 1980): Satellites of Jupiter. (Discovery of 1979 J 3, later named Metis.) http://www.cbat.eps.harvard.edu/iauc/03500/03507.html.

**Table 4** Overview of spacecraft closest approach distances to the small inner moons

| Spacecraft | Date | Metis | Adrastea | Amalthea | Thebe |
|---|---|---|---|---|---|
| *Voyager 1* | Mar 1979 | 355,400 | 230,900 | 421,000 | 130,300 |
| *Voyager 2* | Jul 1979 | 619,600 | 599,300 | 558,100 | 639,500 |
| *Galileo* JOI | Dec 1995 | 267,600 | 252,800 | 334,600 | 390,400 |
| *Galileo* prime | 1996-1997 | 521,800 | 518,100 | 460,300 | 436,800 |
| *GMM* E26 | Jan 2000 | 285,400 | 284,600 | 232,500 | 188,200 |
| A34 | Nov 2002 | 51,570 | 50,010 | 249 | 49,850 |
| *Cassini* | Dec 2000 | 9,666,000 | 9,665,000 | 9,614,000 | 9,570,000 |
| *New Horizons* | Feb 2007 | 2,180,000 | 2,179,000 | 2,142,000 | 2,149,000 |
| *Juno* | 2016-2025 | 38,860 | 33,510 | 59,350 | 32,780 |
| JUICE | 2031-2034 | 548,500 | 545,300 | 498,600 | 446,000 |

*Notes:* In units of km. *Galileo* values are for the arrival day (day of Jupiter Orbit Insertion), the prime mission, *GMM* orbit E26, and the Amalthea targeted flyby (A34). Data derived from JPL's SSD HORIZONS website (https://ssd.jpl.nasa.gov/horizons/app.html). JUICE values are for orbit tour CReMA_5_0.

The discovery images of Adrastea, Thebe, and Metis shown in Fig. 11 are reprocessed versions. Names and permanent IAU designations of the small inner moons discovered in *Voyager* images were announced in 1983.[26] Note there exist three Main Belt Asteroids with same names as the inner Jovian moons: (9) Metis, (239) Adrastea, and (113) Amalthea.

### 3.1.2 Spacecraft Observations

Various spacecraft have visited Jupiter in the past, or, as is the case for *Juno* (Bolton et al. 2017), are visiting at the time of this writing. So far, the *Galileo* orbiter performed the only targeted flyby of one of the inner moons. On 05 Nov 2002 06:18:41 UTC, *Galileo* came within 250 km to Amalthea's center of mass and passed over the southern side and inside the orbit at a relative velocity of 18.4 km/s on the inbound leg of its trajectory before reaching perijove (Fieseler et al. 2004). During the flyby, which was dubbed "A34", the spacecraft performed field-and-particle measurements, with its path being tracked precisely to determine the mass of Amalthea. Because the activities of the remote sensing instruments had been terminated on January 2002, no pictures or spectra have been obtained during the Amalthea flyby. The spacecraft went into safe mode 16 minutes after Amalthea closest approach (Bindschadler et al. 2003), which fortunately did not affect the Amalthea science. No other close flyby of a small inner Jovian moon has since been performed or is announced for upcoming missions.

All other spacecraft observations of the Jovian small inner moons were performed from larger range. Table 4 gives an overview of closest approach distances. First dedicated observations were planned and executed for Amalthea by the two *Voyager* spacecraft. *Voyager* images of Jupiter or the rings led to the discovery of the three other inner moons. The *Galileo* spacecraft performed an observation campaign during the primary mission in 1996 and 1997 where all four small inner moons were aimed at during eight of the eleven orbits.

[26] IAU circ. no. 3872 (30 Sep 1983): Satellites of Jupiter and Saturn. (Naming of inner moons Metis, Adrastea, Thebe.) http://www.cbat.eps.harvard.edu/iauc/03800/03872.html.

The total number of images[27] was unfortunately very limited because of the unavailability of the spacecraft's high-gain antenna (O'Neil et al. 1993). During the *Galileo* Europa Mission (GEM), the first mission extension from end of 1997 to early 1999, no further small-moon pictures were taken. With the perijove reduction toward Io in the second extended mission phase named *Galileo* Millenium Mission (GMM), the *Galileo* spacecraft came closer than ever to these moons, and again obtained images on a few occasions. On 04 Jan 2000 (orbit E26), the best-resolved images to date of Thebe, Amalthea, and Metis were taken while *Galileo* came closest to these objects (Table 4; panels [5|3], [3|4], and [6|9] in Fig. 10).

The *Cassini* spacecraft passed the Jovian system at a rather remote distance of 10 Gm. The innermost moons Metis and Adrastea were observed to determine the orbit inclinations, the relation of these two objects to the Jovian main rings, and for a moon search (Porco et al. 2003). *New Horizons*, en route to Pluto, took advantage of Jupiter's huge mass for performing a gravity assist at 2.3 Gm range, and also searched for moons and studied the main ring (Showalter et al. 2007; see Sect. 3.2.3 for a short review of these search campaigns).

The *Juno* spacecraft is the second Jupiter orbiter, arrival was in July 2016. During the extended mission (since mid-2021) with close flybys of the Galilean moons Ganymede, Europa, and Io, the perijove point shifted so that the spacecraft is also passing the small inner moons repeatedly at ranges below 100,000 km (Table 4). Since the imagers onboard *Juno* are wide-angle devices,[28] spatial resolution of potential images taken at nearest distances would be comparable to the *Galileo* images taken in the prime mission (Fig. 10). However, the small inner moons could not be observed because *Juno* is a power-optimized spinning spacecraft, and any deviation from the regular attitude (solar arrays pointing to the Sun) requires very strong science or engineering cases. From greater distances, Amalthea has been imaged over the Jovian cloud deck as a tiny dark spot.[29]

## 3.2 Review of Knowledge

This section provides an overview of the knowledge that has been gained about the small inner moons to date. Far more is known about Amalthea than about the other three moons, warranting to give it an own sub-section. In the middle part, the physical and orbital properties of all four inner Jovian moons are described in detail. The section concludes with a description of the numerous attempts to discover more ring moons. The three sub-sections are largely organized chronologically. Such a structure makes it possible to follow the development of the discoveries. It also allows older papers to be cited which were significant in their time but have since been replaced by more recent research results.

### 3.2.1 Amalthea

Among the four small inner Jovian moons, the most knowledge was gained about Amalthea. The major discoveries stem from data of the two *Voyager* spacecraft in 1979 and of the

[27] Observations of the small inner moons by *Galileo*'s near-IR spectrometer NIMS to obtain spectra have been performed as well, but the objects were too faint to show any useful signal in the data.

[28] Instantaneous Field of View (IFOV) of imaging devices of Jupiter missions (in µrad/pix) (with 1 µrad = 0.206"): *Voyager* NAC and WAC: 9.25 and 69.4 ("angle subtended by scan line"); *Galileo* SSI: 10.16; *Cassini* NAC and WAC: 5.99 and 59.75; *New Horizons* LORRI: 4.95; *Juno* JIRAM: 238; JunoCam: 673; JUICE JANUS: 15; JUICE MAJIS: 150 (Smith et al. 1977; Belton et al. 1992; Porco et al. 2004; Cheng et al. 2008; Tosi et al. 2024a; Hansen et al. 2017; Palumbo et al. 2025; Poulet et al. 2024, respectively). For comparison: The telescope used by Galileo Galilei to discover the Galilean moons had a resolving power of ∼50 µrad (Greco et al. 1993).

[29] Amalthea in front of Jupiter on 07 Mar 2024: https://web.archive.org/web/20250408074126/https://photojournal.jpl.nasa.gov/catalog/PIA25728.

*Galileo* spacecraft between 1996 and 2003, which have provided disk-resolved views (upper half of Fig. 10) and a targeted flyby. Fundamental information from the initial *Voyager-1* imaging team report (Smith et al. 1979a) included values for the $a$ and $c$ axes (longest and polar axes) of the object, a very low average geometric albedo of ∼0.04 to 0.06, a very reddish surface color, and that there are bright areas with albedos up to ∼0.15 that are less reddish. Suspected synchronous rotation has been confirmed, with the long axis pointing toward Jupiter, as expected. The images showed the leading, trailing, and anti-Jupiter side of Amalthea at spatial resolutions up to ∼8 km/lp (line pair). *Voyager-2* imaging three months later (Smith et al. 1979b) provided information on the $b$ axis dimension from data showing Amalthea in transit above the Jovian clouds; the Amalthea size was at that time determined to 270 × 170 × 155 km (accuracy about ±15 km). Closest approach distances are given in Table 4.

A major analysis of the *Voyager* Amalthea data was published by Veverka et al. (1981), investigating images at phase angles between 0.8° and 42°. They again emphasized the very irregular shape of the object and noted that it could not be approximated very well by a triaxial ellipsoid. The surface gravity was estimated to ∼1% of Earth's. The mean opposition magnitude (in the *Voyager* NAC clear filter) was determined to 14.1 mag. Before that, only Millis (1978) had published photoelectric measurements of Amalthea's apparent magnitude near western elongation ($V = +14.1 \pm 0.2$ mag) – all preceding brightness estimates had been guesses. For example, E. Barnard estimated ∼13 mag (Barnard 1892), as did an overview chapter on photometry of planets and satellites by Harris (1961) many decades later. From the *Voyager* data, Veverka et al. (1981) determined the normal reflectance of Amalthea to very low ∼5-6% and concluded that Amalthea is a very dark body, confirming a similar conclusion from ground-based thermal measurements in 1974 (Rieke 1975). The disk-integrated linear phase coefficient (*Voyager* 'clear' filter) for the solar-phase angle range of 0.8° to 42° was measured to 0.042±0.004 mag/deg. The color was confirmed to be "very red" in the spectral range the *Voyager* cameras could observe the object ('violet' to 'orange'; 410-590 nm), being redder than typical Trojans and planet Mars, but less red than Io. The Amalthea trailing side was also found to be somewhat redder than the leading side. It was suggested by Gradie et al. (1980) and by Veverka et al. (1981) that contamination of the surface by sulfur is a likely cause, with material from the Io volcanoes as the potential source. Gradie et al. (1980) suggested that the Amalthea surface was highly modified by high-velocity impacts and by the interaction with ions of the Jovian magnetosphere. Charged particles from the Jovian magnetosphere, exogenic contaminants such as sulfur from Io, and high-velocity micrometeoritic matter combined should have darkened, reddened, and altered Amalthea's surface.

Among geologic landforms, Veverka et al. (1981) noted large craters, sharp ridges, "bright markings", plus other unspecified "prominent" topography. The bright spots appeared significantly brighter than the dark surrounding area and showed a less red color. The largest craters were named Pan and Gaea; they are located on the northern sub-Jovian leading hemisphere and near the south pole, are ∼90 and 75 km wide, and ∼10-20 km deep. At least five more potential craters of sizes ∼20 to ∼40 km have been discerned, and the crater production rate was estimated to be ∼10-40 times that of Callisto. Despite the extremely high estimated velocity of impactor projectiles (∼38 km/s; Smith et al. 1979b), Veverka et al. (1981) suggest that all impact debris should have been reaccreted, possibly forming a regolith cover (debris mantle) of ∼1-3 km thickness. They also note that the bright markings occur on local slopes like crater walls or ridges and suggest that these represent exposures of fresher materials at locations where downslope movement is effective. This is particularly notable in light of later *Cassini* images of Saturnian moon Phoebe where

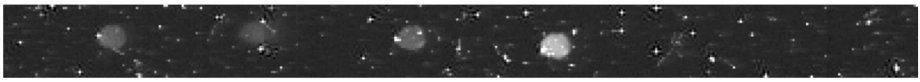

**Fig. 12** *Galileo*-SSI color "on-chip" mosaic of Amalthea (C0374546001; orbit E4) illustrates the effect of high-energy radiation for image quality over about half a minute residence time. Images in four different color filters (from right to left: green, violet, 1-micron, methane-889) have been taken before the CCD was read out. The respective times in the image labels are (seconds after 1996-12-18T07:13:00 UTC): 07.847; 16.614; 25.414; 34.081. The subsequent CCD readout added a few more seconds. Spacecraft-Jupiter distance was 1.23 Gm

exactly this phenomenon has been seen (e.g., Porco et al. 2005). With respect to the question of Amalthea's formation, Veverka et al. (1981) could not give a definitive answer, but suggested the object's bulk density as a major criterion.

More disk-resolved images of Amalthea have been provided by the *Galileo* spacecraft between 1996 and 2001. Despite the spacecraft's high-gain antenna anomaly (O'Neil et al. 1993), a small fraction of the strictly budgeted data volume was assigned to the small inner moons, providing additional views of Amalthea (Fig. 10; Carr et al. 1995). Major analyses of the imaging data taken during the *Galileo* prime mission were published by Thomas et al. (1998) and Simonelli et al. (2000). While Thomas et al. (1998) used data until *Galileo*'s 9th perijove passage (G2 to C9; last two panels in top row and 1st to 6th panel in 2nd row of Fig. 10) plus some *Voyager-1* images for a geology-oriented interpretation of the data, Simonelli et al. (2000) used about a dozen *Voyager* pictures and almost all *Galileo* prime-mission images, and concentrated on photometric properties. Although the observation distances were comparable, the *Galileo* images showed more details than previous *Voyager* images with respect to shape, color, or photometric properties. Thomas et al. (1998) produced a new shape model and revised the dimensions of the prime axes (250 × 146 × 128 km; uncertainty ∼4 km). The model implied that Amalthea shows no bifurcated or contact-binary shape. The albedo (in the *Galileo* SSI "clear" filter) was determined to 0.091±0.0082, with the leading side being ∼1.25x brighter than the trailing side (thus confirming the impression of E. Barnard a century before). The bright spots appear as rather small patches or ridges, but with a significant albedo contrast >2:1. The reddish slope of the spectrum is found throughout the whole SSI wavelength range from 0.4 to 0.9 μm, with a possible absorption at 1.0 μm. The colors of bright spots appear slightly less red compared to their dark surroundings. In the short wavelength range (violet-to-green filter ratios), the trailing side is redder than the leading side. However, the color measurements from *Galileo* SSI camera data have some uncertainties because of the need to use the "on-chip mosaic" technique during data acquisition to preserve tape-recorder space (Carr et al. 1995; Klaasen et al. 1999). Here, multiple exposures in different filters have been placed on different parts of the CCD with the side effect of a long residence time on the detector and thus a large "pollution" by high-energy electron and proton hits. Fig. 12 shows an example.

Thomas et al. (1998) confirmed that the Amalthea surface is highly cratered, likely near equilibrium (saturation) for crater diameters >35 km. Impact craters and the bright albedo spots are the major geologic landforms. Because the *Galileo* spacecraft never left the Jovian equatorial plane, the polar regions of the small inner moons were only viewed at high emission angles and we do not really know how they look like. The depth of the largest crater Pan was measured to be at least 8 km, the diameter as 89±4 km. This is even larger than the mean radius of Amalthea (83.5±2 km). Five more craters were identified with diameters larger than half of the moon's mean radius. No crater ejecta and no color units were identified.

Burns et al. (2004) gave descriptions on the *Galileo* observations of Amalthea during the GMM not covered in other publications before. They emphasize that Amalthea's surface exhibits a complex appearance including ridges, large and small craters, and albedo splotches. The latter show a high contrast and are found along rims of craters like Gaea and Pan. Intriguingly, in the highest resolved image from orbit E26 (panel [3|4] in Fig. 10), the bright terrain at Gaea is even greatly overexposed. In the same picture, a "saw-tooth" shape of Amalthea's terminator is considered indicative for a very rough surface with many small hills and valleys. Ida Facula, originally known from Voyager images (panel [1|3]), was identified as a ∼50-km long bright streak in GMM images (panels [3|1] and [3|3]) and might mark the crest of a local ridge. Downslope motion of loose debris, exposing brighter material from below, is considered as a formation process.

Simonelli et al. (2000) performed photometric studies and produced a clear-filter albedo map of Amalthea using *Galileo* data until orbit E11. Images taken at low solar phase angles up to 10° were used for the albedo map, and images up to 56° phase plus *Voyager* images for photometry. From modelling the photometric behavior with the Hapke function, the geometric albedo (*Galileo* SSI clear filter) of Amalthea was determined to 0.090±0.005, and the phase coefficient to 0.034±0.004 mag/deg (for solar phase angle range 15°-30°). According to the modelling, the Amalthea regolith appears relatively smooth and strongly backscattering. In the albedo map, most of the clear-filter normal reflectances lie between 0.07 and 0.12. The brightest albedo spot on Amalthea was found inside crater Gaea near the south pole, with a (clear filter) albedo of >0.25. Almost as bright are the high albedo areas inside largest crater Pan. The map shows again that the leading side of Amalthea is by about 25% brighter than the trailing side.

From gravity measurements during the targeted "A34" flyby, Anderson et al. (2005) determined the mass of Amalthea (via $Gm_{Ama} = 0.139\pm0.010$ km$^3$/s$^2$) to $m_{Ama} = (2.08\pm0.15)\cdot10^{18}$ kg. Combined with the volume estimate by Thomas et al. (1998) ($V_{Ama} = (2.43\pm0.22)\cdot10^6$ km$^3$), a surprisingly low bulk density of $\rho_{Ama} = 0.857\pm0.099$ g/cm$^3$ was found. According to Anderson et al. (2005), this low number results from a relatively low-density material and from bulk porosity. Water ice could be a major constituent of Amalthea, but given very high porosities of some other small objects, the uncertainty of the mean density, and the presence of non-water-ice materials in the system, the amount is very uncertain.

The absence of absorption features near the one- and two-micron wavelength region of Amalthea's spectrum in Mauna Kea IRTF (Infrared Telescope Facility) data from 1980 was originally interpreted as being inconsistent with water, ammonia, or methane frosts (Neugebauer et al. 1981). On the other hand, the discovery of a deep 3-μm absorption feature by Subaru and IRTF data obtained between 2002 and 2004, and by Keck-telescope NIRSPEC data from December 2002, was considered strongly supportive for the existence of $H_2O$ in some form on Amalthea (Takato et al. 2004; Wong et al. 2006). The requirements of water ice as a major constituent of Amalthea (inferred by the gravity measurements) and of hydrous minerals as products of a low-temperature environment (implicated by IR spectra), pose a big challenge to formation hypotheses. In the first reviews of *Voyager* results from Jupiter and Saturnian satellites, Pollack and Fanale (1982) and Morrison (1982) speculated that Amalthea should be composed of refractory material that was able to survive formation so close to Jupiter. This is currently not a likely option anymore (Anderson et al. 2005).

From the shape model, the escape velocity off the surface into a Jupiter orbit varies widely between almost zero and ∼75 m/s. The location of some of the prominent bright spots on the antijovian end of Amalthea might be consistent with very low gravity and a possibly enhanced removal of materials, exposing brighter underlying ice. Models of local topography, slope, surface acceleration ("gravity"; includes tidal and rotational effects, see

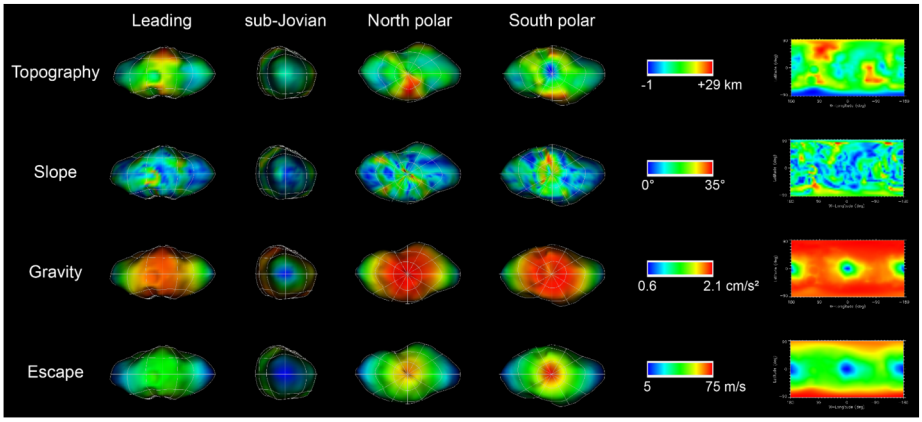


**Fig. 13** Amalthea models of local topography, slope, gravity (surface acceleration), and escape speed. Updated from models of Thomas et al. (1998), now including *Galileo* GMM data. The axes dimensions are 251 × 147 × 126 km. Jupiter is towards right for all views except sub-Jovian (2nd column) where Jupiter is towards the reader

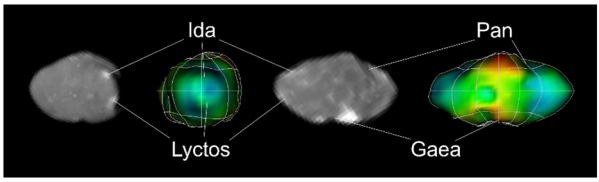


**Fig. 14** Locations of named craters (Pan, Gaea) and faculae[¶] (Ida, Lyctos) on Amalthea.
Equatorial views, north is up. Ida and Lyctos are near 175°W longitude, i.e., close to the center of the anti-Jupiter hemisphere. Pan is located at mid northern latitudes (∼55°N) at the sub-Jupiter side, Gaea is close to Amalthea's south pole. Several of the subtle small spots visible in the images are likely not real surface features, but result from cosmic ray hits. For the scale of the topographic maps (color coded), see Fig. 13. The names' theme of Amalthea surface features is from Greek mythology.[♯]
*Image identification and details:*
*Left:* From Galileo SSI; ID: C0512335101R; observation date: 12 Aug 1999; orbit C22; image scale: ∼5 km/px; solar phase: 16°; sub-observer longitude: 215°W; panel [3;2] in Fig. 10.
2*nd*: Topography model; sub-lon: 180°W.
3*rd*: Galileo SSI; C0401762600R; 27 Jun 1997; C9; ∼7 km/px; phase: 10°; sub-lon: 123°W; [2;5].
*Right:* Topography model; sub-lon: 90°W (from Fig. 13).
*Notes:*
[¶] The term *Facula* ("litle forch") is used for namings of bright spots on the surface of a planet or moon.
[♯] USGS Gazeteer of Planetary Nomenclature: https://planetarynames.wr.usgs.gov/Page/AMALTHEA/target

Thomas 1993 for details), and escape speed, based on *Galileo* and *Voyager* imaging data, are shown in Fig. 13. A comparison of images and topography, with named surface features marked, is given in Fig. 14.

### 3.2.2 Physical and Orbital Properties of the Inner Moons

Much less is known about the other three inner moons than is known about Amalthea. The simple reason is that the objects themselves and thus the surface features are significantly smaller, while the spatial resolutions of the images are similar, with the consequence that the

tiny disks in the data reach the limits of interpretability. Nevertheless, a surprising amount of information could be acquired about details of the surfaces of Thebe and Metis. In addition, much information could be obtained with disk-integrated data. For all four moons, a significant fraction of the research concentrated on dynamical aspects and the roles of the moons related to the faint Jovian rings. After their discoveries in *Voyager* data, it was soon recognized that Metis and Adrastea have very similar orbital elements and that they might play an important role for the Jovian main ring, either as shepherds similar to some Saturnian moons (Atlas, Prometheus, Pandora), or that the ring might even be maintained by erosion of dust particles from these moons. A strong interaction with the Jovian magnetosphere was also suspected (e.g., Morrison 1982).

Concerning physical properties, *Voyager* imaging gave first hints for apparent magnitudes ($V \sim 16$ mag for Thebe; $V \sim 17$ mag for Metis and Adrastea; see Table 3 for actual values). They revealed that all four are very dark objects (albedo $\leq$0.1), and allowed for a first-order calculation of their approximate sizes ($\sim$80$\pm$10 km for Thebe; $\sim$40$\pm$10 km for Metis and Adrastea; Morrison 1982). After *Voyager-2*, the inner two moons remained unseen for almost a decade until Nicholson and Matthews (1991) performed ground-based near-IR observations in December 1988. To see the objects so close to Jupiter, they took advantage of the strongly reduced straylight of Jupiter at 2.2$\pm$0.4 μm wavelength (K band) caused by a deep methane and hydrogen absorption of the planet's atmosphere. These observations greatly improved the mean orbital motions of Metis and Adrastea from Synnott (1984), and allowed predictions of the positions at an accuracy of $\sim$1300 km at the time of the arrival of the *Galileo* spacecraft half a decade later. An approximate K-band brightness was determined by Nicholson and Matthews (1991) for Metis ($\gtrapprox$15.1 mag), guessed for Adrastea ($\gtrapprox$16.5 mag), and adopted from the work of Neugebauer et al. (1981) for Amalthea (12.2 mag). De Pater et al. (1999) provided a more accurate determination with Keck images from 1997 (using a 2.19-2.35 μm filter instead of a broader standard K-filter to better suppress the Jovian straylight). These values are listed in Table 3.

Disk-resolved images of Metis and Thebe, as well as just barely resolved views of Adrastea were provided by the *Galileo* spacecraft (bottom half of Fig. 10), and Metis and Thebe were analyzed in detail by Thomas et al. (1998). As expected, these two moons were found to be in a synchronous rotation state with the largest axis pointing toward Jupiter. For Adrastea, this is likely, too, but the data base was insufficient for a clear claim. The global clear-filter albedos were determined to 0.063$\pm$0.006 (Metis) and 0.049$\pm$0.0045 (Thebe), which makes these two objects significantly darker than Amalthea. Bright spots were also suspected on Thebe and Metis. The albedos and the distances to Jupiter did not seem to correlate in some way, but as for Amalthea, the leading sides were also brighter than the trailing sides by $\sim$25 to $\sim$35%. This is remarkable because Metis orbits inside the synchronous orbit, and if this difference would be due to ion implantation from the magnetosphere and subsequent chemical changes, one might expect a flip at Metis compared to Amalthea and Thebe. Thomas et al. (1998) instead noted that this is in principle consistent with an influence of micrometeoroid impacts.

All three satellites showed reddish colors from 0.4 to 0.9 μm. In the shorter wavelength range, the spectral slopes correlated to the distances to Jupiter, with Metis showing the reddest color. Material lost from Io was suspected to be an important color agent on the surfaces. de Pater et al. (1999) confirmed the reddish color continuing into the infrared for Metis, Adrastea and Thebe, Wong et al. (2006) did so for Amalthea.

Thomas et al. (1998) provided ellipsoidal axes and mean radii for all four small inner moons (Table 3), and shape models for all but Adrastea. For this smallest of the regular Jovian moons, the axis dimensions are the only information that could be derived from the

data. For surface features like ridges, craters, etc., the spatial resolution of the images was not sufficient. As Amalthea, the other small inner moons showed no binary nature. The $a/c$ axis ratio of Metis is also quite large, while Thebe and Adrastea appear to be less elongated (Table 3). On Thebe and Amalthea, impact craters appeared to be the most prominent landform, craters in diameter up to the satellite's mean radius were visible, and the size-frequency distribution of the largest visible craters appeared to be near equilibrium. For Metis, it appears that some of the area might have outward-directed surface accelerations, unless its density is much higher than Amalthea's (Table 3). For a low density, loose material on Metis would be subject to loss from significant fractions of its surface.

Simonelli et al. (2000) also produced albedo maps for Thebe and Metis from *Galileo* data of orbits C3 to E11 (Thebe) and G8 to E11 (Metis), and modeled the photometry in a similar way as for Amalthea. The phase coverage for Thebe spans solar-phase angles from 3° to 72°, for Metis from 12° to 61°. Hapke modelling showed that the surface properties of these three moons are not identical. Amalthea likely has the smoothest and most backscattering regolith among them, while the Metis regolith appears significantly rougher and scatters much more isotropic than Amalthea or Thebe.

Simonelli et al. (2000) confirmed the finding of Thomas et al. (1998) that the leading hemispheres are significantly brighter than the trailing hemispheres. The proposed reason is that macroscopic meteoroid impactors, originating from outside the Jovian system, should be responsible for brightening the leading sides of these satellites. These impactors are also suggested to be the cause of the dusty ejecta that forms the rings. Simonelli et al. (2000) note the tremendous differences between leading and trailing hemisphere impacts, and of impacts by ring particles: $\sim$50 km/s versus "a few" km/s versus $\lessapprox$1 km/s, respectively. However, they admit that the exact physical mechanism brightening the leading sides is not understood. Possible mechanisms that have been proposed are an increase in impact-melt fraction, a comminution-related decrease in the particle sizes, or uncovering of brighter underlying material through gardening. As above-mentioned, bombardment by energetic electrons, protons, and ions trapped in the Jovian magnetosphere were considered unlikely by Simonelli et al. (2000) as the cause, mainly because the Metis asymmetry should be opposite in direction to Amalthea and Thebe. Simonelli et al. (2000) also give numbers for the strength of the local magnetic field in Jupiter's equatorial plane at different distances to the planet. Just outside the orbits of Metis and Adrastea at 2 $R_J$, it is 0.5-0.7 Gauss. At Amalthea's orbit, the strength is 0.2-0.3 Gauss, and at Thebe's orbit $\sim$0.1 Gauss.

The relation of the small inner moons to the rings was a topic of the paper by Ockert-Bell et al. (1999). They asked if the moons might be suppliers or sinks or shepherds for the rings, and concluded clearly that all four moons supply material to maintain the Jovian ring system. Adrastea's orbit marks the outer edge of the main ring, while the Metis orbit marks a localized reduction in ring particle density.

For Amalthea and Thebe, Ockert-Bell et al. (1999) measured the radial and vertical oscillations of the orbits due to eccentricity and inclination, respectively. For Amalthea, they found a radial deviation of $\pm$400 km and a vertical of $\pm$1160 km. For Thebe, the respective values are $\pm$3900 km and $\pm$4310 km. These vertical excursions of the two moon's orbits fit very well with the measured vertical extents of the two "gossamer" rings. The anomalously high orbit inclinations of Amalthea and Thebe themselves might be explained by former resonances with the orbit of Io that swept across the Amalthea and Thebe orbits while Io was moving outward due to forces from the tidal bulges it raises on Jupiter, and before having been trapped into the Laplace resonance with Europa and Ganymede observed today (Hamilton et al. 2001). Interestingly, most of the ring structures are constrained and can be explained by the orbits of the moons, except for an observed extension of the Thebe gossamer ring. Here, not the satellites, but the Jovian magnetosphere is responsible by charging

and discharging dust grains while entering and leaving the planet's shadow and thus exciting the orbital eccentricities of the Thebe gossamer ring particles (Hamilton and Krüger 2008).

Similar research was performed for Metis and Adrastea with images from the Jupiter flyby of the *Cassini* spacecraft. Porco et al. (2003) determined the orbit inclinations and thus the vertical displacements of these two moons from the Jovian equator plane. As Ockert-Bell et al. (1999), they found ∼100 km, which confirmed that Metis and/or Adrastea are the sources of the main ring, and their orbit inclinations determine the ring's vertical thickness.

The chapter by Burns et al. (2004) about Jupiter's ring-moon system in the "Jupiter Book" somehow marks a preliminary closure for the research of the small inner moons with respect to their surfaces and physical properties. It reviews research on Jupiter's small inner moons and rings. They note that the results from color measurements of dark and bright material by *Galileo* and *Voyager* are quite limited, and that improved color observations for the dark terrain as well as the bright crests with higher SNR are very much desired. Furthermore, with respect to formation, Burns et al. (2004) consider it possible that Metis and Adrastea condensed as "typical ring moons" from a disk of dust and gas around proto-Jupiter. Their orbital proximity might be a hint that they have been originally one body that broke up long ago. Burns et al. (2004) speculate that smaller fragments from this disruption event might still exist on similar orbits. Amalthea and Thebe are also assumed to have formed close to their nowadays locations.

In general, they again emphasize the very unique location of the small inner moon within the Solar system. These moons are enveloped by the most energetic magnetosphere, and orbital velocities are measured in several tens of km/s. Velocities for escaping from the entire system from circular orbit are even higher (by a factor of $\sqrt{2}$), which implies, the other way round, that projectiles approaching from outside the system move at least that fast. Mean collision speeds are many tens of km/s, with head-on impacts occuring at velocities as high as 80 km/s, producing substantial ejecta. This implies that significant regolith should cover the surfaces, although it is unclear if low gravities and locally large fictitious forces might result in a loss of loose material from the surfaces, especially on Metis and Adrastea, and on the tips of Amalthea. Note the escape speeds in Table 3 (and the Amalthea escape-speed map in Fig. 13); they radically illustrate the large variations of forces acting on the surfaces between the moons and between different areas on a moon due to their irregular shapes.

### 3.2.3 Search for Additional Objects

The numerous small inner moons in the Saturnian, Uranian, and Neptunian systems suggest that more small satellites could also exist nearby Jupiter. Of several papers reporting either dedicated or serendipitous searches around Jupiter, we review seven, three of which performed by spacecraft (*Galileo*, *Cassini*, *New Horizons*). New "objects" were indeed found, but their true physical nature remained unclear and thus no further moon discovery could be announced.

On 03 Dec 1988, Nicholson and Matthews (1991) observed the Jupiter main ring and the moons Metis and Adrastea with the 5-m Hale telescope at Palomar Observatory. As noted above, they used the relatively narrow K-band filter to suppress Jovian straylight and improve the signal-to-noise ratio (SNR). In their 119 images spread over nearly 7 hours (>80% of the orbit periods of Metis/Adrastea, or >50% of the Amalthea period), no additional satellites were found down to the K-band magnitude of Adrastea. This indicated that, if more inner moons did exist, they must be smaller than the four known ones, or that they orbit Jupiter at distances similar to or larger than Amalthea's, or much closer to Jupiter than Metis.

A similar approach was adopted by de Pater et al. (1999) who observed the Jovian ring at 2.27 μm with the 10-m Keck telescope in mid-August 1997. They concluded that no

additional moons larger than ∼9 km should exist in the main ring, and no object >6 km in the Amalthea gossamer ring.

During the *Cassini* Jupiter flyby, a dedicated satellite search was performed with the ISS NAC on approach from 04 Oct to 06 Dec 2000 from ranges between 82 and 25 Gm and at phase angles from 20° to 8° (Porco et al. 2003, paper and SOM). The search area covered Jupiter projected distances from 2.6 to 20 $R_J$ or the area between the orbits of Amalthea and Callisto. Under this viewing configuration, the angular separation to Jupiter was between 7.5 and ∼30 arcmin for the Amalthea orbit, and between ∼1.3° and ∼4° for Callisto's orbit. Because of observing time constraints, 1×4 NAC image mosaics could only be taken at a slow cadence of many hours to even days. This precluded the application of a simple object detection scheme based on the motion detection against a fixed star background, but required more complex search algorithms and restricted the search to orbits with near zero eccentricities ($e < 0.0002$) and inclinations ($i < 1.6°$). No new object was found with a visual magnitude brighter than 14.5 (which corresponds to an object diameter of 15 km for an albedo of 0.1), and the only object automatically detected turned out to be the known moon Thebe.

Showalter et al. (2003) reported ring observations between December 2002 and February 2003 with the then new ACS (Advanced Camera for Surveys) of the Hubble Space Telescope.[30] During seven visits targeting the main ring, each lasting ∼50 min, they could clearly detect Metis and Adrastea, but no other object. Based on those (non) detections they placed an upper bound of 6 to 8 km to the size of putative moons.

An unusual and interesting report about macroscopic objects in the vicinity of Amalthea was published by Fieseler et al. (2004). Their data suggest the existence of a thin "ring" of rocks orbiting Jupiter at Amalthea's orbit. During the targeted 250-km flyby of *Galileo* on 05 Nov 2002 (see Sect. 3.1.2), the spacecraft's star scanner telescope (a photomultiplier tube mounted on the spinning part of the spacecraft; Birnbaum et al. 1983) observed a series of bright flashes near Amalthea.[31] These were brighter than $6\sigma$ of radiation noise, in some cases even $>100\sigma$. The interpretation of the adopted signals is that about seven to nine small moonlets with possible sizes up to ∼3.5 km at distances $\lessapprox$2000 km are located near Amalthea. (One apparently much brighter object might have been further away and even larger.) A further eleven possible signals were not reported because these were marginal detections not well above the radiation noise.

The objects detected by the star scanner were positioned in space somewhere along a "sighting" vector centered on the spacecraft, but the data were not suitable to make any calculations of the exact distances or sizes of the observed objects. Nevertheless, some size and distance constraints could be placed via geometric and detector sensitivity considerations. For example, because no object was observed for a second time after one rotation of the spacecraft (i.e., after 19 s), Fieseler et al. (2004) estimated a maximum distance – objects further away should have appeared twice in succession in the star scanner's field-of-view. Furthermore, the threshold of the star scanner was set such that objects darker than the equivalent of $V$ magnitude +2.0 were not detectable. On the other end, the brightest measured object had an equivalent $V = -2.9$ mag.

Assuming the objects were residing close to the Amalthea orbit, they would have been on the order of 250 km away from *Galileo* during detection. In this case and according to Fig. 4 of Fieseler et al. (2004), the brightest signal would have stemmed from a $\gtrapprox$2-km

[30] *HST* Proposal 9426 (https://archive.stsci.edu/proposal_search.php?id=9426&mission=hst).

[31] IAU circ. no. 8107 (04 Apr 2003): Objects near Jupiter V (Amalthea). http://www.cbat.eps.harvard.edu/iauc/08100/08107.html.

sized object, and the darkest from an $\sim \frac{1}{4}$-km sized body. These are very rough estimates which depend on assumtions about albedo, phase-angle behavior, and other parameters. As a comparison, the best *Galileo*-SSI images of Amalthea have pixel scales of 2.4, 3.7, and 4.5 km/px (Fig. 10, panels [3|4], [3|2], [3|1], respectively). Such objects might have gotten lost in the speckles of electron and proton hits, or might have been located ouside the cut-out windows that have been downlinked to Earth. The latter statement is not true for the final Amalthea images from orbits I32 (panel [3|6]) and I33 (panels [3|7+8]) where significant fractions of the images have been downlinked (most of this "empty" space is not reproduced in the panels in Fig. 10), but these images were taken from ∼1 Gm range with a pixel scale of ∼10 km/px and short exposure times, making sub-kilometer-sized objects hard to discern between cosmic-hit speckles and background stars.

Another signal was observed by the star scanner one orbit later on 21 Sep 2003 just 1 h before spacecraft plunge into Jupiter (Fieseler et al. 2004). At that time, Amalthea was located on the other side of Jupiter, thus, this object might share the orbit of Amalthea, but was not located in the moon's immediate vicinity. After various checks of potential instrument failures and possible other causes for the signals, Fieseler et al. (2004) conclude that they do not see any alternative to the interpretation of real physical objects near Amalthea's orbit. They argue that it is statistically extremely unlikely that such events are detected quite exactly at the Amalthea passage by coincidence without any relation to Amalthea. Another important argument was that in 13 years of operation, no other set of observations has shown similar features.

*New Horizons* was another spacecraft using Jupiter's gravity to accelerate toward its ultimate target. Among other science, it used its LORRI camera for a new search of Jovian ring moons; results were reported by Showalter et al. (2007). During approach at low solar phase angles, first on 24 and again on 25/26 Feb 2007, two ring "movies" have been recorded. Forty-nine images have been taken every 10 min over 7.2 h on the first occasion, and 63 images every 8 minutes also over 7.2 h on the second. In both cases, the left ansa of the main ring was targeted (Fig. 15). The first ring movie was longitudinally complete between radial limits 104,000 to 185,000 km ($0.81 \cdot a_{Met}$ to $1.02 \cdot a_{Ama}$) and was sensitive to moons down to a diameter of ∼2 km. The second movie had narrower limits of 108,000 to 154,000 km ($0.84 \cdot a_{Met}$ to $0.85 \cdot a_{Ama}$) and was sensitive to moons with diameters down to ∼1 km.

No new satellite was discovered, but instead "clumps" orbiting just interior to Adrastea. Two "families" of clumps have been distinguished, one contained three to five, the other two distinct features. Each "clump" has a longitudinal extent of about 0.1° to ∼0.3°. The brightest features were found to be two to three times as bright as the local ring, with integrated intensities of about 1% that of Adrastea. These numbers convert into cross sections equivalent to moons with diameters of ∼2 km. Interestingly, clumps were not seen in the high phase images taken a couple of days later, leading Showalter et al. (2007) to conclude that they must be primarily concentrations of larger bodies, not of dust.

Showalter et al. (2007) note that with respect to small inner moons, the situation at Jupiter appears to be fundamentally different from that of Saturn. At Jupiter, no moons with sizes of a couple of kilometers were found; if Adrastea (∼16 km) is indeed the smallest, there is an abrupt cutoff in the size-frequency distribution. At Saturn, there are multiple inner moons at the kilometers-size level, and no such cutoff is observed. This surprising finding at Jupiter requires an explanation. Showalter et al. (2007) speculate that a massive erosive process is at work in the inner Jovian moon system. For such a process, the erosion rate $\mathrm{d}r/\mathrm{d}t$ would be about constant, independent of object radius $r$. Hence, simply spoken, in the same time that Adrastea shrinks from 26 to 16 km, or Amalthea from 177 to 167 km, all objects in the (inner) system with diameters 10 km or smaller would vanish. This hypothesis requires that

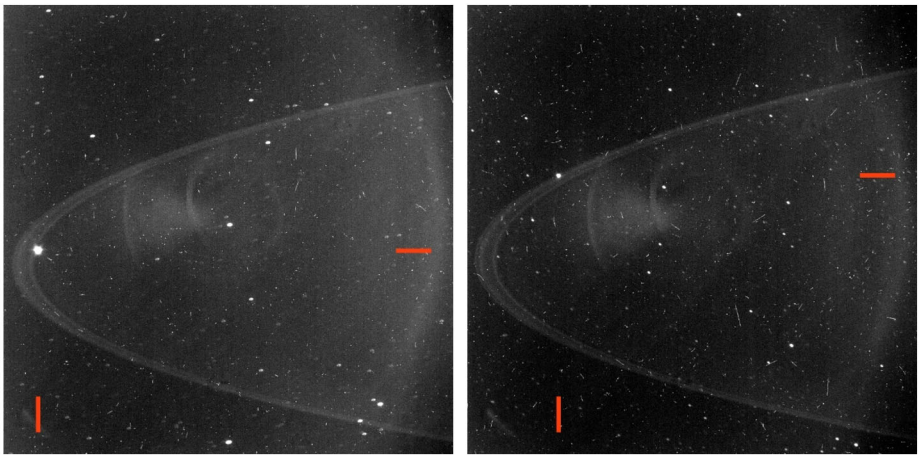

**Fig. 15** Jovian ring with satellites Metis (left) and Adrastea (right), observed by *New Horizons*. LORRI images 0034765323 (left; 26 Feb 2007 03:10 UTC) and 0034772943 (26 Feb 2007 05:17 UTC); exposure times: 4 s

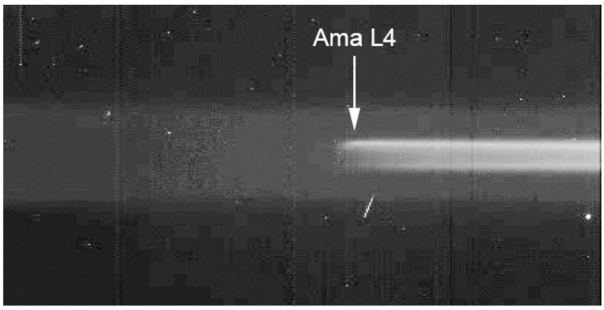


**Fig. 16** Jovian gossamer rings at Amalthea's orbit L4 location, observed by *Galileo* during orbit C10 from 6.6 Gm distance at phase angle 178.5° (SSI image C04160889.68; 05 Oct 1997 23:58 UTC)

material reaccretion should be orders of magnitude less efficient, which might be reasonable so close to Jupiter's Roche limit, but is completely at odds with the Veverka et al. (1981) suggestion that all impact debris should have reaccreted and should form a kilometers-thick regolith, as noted in Sect. 3.2.1. Arguing with the surface escape speed, Burns et al. (2004) also expect significant regolith on Amalthea and maybe Thebe, but possibly not on smaller Metis and Adrastea.

In their paper about exploration of the gossamer rings of Amalthea and Thebe with *Galileo*, *Voyager*, *HST* and Keck images, Showalter et al. (2008) note that additional material appears to be concentrated just interior to the orbits of these two moons and might be locked in 1:1 resonances with them. At least in the case of Amalthea's ring, material appears to be located in the same orbital plane as Amalthea's inclined orbit and might be trapped at the Lagrange points (Fig. 16).

The small inner Jovian moons have been observed again recently with the *James Webb Space Telescope* (*JWST*) as part of the Early Release Science (ERS) program.[32] At the time of this writing, the data reduction and analysis was still ongoing. Based upon early calcu-

[32] *JWST* ERS #1373: https://www.stsci.edu/jwst/science-execution/approved-programs/dd-ers/program-1373.

lations, the ERS team expects to be able to detect objects as small as ∼100 m in size. If present, it may confirm the viability of the currently dominant model (see, e.g., review by de Pater et al. 2018) that requires for the continued presence of the dusty Jovian ring a population of embedded source bodies, perhaps hundreds of meters in size. If no bodies of this size range will be found, new theories about the continued presence of the rings might be necessary.

### 3.3 Small Inner Moons' Science Objectives for JUICE

The 2014 JUICE mission Definition Study Report (ESA 2014) remarks small inner moon observations as a general mission goal. Herein, it is noted that "[t]he study of the diversity of the satellite system will be enhanced with additional information gathered remotely on [...] the smaller moons." In addition, the report states that "JUICE will shed light on the physical shape and bulk composition of these small moons. At least for the largest objects Thebe and Amalthea, JUICE will investigate their individual relationships with the ring system. JUICE will also improve their orbital elements, ultimately constraining their origin." Especially for MAJIS, the determination of "composition and physical properties of Io, small moons, rings and dust in the Jupiter system" are mentioned. Table 4-10 ("Estimated contribution of the JUICE experiments in achieving major science objectives") in the report has listed "Study the main characteristics of rings and small satellites" as the item related to the small inner moons.

These generalized statements comprise science goals like the investigation of the formation history and evolution of the small inner moons, as well as surface and bulk properties. Key aspects of these goals are the study of the cratering record, of the orbital evolution and of the geological processes, or of the determination of object masses and densities. Adding potentially existing, yet undiscovered objects to the inventory is another part of the task.

For a spacecraft mission with no close flybys at the inner moons, these science questions will not easily be solved. Though, they can be pursued by tackling the following objectives:

*Objects characterization — global properties:* Determine or refine sizes, shapes, volumes, albedos, colors, surface compositions (especially water ice and refractory components), states of surfaces (roughness, slopes, porosities, regolith properties, etc.), phase-angle behavior, rotation states; possibly estimates of bulk densities ("rubble pile" vs. "solid rock"). For JANUS, this can be addressed through complete longitude coverages at low (∼0°-20°) and mid solar phases (∼40°-60°) at closest possible distance in multiple filters, by observations during the inclined orbits, and by observations at various phase angles. MAJIS, UVS, and SWI are suited to obtain data from Amalthea revealing information about the roles of water ice and other surface components. See Sect. 3.4.3 for details.

*Surfaces characterization — local properties:* Identify additional geologic features like craters, bright spots, scarps, grooves, plains. For this task, the same data, obtained from lowest possible distance, might provide the information (also see Sect. 3.4.3).

*High-accuracy astrometry:* These observations refine the orbits' $e$ and $i$ elements; they provide masses and thus densities of the small inner moons; they possibly allow for a determination of the internal mass distributions and for a quantification of tides. Section 3.4.4 goes into more details on this topic.

*Search for unknown objects:* Within the orbit of Io; track and investigate objects potentially discovered by other means (Sect. 3.4.5).

**Table 5** Apparent object sizes and pixel scales of the small moons

| Moon | | 1 pixel fill at range | Perijove | C/A | Phase | JANUS pixel scale | Apparent size ($a \times b \times c$) |
|---|---|---|---|---|---|---|---|
| | | | | [km] | [°] | [km/px] | [px] |
| 516 | Metis | 2.9 Gm | 9 | 635,100 | 61 | 9.5 | 6.3 × 4.2 × 3.6 |
| | | | 12 | 638,300 | 8 | 9.6 | |
| 515 | Adrastea | 1.1 Gm | 9 | 637,800 | 65 | 9.6 | 2.1 × 1.7 × 1.5 |
| | | | 12 | 634,200 | 18 | 9.5 | |
| 505 | Amalthea | 11.1 Gm | 9 | 578,400 | 55 | 8.7 | 29.0 × 17.1 × 14.5 |
| | | | 12 | 581,700 | 20 | 8.7 | |
| 514 | Thebe | 6.6 Gm | 9 | 533,200 | 50 | 8.0 | 14.5 × 12.3 × 10.5 |
| | | | 12 | 542,200 | 14 | 8.1 | |

*Notes:* Apparent object sizes and pixel scales for JANUS during closest approaches near the two perijoves PJ9 and PJ12 for orbit tour CReMA_5_0. In this tour, these are the best opportunities for the small inner moons after the two "Europa-orbit" perijoves. The apparent sizes (of the objects) are given for the assumption of full illumination. The phase column indicates the solar-phase angles which are moderate in PJ9 and low in PJ12. The '1 pixel fill at range' column gives the distance between JUICE and the object for the case where the mean size of the object (see Table 3) would fit in one JANUS pixel. For MAJIS, with a ten times lower pixel scale, corresponding numbers for '1 pixel fill', pixel scale and apparent size can be obtained by just shifting the decimal points by one digit.

## 3.4 Observing the Small Inner Moons with JUICE

After presentation of the science goals, a description of the observation plans and constraints for the small inner moons will follow. But before that a comparison of the capabilities of spacecraft and ground-based telescopes is made.

Because the spacecraft will never come closer to Jupiter than the orbit of Europa (perijove PJ7 and PJ8; Boutonnet et al. 2024, this collection), only observations from remote distances (>0.5 Gm) will be possible. Table 5 lists the spatial resolutions (pixel scales) and apparent object sizes for the best opportunities outside the two Europa orbits (which are unlikely to get observation slots for the small inner moons, see Sect. 3.4.3 below). Despite the lack of close flybys, there is lots of science that can be achieved with JANUS, MAJIS, UVS, and SWI, and that complements and augments the results from *Voyager*, *Galileo*, ground-based and spaceborne telescopes significantly.

### 3.4.1 Spacecraft at Jupiter Versus Earth-Based

Many of the science objectives described in Sect. 3.3 cannot be reached (either at all or with the desired precision) with ground-based telescopes or space telescopes operating near Earth, but only by spacecraft operating in the vicinity of the objects. Here is a short compilation what makes spacecraft observations particularly unique for the small inner moons of Jupiter.

*Astrometry:* Observations at close range, from above/below the ecliptic, and at high frequency allow for a much more precise determination of the elements describing the shapes and orientations of the orbits.

*Phase coverage:* The reachable solar-phase angles range can be high, in principle between 0° and 180°. The upper limit is set by possible Sun-avoidance angle restrictions of the spacecraft's optical sensors and by the apparent magnitude of the object which also de-

pends on the observation distance. Practically, Amalthea might become too dark at phases $>160°$, Adrastea $\gtrapprox 150°$. Other constraints might be set by straylight of the Sun in the imaging devices. Reflected light from Jupiter ("Jupitershine") or the Galilean moons will also limit the observation opportunities. From Earth, only the phase-angle range between 0° and 12° can be observed.

*Polar views:* Earth, Sun, and the inner moons of Jupiter are located on the same plane within a few degrees, and the pole axes of the moons are almost perpendicular to this plane. Thus, from Earth, the polar areas can only be seen very obliquely, if at all. During the inclined-orbits phase, JUICE will have viewing geometries that allow disk-resolved polar views. The highest sub-spacecraft latitude might reach ∼27° for Amalthea and Thebe, and ∼18° for Metis. For comparison, during the *Galileo* mission, which did not leave Jupiter's equatorial plane, the sub-spacecraft latitudes ranged from −1.0° to +0.9° (Metis, Amalthea, Thebe). During the *Voyager* flybys, Amalthea was also imaged equatorially, with sub-spacecraft latitudes from −4.5° to +4.0° (Simonelli et al. 2000).

*Spatial resolution:* In the era of modern giant telescopes, this topic poses an interesting question: Is proximity to the targets still a resolution argument even for a moderately-sized "wide angle" telescope like JANUS (angular resolution: 3094 milli-arcseconds (mas)); how does JANUS compare to the largest Earth-based observatories? As seen from Earth during opposition, a distance of ∼3 km appears under a viewing angle of 1 mas from Earth. This corresponds to an angular size of $\sim 44 \times 86$ mas for Amalthea, and about $2 \times 3$ mas for Adrastea. These are just barely or not at all resolvable for *HST* ($\geq$40 mas)[33] or *JWST* (∼100 mas).[34] However, with future giant telescopes (ELT, TMT, GMT), it might be possible to achieve an angular resolution of ∼5 mas. At Jupiter opposition distance, this corresponds to a spatial resolution of ∼15 km/px which is equivalent to JANUS images taken from a distance of ∼1 Gm. Keeping in mind that these ∼5 mas are likely an ideal value that might be rather hard to achieve in practice for tiny moving targets in the vicinity of giant glaring Jupiter, it can be expected that in-situ remote sensing instruments will remain the superior choice for the task to map the surfaces of the small Jovian moons in the foreseeable future.

### 3.4.2 Comparison of JUICE/JANUS with *Galileo* and *Voyager* Imaging

The closest distances of JUICE to any of the small inner moons (Table 4) will be larger than the closest ranges for *Voyager* or *Galileo*, but similar to the average distances from which images have been taken by these two missions (e.g., see Table 1 in Simonelli et al. 2000). Except for this "distance disadvantage", the JUICE mission and instruments are better in all other aspects. Compared to *Voyager* ISS (with a vidicon) and *Galileo* SSI (with a CCD sensor), the JANUS camera has superior capabilities. This includes the readout (line time below 1 ms on JANUS thanks to the detector with rolling shutter); for short exposure times, a faster readout reduces the time the data are susceptible to charged-particle radiation while residing on the chip between exposure start and readout. In addition, there was no capability for *Voyager* and *Galileo* to obtain spectral data of minor moons in the UV or near-IR wavelength range as will be possible for UVS and MAJIS. Furthermore, co-adding JANUS images taken twice or three times in direct succession (within seconds) might help to improve spatial resolution. Another unique feature of JUICE compared to *Voyager* and *Galileo* are the already mentioned inclined orbits. They will allow more direct views of the south poles of Amalthea, Thebe, and Metis, and of the north pole of Amalthea at moderate emission angles.

[33] *Hubble* by the Numbers: https://science.nasa.gov/mission/hubble/overview/hubble-by-the-numbers/.

[34] *JWST* key facts: https://webb.nasa.gov/content/about/faqs/facts.html.

While this is all very significant, the major advantage of JUICE will be the potentially large amount of data. Compared to *Galileo*, which obtained only a few dozen images due to the main antenna anomaly, and to *Voyager*, which imaged only Amalthea spatially resolved during two flybys (Fig. 10), JUICE can perform systematic surveys of all four small inner moons in multiple color filters, over a large range of phase angles, over all sub-surface longitudes, and for astrometry purposes.

### 3.4.3 Observing the Small Inner Moons with JANUS, UVS, MAJIS, and SWI

**JANUS:** The camera will be a major driver for the design of the small inner moon observations by JUICE. To tackle the goals introduced in Sect. 3.3, four types of observations are currently under consideration:

- High spatial resolution – image the moons from as close as possible while aiming at full geographic longitude coverage.
- High-latitude views – schedule observations during parts of the inclined orbits (late 2032 to mid 2033 in CReMA_5_1) based on criteria like 'proximity', 'low phase', 'high sub-spacecraft latitude' (emission angles at the poles much lower than 90°), or 'longitude coverage'.
- Large phase coverage – observe at various phase angles from close to zero phase up to >140°; spatial resolution is not critical here, the objects might remain sub-pixel in size.
- Astrometry – see Sect. 3.4.4 for details.

Besides the broadband PAN filter, color imaging will be an important part of the observations. Several JANUS color filters will be considered to evenly cover the spectral range of the instrument from 0.38 to 1.02 µm. JANUS color observations will show the general spectral slope from near-UV to near-IR, might identify possible color variations between the objects, and between the hemispheres of the same object. Also, JANUS might detect the putative 0.7-µm bands indicative of aqueous alteration (e.g., Vilas et al. 2006 and Vilas and Hendrix 2024 discuss this for some of the large Irregular Jovian moons). One-micron absorptions measured by Thomas et al. (1998) on Amalthea and Thebe with *Galileo* SSI have not been confirmed from reflectance spectra of Amalthea measured with IRCS on Subaru and SpeX on IRTF by Takato et al. (2004), thus JANUS color data might confirm or disprove the existence of this feature.

As mentioned before, for spatial resolution as a quite precise rule of thumb, the lower the orbit periapsis of JUICE, the closer the lowest altitudes to the moons and thus the better the spatial resolution. This is expected because closest approach of JUICE to Jupiter will always be at least 3x farther away than the distance of Thebe from Jupiter, and even more for the other moons. The best observation opportunities will be the two Europa-flyby orbits in July 2032 with Jupiter periapsis altitudes of 599,100 (perijove PJ7) and 601,200 km (PJ8). Unfortunately, these cannot be used for the small moons because they are conflicted with top-priority Europa science. The next lowest periapses (for orbit tour CReMA_5_1) are PJ9 (687,500 km), PJ12 (691,300 km), PJ6 (697,700 km), PJ31 (733,600 km) and PJ13 (738,200 km); occurring between June and October 2032 (PJ31 in August 2033). For these opportunities, closest JANUS imaging might provide apparent mean object sizes of ∼4.5 pixels for Metis, ∼1.7 pixels for Adrastea, ∼19 pixels for Amalthea, and ∼12 pixels for Thebe in JANUS images (Table 5; compare in Fig. 10 to images of similar sizes achieved during the *Galileo* prime mission).

Concerning the high latitude views, the JUICE orbit plane allows for a better view of the southern hemispheres than of the northern ones. For the south, there are opportunities at $\lessapprox$1 Gm distance, allowing for imaging at ∼14 km/px, which is useful for Amalthea

(including crater Gaea), Metis and Thebe. For imaging of the northern parts, JUICE will be ∼1.5 Gm away from the inner moons; this corresponds to pixel scales of ∼22 km/px. This will be useful for Amalthea, and barely for Thebe. These numbers refer to trajectory CReMA_5_1 and will change somewhat with future orbit tour updates.

Solar-phase angle coverage to constrain the physical properties of the surface regolith is ideally performed in one single or two adjacent orbits to keep possible variations of other parameters low (especially sub-solar latitude variations). Here, particularly useful appear orbits where phase angles remain low for a few days after perijove and then steadily increase to high values until before next perijove. Covering a wide phase range from ∼0° to ∼140° or even higher would provide high-quality phase curves for all four objects, and even for additional moons in case more will have been discovered prior to JUICE's arrival at Jupiter.

**UVS:** JUICE's Ultraviolet Spectrograph will attempt to obtain UV spectra of the inner Jovian moons during ride-along observations with JANUS, with the main challenge being background counts due to charged particle radiation trapped in the Jupiter magnetosphere. The best opportunities to view the inner satellites occur at JUICE-Jupiter distances of $<10$ $R_J$. Based on the performance of *Juno* UVS (Gladstone et al. 2017), we expect that in this region JUICE UVS will experience background count rates of a few hundred kHz (summed over the full detector area). For comparison, for observations of the Irregular satellites at $>100$ $R_J$ the background count rate is expected to be close to that measured in cruise (tens of Hz). Although the maximum angular diameter of the inner moons will be a factor of about 1-11 larger than that of Irregular moon Himalia (see Sect. 4.3.3), thereby increasing the signal from reflected sunlight, the increased particle background will have a detrimental effect on the SNR of any UV observations. However, UVS can discriminate spurious events based on the observed pulse height distribution (PHD; Retherford et al. 2026, this collection), which can potentially be used to subtract background counts since energetic particles and UV photons produce different PHDs. Hence, it may be possible to extract some UV spectral information despite the high background count rate. The main spectral feature UVS will search for is a characteristic signature of water ice near 160 nm; this is described in more detail in Sect. 4.3.3 and Fig. 24.

**MAJIS:** As described in Sect. 3.2.1, the composition of Jupiter's four small inner moons remains a debated matter. While their formation in the circumjovian nebula would favor a composition rich in high-density refractory materials (Pollack and Fanale 1982), the average density of Amalthea is lower than the density of water (Anderson et al. 2005) and the surface shows an absorption band at 3 μm, potentially indicative of hydrated minerals and perhaps of organic compounds (Takato et al. 2004). Visible to near-infrared observations of the ring system and these moons (at least the two largest ones, Amalthea and Thebe) by MAJIS can clarify the interconnections existing between the ring material and the surface composition of these objects. During JUICE's tour of Jupiter, MAJIS will have about ten opportunities to tentatively observe both Amalthea and Thebe at spatial resolution $<100$ km/px (targets seen over 1 to 2 pixels). These observations will ultimately provide full-disk spectral profiles in the overall range 0.5-5.5 μm with good SNR. Observations carried out at substantially different solar phase angle values will further allow deriving phase curves at multiple wavelengths, useful for constraining the surface regolith properties of these objects and complementing the JANUS observations. Finally, simultaneous UVS observations will allow broadening the spectral range and further constrain the compositional and physical properties of the surface material of these moons.

**SWI:** The Submillimetre Wave Instruments (Hartogh et al. 2026, this collection) observes the moons in the far infrared in two bands around 250 and 500 μm wavelengths and is therefore sensitive to low-temperature thermal emissions of the bodies. Surface properties of the moons, like the thermal inertia of the upper few centimeters can be derived by

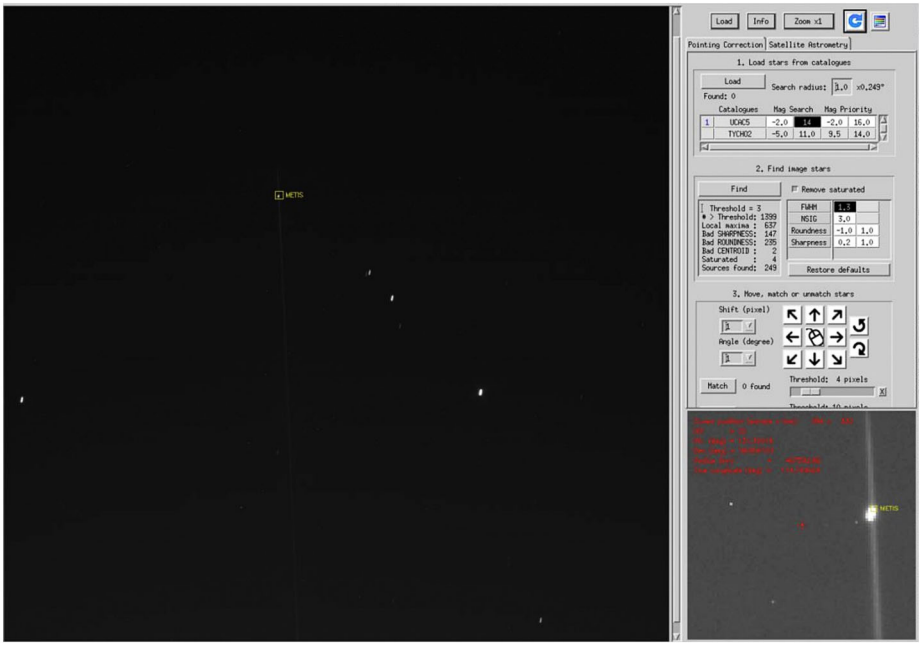


**Fig. 17** Astrometric measurement of Metis from *Cassini*-ISS image N1356864415 using the Caviar software (Cooper et al. 2018). One can see the presence of stars in the background field that are used for calibration. Similar but more accurate measurements will be performed with the JANUS camera for the four inner Jovian moons

detecting the wavelength-dependent far infrared brightness responses to solar illumination. Considering the radiometric accuracy of SWI and the large distances and small sizes of all Jovian minor moons, this may only work for Amalthea with sufficient sensitivity. The low density of Amalthea suggests that it is a rubble pile or an icy body or something in between (Anderson et al. 2005; Sect. 3.2.1). The substantially higher brightness at its leading hemisphere suggests the excavation of ice by the higher velocity and frequency of impacts (Simonelli et al. 2000; see also Sect. 3.2.2). This process, together with sublimation (assuming ice temperatures above 130 K), may create a thin cloud of water vapor that due to the low gravity will expand rather quickly and fill the SWI beam within about 1 hour (i.e., photodissociation by Lyman-$\alpha$ radiation is small). Due to SWI's very high spectroscopic sensitivity ($<10^{15}$ water molecules/m$^2$ column density) the spectroscopic observation will constrain the production rate of water vapor and help to understand the nature of the observed higher brightness of the leading hemisphere of Amalthea.

### 3.4.4 Astrometry of Inner Moons

JUICE's repeated circumnavigation of Jupiter over several years will be an opportunity to obtain astrometric positions of the moons with much improved precision than from Earth (Fig. 17). In particular, an accuracy of a few kilometers (Cooper et al. 2015; Lainey et al. 2023) for the inner moons (depending on the distances at the time of the observations) should be possible. Such data will greatly enhance our knowledge of the inner Jovian system. With the exception of Amalthea, the masses of these four satellites are barely known. However, it was shown that mutual gravitational perturbations between Metis and Adrastea induce

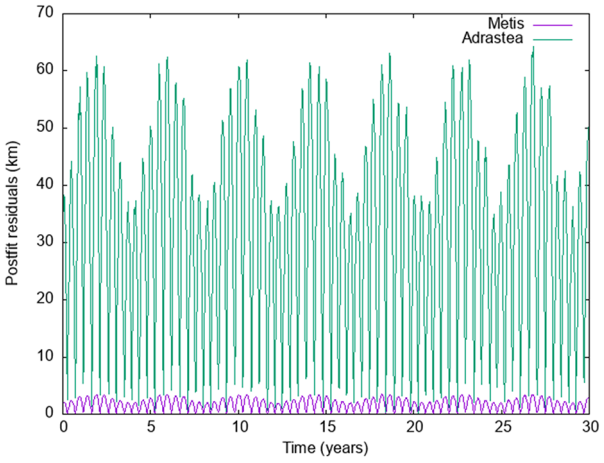


**Fig. 18** Post-fit residuals associated with the effect of Metis' and Adrastea's mutual perturbation, assuming a density of 0.86 g/cm$^3$ for both moons

a periodic signal of around ∼2-3 km and ∼35-65 km on the orbital longitude of Metis and Adrastea, respectively (Fig. 18; Lainey and Van Hoolst 2009). Consequently, tracking the orbits of these inner moons will enable us to derive their masses and, as a consequence, their densities. In particular, only the density of Amalthea was obtained from a single *Galileo* flyby in November 2002 (Anderson et al. 2005). As discussed in Sect. 3.2.1, the low value of ∼0.86 g/cm$^3$ suggests high porosity. Such large porosity is observed in the inner Saturnian system, too (Lainey et al. 2023). This may be the consequence of accretion at the edge of a massive ring, when material crosses the Roche limit (Charnoz et al. 2010). However, we lack the information at this stage to conclude if a similar formation mechanism occurred in the Jovian system. In particular, it is currently unknown whether or not Jupiter once had a dense ring as well, similar to the Saturnian one, which was eventually removed by ballistic transport due to micrometeoroid bombardment (Estrada and Durisen 2023).

Astrometric data can infer the internal mass distribution as well. Indeed, the coupling between the rotation of the inner moons on their orbit can provide useful information. The physical libration of inner moons induces a specific trend on the periapses (Borderies and Yoder 1990; Lainey et al. 2023) that can be constrained from JANUS. It should be noted that the amplitude of physical librations is directly related to the mass distribution inside the body (Comstock and Bills 2003; Rambaux et al. 2022). As a result, and depending on the sampling and precision of the final data, JANUS astrometric data from JUICE could allow us to infer even more interior properties such as homogeneity. In particular, this method has proven fruitful in the case of Phobos (Jacobson 2010) and Saturn's inner moons (Lainey et al. 2023). Combined with JANUS-derived shape models, and surface analysis, this will give us a much better overview of Jupiter's inner moons physical and dynamical properties, including their possible formation history.

Quantification of tides is an important aspect of astrometry, too. It has been suggested that tidal dissipation within giant gas planets could be extremely frequency-sensitive (Ogilvie and Lin 2004; Auclair-Desrotour et al. 2015; Fuller et al. 2016). Therefore, we cannot exclude the possibility of determining tidal dissipation within Jupiter at the tidal frequencies of the inner moons. At least, a constraint on the Jovian $k_2/Q$ at these frequencies will be obtained.[35]

[35] We recall to the reader that $k_2$ (the so-called Love number of degree 2) characterises the response of a body suffering tidal distorsion in the gravitational potential; it allows to characterize the internal structure of the

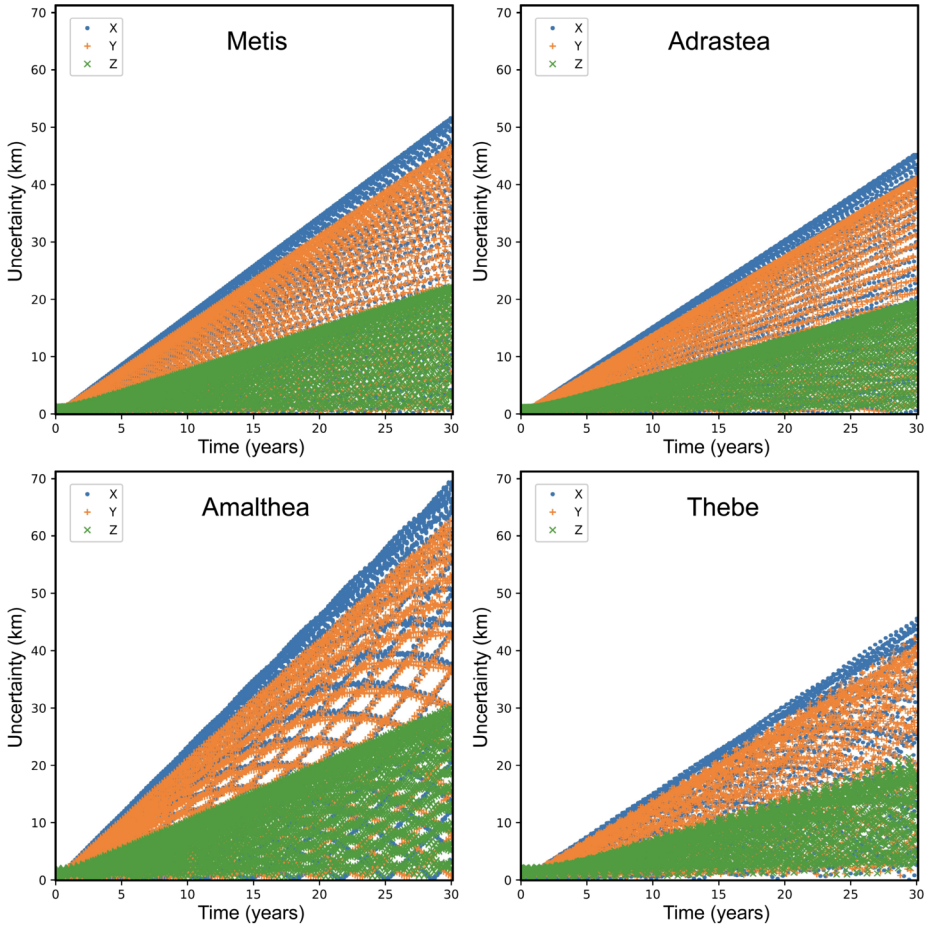


**Fig. 19** Uncertainty ($1-\sigma$) of the 3-D position of the inner Jovian satellites (EME2000 and initial epoch J2000 – 01 Jan 2000 at 12:00 UTC) from year 2000 to 2030. These uncertainties were derived from the last ephemerides kernel NOE-5-2023 provided by IMCCE/Paris Observatory, and derived from ground and space based astrometric data (including *New Horizons* and *Cassini*)

Finally, we cannot rule out the possibility of detecting tiny moons that are not yet known (cf. Sects. 3.2.3 and 3.4.5). If such objects exist, constraining their orbits will be the first task to be carried out, at least to recover these objects during a subsequent observation sequence. A study of the orbital characteristics, including the possible resonance mechanism and sensitivity to the gravity field of other moons, will be carried out.

From a practical point of view, astrometric data will be extremely valuable at close range from the spacecraft (Fig. 19). This raises the question of the accuracy of the ephemerides to catch the moons in the field of view under optimal conditions. Thanks to the *New Horizons* and *Cassini* astrometric data, the ephemerides of the inner moons are globally constrained within about 70 km (200 km at a $3\sigma$ level) at the time of JUICE arrival. This precision is

object. Q is the "quality factor"; 1/Q characterises the amount of mechanical energy dissipated per cycle by tides. When only $k_2$/Q is measured, it provides the dissipated mechanical energy $\dot{E}$.

sufficient to allow sub-frame images to be taken, with stars in the background. Interestingly, we could investigate the possibility of making mutual event observations, i.e., observations of two or more inner moons on the same images. While increasing the amount of data without increasing the download volume, mutual events also offer the possibility of performing an intersatellite astrometric adjustment, significantly reducing the impact of JUICE's positioning error. Consequently, a study of the opportunity for mutual events should be carried out prior to the image acquisition procedure.

### 3.4.5 Potentials of a Satellite Search Campaign Inside Io's Orbit

The past satellite search efforts described in Sect. 3.2.3 covered three different "regions": The main ring (confined by Metis and Adrastea), the Amalthea orbit, and "everywhere" (i.e., all regions between the orbits inside Metis up to Callisto). Their results define the minimum requirements for any future search. For the main-ring area, Showalter et al. (2007) expected for LORRI/*New Horizons* a search sensitivity down to objects of approximately 1 km in size, and reported no moon finding, but potential "clumps" in the ring. For the Amalthea orbit, Fieseler et al. (2004) detected signals in *Galileo* star-scanner data that appear hard to interpret otherwise than as objects of sizes of a few hundred to maybe ∼2 km in the direct vicinity as well as in the entire orbit of Amalthea. Moreover, Showalter et al. (2008) suspected a "concentration of material trapped in Amalthea's leading Lagrange point" (L4; 1:1 resonance). Off the orbits of the three innermost moons, Showalter et al. (2007) expected that no additional moon >2 km exists inside the Amalthea orbit. Outside Amalthea up to Callisto, Porco et al. (2003) found no object down to the size of Adrastea (∼16 km) in the *Cassini* NAC images, but this search had the restriction to almost zero orbit eccentricity and inclination.

These works offer a guidance to potential JUICE JANUS satellite search strategies. In general, a rather large distance is needed to restrict the search area in the sky and the number of images. Unfortunately, the orbit tour of JUICE is not well suited for inner moons searches because the solar phase angles are rather high while the spacecraft is in the apoapsis parts of its orbit. Furthermore, the apojove distances will shrink below ∼3 Gm rather early in the mission, with only few exceptions of which none offers low phase angles. Note that ∼90° solar phase means a drop in object brightness by ∼4 mag compared to near zero phase. Evaluating the best possible search strategies is a task for upcoming observation planning.

## 4 Irregular Moons

As of the end of 2025, there are 357 Irregular moons known in our Solar System, 89 of which belong to the Jupiter system (Fig. 2, Table 6). Their distances to their center planets are of the order of many million kilometers, but well within the planets' Hill spheres.[36] The orbits are much more eccentric and inclined than observed for the regular moons, with the vast majority even residing on retrograde paths. The semi-major axes of the Jovian Irregular moons on prograde orbits range between 7.4 and 18.7 Gm (∼100-260 $R_J$) and for the retrograde objects between 19.3 and 24.2 Gm (∼270-340 $R_J$). The higher stability of retrograde orbits at large distances to Jupiter is attributed to the Coriolis acceleration (e.g., Hamilton and Burns 1991; Shen and Tremaine 2008).

[36]The largest semi-major axis in the Solar System in units of Hill radii of the center planet belongs to Jovian moon Kore (J XLIX; 0.456 $R_{H,J}$); see also Fig. 1 in Sheppard et al. (2023).

**Table 6** Irregular moons of Jupiter – overview table

| JPL ID | IAU desig. | Moon name | Prov. desig. | Abbr. (TD) | $a$ [Gm] | $e$ [ ] | $i$ [°] | $P_{sid}$ [d] | $P_{syn}$ [d] | $H$ [mag] | $p_v$=0.06 Size [km] | $p_v$=0.03 Size [km] | Apparent mag. from Earth ($\Delta$) [mag] | Juice ($V$) [mag] | Closest range to Juice [Gm] | Lowest phase for Juice [°] | Revs from JOI to GOI [ ] | Abbr. (TD) |
|---|---|---|---|---|---|---|---|---|---|---|---|---|---|---|---|---|---|---|
| 518 | J XVIII | Themisto | S/2000 J 1 | Thm | 7.4 | 0.34 | 44 | 130 | 134 | 13.3 | 12 | 17 | 21.0 | 9.0 | 3.46 | 4.5 | 9.31 | Thm |
| 506 | J VI | Himalia | -- | Him | 11.4 | 0.16 | 28 | 251 | 266 | 8.0 | 140 | 197 | 14.8 | 5.6 | 3.91 | 2.7 | 4.69 | Him |
| 507 | J VII | Elara | -- | Ela | 11.7 | 0.21 | 28 | 260 | 276 | 9.7 | 64 | 90 | 16.6 | 7.7 | 4.32 | 12.7 | 4.52 | Ela |
| 510 | J X | Lysithea | -- | Lys | 11.7 | 0.12 | 27 | 259 | 276 | 11.2 | 32 | 45 | 18.2 | 9.3 | 7.32 | 1.5 | 4.53 | Lys |
| 513 | J XIII | Leda | -- | Led | 11.1 | 0.16 | 29 | 241 | 255 | 12.7 | 16 | 23 | 20.2 | 10.9 | 5.70 | 3.8 | 4.89 | Led |
| 571 | J LXXI | Ersa | S/2018 J 1 | Ers | 11.4 | 0.12 | 29 | 249 | 264 | 16.0 | 3.5 | 5.0 | 22.9 | 14.7 | 4.71 | 16.7 | 4.72 | Ers |
| 553 | J LIII | Dia | S/2000 J 11 | Dia | 12.3 | 0.23 | 29 | 278 | 297 | 16.1 | 3.3 | 4.7 | 22.4 | 15.1 | 7.53 | 17.4 | 4.20 | Dia |
| 565 | J LXV | Pandia | S/2017 J 4 | Pdi | 11.5 | 0.18 | 29 | 252 | 267 | 16.2 | 3.2 | 4.5 | 23.0 | 14.4 | 4.21 | 5.8 | 4.67 | Pdi |
| 55509 | | | S/2011 J 3 | 1133 | 11.7 | 0.19 | 28 | 260 | 276 | 16.3 | 3.1 | 4.3 | 23.1 | 14.4 | 4.18 | 9.9 | 4.52 | 1133 |
| 55510 | | | S/2018 J 2 | 1832 | 11.4 | 0.15 | 28 | 250 | 265 | 16.5 | 2.8 | 3.9 | 23.3 | 15.0 | 7.89 | 17.0 | 4.71 | 1832 |
| 546 | J XLVI | Carpo | S/2003 J 20 | Crp | 17.0 | 0.42 | 53 | 456 | 510 | 16.2 | 3.2 | 4.5 | 23.0 | 14.5 | 5.25 | 1.6 | 2.45 | Crp |
| 55520 | | | S/2018 J 4 | 1834 | 16.3 | 0.18 | 50 | 428 | 474 | 16.7 | 2.5 | 3.6 | 23.5 | 15.2 | 11.61 | 0.9 | 2.63 | 1834 |
| 562 | J LXII | Valetudo | S/2016 J 2 | Val | 18.7 | 0.22 | 35 | 528 | 601 | 17.0 | 2.2 | 3.1 | 24.0 | 15.7 | 6.45 | 4.2 | 2.08 | Val |
| 512 | J XII | Ananke | -- | Ana | 21.0 | 0.24 | 148 | 630 | 550 | 11.7 | 25 | 36 | 18.9 | 10.6 | 15.52 | 3.8 | 2.27 | Ana |
| 527 | J XXVII | Praxidike | S/2000 J 7 | Pra | 20.9 | 0.25 | 148 | 625 | 547 | 14.9 | 5.8 | 8.2 | 21.2 | 15.2 | 11.44 | 20.9 | 2.28 | Pra |
| 524 | J XXIV | Iocaste | S/2000 J 3 | Ioc | 21.1 | 0.23 | 149 | 632 | 551 | 15.5 | 4.4 | 6.2 | 21.8 | 15.2 | 14.21 | 11.1 | 2.26 | Ioc |
| 530 | J XXX | Hermippe | S/2001 J 3 | Her | 21.1 | 0.22 | 150 | 634 | 553 | 15.5 | 4.4 | 6.2 | 22.1 | 15.9 | 13.58 | 22.0 | 2.26 | Her |
| 529 | J XXIX | Thyone | S/2001 J 2 | Thy | 21.0 | 0.23 | 148 | 627 | 548 | 15.8 | 3.8 | 5.4 | 22.3 | 15.1 | 12.61 | 0.3 | 2.28 | Thy |
| 522 | J XXII | Harpalyke | S/2000 J 5 | Har | 20.9 | 0.23 | 148 | 623 | 545 | 15.9 | 3.7 | 5.2 | 22.2 | 14.8 | 14.36 | 1.7 | 2.29 | Har |
| 545 | J XLV | Helike | S/2003 J 6 | Hlk | 20.9 | 0.15 | 154 | 626 | 547 | 16.0 | 3.5 | 5.0 | 22.6 | 15.3 | 12.10 | 3.8 | 2.28 | Hlk |
| 570 | J LXX | | S/2017 J 9 | 1739 | 21.8 | 0.20 | 156 | 666 | 577 | 16.2 | 3.2 | 4.5 | 22.8 | 13.5 | 8.25 | 1.7 | 2.16 | 1739 |
| 534 | J XXXIV | Euporie | S/2001 J 10 | Eup | 19.3 | 0.15 | 146 | 551 | 489 | 16.3 | 3.1 | 4.3 | 23.1 | 15.7 | 14.61 | 8.4 | 2.55 | Eup |
| 540 | J XL | Mneme | S/2003 J 21 | Mne | 20.8 | 0.25 | 148 | 620 | 542 | 16.3 | 3.1 | 4.3 | 23.3 | 14.8 | 11.89 | 1.1 | 2.30 | Mne |
| 55506 | | | S/2003 J 16 | 3316 | 20.9 | 0.24 | 148 | 623 | 545 | 16.3 | 3.1 | 4.3 | 23.3 | 15.1 | 12.47 | 2.7 | 2.29 | 3316 |
| 542 | J XLII | Thelxinoe | S/2003 J 22 | Tlx | 21.0 | 0.23 | 151 | 628 | 549 | 16.3 | 3.1 | 4.3 | 23.5 | 16.0 | 14.37 | 15.5 | 2.28 | Tlx |
| 533 | J XXXIII | Euanthe | S/2001 J 7 | Eua | 20.8 | 0.24 | 148 | 620 | 543 | 16.4 | 2.9 | 4.1 | 22.8 | 15.3 | 10.08 | 6.4 | 2.30 | Eua |
| 555 | J LV | | S/2003 J 18 | 3318 | 20.3 | 0.09 | 145 | 598 | 526 | 16.5 | 2.8 | 3.9 | 23.4 | 16.8 | 11.46 | 21.4 | 2.37 | 3318 |
| 564 | J LXIV | | S/2017 J 3 | 1733 | 20.9 | 0.23 | 148 | 626 | 547 | 16.5 | 2.8 | 3.9 | 23.4 | 15.4 | 13.49 | 4.4 | 2.28 | 1733 |
| 560 | J LX | Eupheme | S/2003 J 3 | Eph | 20.8 | 0.24 | 148 | 618 | 541 | 16.6 | 2.7 | 3.8 | 23.4 | 15.1 | 9.36 | 0.7 | 2.31 | Eph |
| 535 | J XXXV | Orthosie | S/2001 J 9 | Ort | 20.9 | 0.30 | 144 | 623 | 544 | 16.6 | 2.7 | 3.8 | 23.1 | 15.5 | 11.51 | 7.1 | 2.29 | Ort |
| 568 | J LXVIII | | S/2017 J 7 | 1737 | 21.0 | 0.23 | 147 | 627 | 547 | 16.6 | 2.7 | 3.8 | 23.6 | 15.8 | 14.55 | 6.7 | 2.28 | 1737 |
| 55501 | | | S/2003 J 2 | 332 | 21.0 | 0.23 | 150 | 629 | 549 | 16.7 | 2.5 | 3.6 | 23.7 | 16.3 | 10.57 | 2.1 | 2.27 | 332 |
| 554 | J LIV | | S/2016 J 1 | 1631 | 20.8 | 0.23 | 145 | 618 | 541 | 17.0 | 2.2 | 3.1 | 24.0 | 16.2 | 15.83 | 9.6 | 2.31 | 1631 |
| 55505 | | | S/2003 J 12 | 3312 | 21.0 | 0.24 | 150 | 627 | 548 | 17.0 | 2.2 | 3.1 | 24.0 | 14.6 | 2.45 | 2.0 | 2.28 | 3312 |
| 55514 | | | S/2021 J 3 | 2133 | 20.8 | 0.24 | 148 | 618 | 541 | 17.2 | 2.0 | 2.9 | 23.8 | 16.8 | 13.86 | 19.5 | 2.31 | 2133 |
| 55513 | | | S/2021 J 2 | 2132 | 20.9 | 0.24 | 148 | 625 | 546 | 17.3 | 1.9 | 2.7 | 24.0 | 17.0 | 4.13 | 23.4 | 2.28 | 2132 |
| 55512 | | | S/2021 J 1 | 2131 | 21.0 | 0.23 | 151 | 627 | 548 | 17.3 | 1.9 | 2.7 | 23.9 | 15.7 | 5.61 | 9.0 | 2.28 | 2131 |
| 552 | J LII | | S/2010 J 2 | 1032 | 20.8 | 0.25 | 148 | 619 | 542 | 17.4 | 1.8 | 2.6 | 23.9 | 16.1 | 9.26 | 3.7 | 2.30 | 1032 |
| 55523 | | | S/2022 J 3 | 2233 | 21.0 | 0.25 | 148 | 631 | 551 | 17.4 | 1.8 | 2.6 | 24.0 | 16.0 | 12.44 | 3.5 | 2.27 | 2233 |
| 511 | J XI | Carme | -- | Car | 23.1 | 0.26 | 165 | 734 | 628 | 10.6 | 42 | 60 | 17.9 | 10.3 | 16.24 | 13.5 | 1.99 | Car |
| 523 | J XXII | Kalyke | S/2000 J 2 | Klk | 23.3 | 0.26 | 165 | 742 | 634 | 15.4 | 4.6 | 6.5 | 21.8 | 15.4 | 16.04 | 3.2 | 1.97 | Klk |
| 520 | J XX | Taygete | S/2000 J 9 | Tay | 23.1 | 0.25 | 165 | 732 | 627 | 15.6 | 4.2 | 6.0 | 21.9 | 14.9 | 5.96 | 10.3 | 1.99 | Tay |
| 557 | J LVII | Eirene | S/2003 J 5 | Eir | 23.1 | 0.26 | 165 | 730 | 625 | 15.8 | 3.8 | 5.4 | 22.5 | 15.2 | 14.24 | 0.8 | 2.00 | Eir |
| 521 | J XXI | Chaldene | S/2000 J 10 | Cha | 22.9 | 0.27 | 165 | 724 | 620 | 16.0 | 3.5 | 5.0 | 22.5 | 15.2 | 7.42 | 9.4 | 2.01 | Cha |
| 526 | J XXVI | Isonoe | S/2000 J 6 | Iso | 23.0 | 0.25 | 165 | 726 | 622 | 16.0 | 3.5 | 5.0 | 22.5 | 15.5 | 15.65 | 3.0 | 2.01 | Iso |
| 525 | J XXV | Erinome | S/2000 J 4 | Eri | 23.0 | 0.28 | 164 | 728 | 624 | 16.0 | 3.5 | 5.0 | 22.8 | 15.2 | 13.99 | 6.8 | 2.00 | Eri |
| 531 | J XXXI | Aitne | S/2001 J 11 | Ait | 23.1 | 0.28 | 165 | 730 | 625 | 16.0 | 3.5 | 5.0 | 22.7 | 15.0 | 14.07 | 0.7 | 2.00 | Ait |
| 547 | J XLVII | Eukelade | S/2003 J 1 | Euk | 23.1 | 0.28 | 165 | 730 | 625 | 16.0 | 3.5 | 5.0 | 22.6 | 15.0 | 14.22 | 4.6 | 2.00 | Euk |
| 543 | J XLIII | Arche | S/2002 J 1 | Arc | 23.1 | 0.26 | 165 | 732 | 626 | 16.2 | 3.2 | 4.5 | 22.8 | 16.3 | 17.27 | 2.5 | 1.99 | Arc |
| 544 | J XLIV | Kallichore | S/2003 J 11 | Kch | 23.0 | 0.25 | 165 | 728 | 624 | 16.3 | 3.1 | 4.3 | 23.7 | 13.4 | 0.96 | 5.6 | 2.00 | Kch |
| 537 | J XXXVII | Kale | S/2001 J 8 | Kle | 23.1 | 0.26 | 165 | 730 | 625 | 16.3 | 3.1 | 4.3 | 23.0 | 15.4 | 15.25 | 1.9 | 2.00 | Kle |
| 563 | J LXIII | | S/2017 J 2 | 1732 | 23.0 | 0.27 | 165 | 725 | 621 | 16.4 | 2.9 | 4.1 | 23.5 | 13.8 | 7.60 | 1.6 | 2.01 | 1732 |
| 550 | J L | Herse | S/2003 J 17 | Hrs | 23.2 | 0.26 | 164 | 735 | 628 | 16.5 | 2.8 | 3.9 | 23.4 | 15.6 | 14.39 | 7.3 | 1.99 | Hrs |
| 551 | J LI | | S/2010 J 1 | 1031 | 23.2 | 0.25 | 165 | 737 | 630 | 16.5 | 2.8 | 3.9 | 23.3 | 16.2 | 7.33 | 13.8 | 1.98 | 1031 |
| 566 | J LXVI | | S/2017 J 5 | 1735 | 23.2 | 0.26 | 165 | 737 | 630 | 16.5 | 2.8 | 3.9 | 23.5 | 15.8 | 14.10 | 2.2 | 1.98 | 1735 |
| 55508 | | | S/2003 J 24 | 3324 | 22.9 | 0.26 | 165 | 722 | 619 | 16.6 | 2.7 | 3.8 | 23.8 | 14.9 | 7.90 | 0.2 | 2.02 | 3324 |
| 561 | J LXI | | S/2003 J 19 | 3319 | 23.2 | 0.27 | 165 | 735 | 628 | 16.6 | 2.7 | 3.8 | 23.7 | 16.3 | 15.42 | 0.2 | 1.99 | 3319 |
| 55518 | | | S/2016 J 3 | 1633 | 22.7 | 0.25 | 165 | 714 | 613 | 16.7 | 2.5 | 3.6 | 23.6 | 15.7 | 15.52 | 2.1 | 2.04 | 1633 |
| 572 | J LXXII | | S/2011 J 1 | 1131 | 23.1 | 0.27 | 165 | 733 | 627 | 16.7 | 2.5 | 3.6 | 23.7 | 16.8 | 15.74 | 9.6 | 1.99 | 1131 |
| 538 | J XXVIII | Pasithee | S/2001 J 6 | Pst | 22.8 | 0.27 | 165 | 719 | 617 | 16.8 | 2.4 | 3.4 | 23.2 | 16.6 | 14.96 | 6.4 | 2.02 | Pst |
| 55516 | | | S/2021 J 5 | 2135 | 23.4 | 0.27 | 165 | 748 | 638 | 16.8 | 2.4 | 3.4 | 23.6 | 16.5 | 15.08 | 6.2 | 1.96 | 2135 |
| 55503 | | | S/2003 J 9 | 339 | 23.2 | 0.26 | 165 | 737 | 630 | 16.9 | 2.3 | 3.3 | 23.7 | 16.0 | 15.01 | 0.1 | 1.98 | 339 |
| 55504 | | | S/2003 J 10 | 3310 | 23.6 | 0.26 | 164 | 755 | 643 | 16.9 | 2.3 | 3.3 | 23.8 | 14.1 | 4.40 | 1.4 | 1.94 | 3310 |
| 55521 | | | S/2022 J 1 | 2231 | 22.7 | 0.26 | 165 | 738 | 631 | 17.0 | 2.2 | 3.1 | 23.8 | 16.2 | 11.32 | 11.9 | 1.98 | 2231 |
| 569 | J LXIX | | S/2017 J 8 | 1738 | 22.8 | 0.26 | 165 | 720 | 617 | 17.1 | 2.1 | 3.0 | 24.0 | 17.1 | 11.25 | 12.6 | 2.02 | 1738 |
| 55517 | | | S/2021 J 6 | 2136 | 22.9 | 0.27 | 165 | 721 | 618 | 17.3 | 1.9 | 2.7 | 23.9 | 16.7 | 13.87 | 11.3 | 2.02 | 2136 |
| 55511 | | | S/2018 J 3 | 1833 | 23.4 | 0.27 | 165 | 747 | 637 | 17.3 | 1.9 | 2.7 | 23.9 | 16.8 | 17.55 | 8.8 | 1.96 | 1833 |
| 55515 | | | S/2021 J 4 | 2134 | 23.0 | 0.27 | 165 | 728 | 624 | 17.4 | 1.8 | 2.6 | 24.0 | 16.9 | 13.69 | 12.0 | 2.00 | 2134 |
| 55522 | | | S/2022 J 2 | 2232 | 23.0 | 0.27 | 165 | 782 | 662 | 17.6 | 1.7 | 2.4 | 24.0 | 15.5 | 1.84 | 7.1 | 1.88 | 2232 |
| 508 | J VIII | Pasiphae | 1908 CJ | Pas | 23.5 | 0.41 | 148 | 744 | 635 | 10.1 | 53 | 75 | 16.9 | 9.9 | 13.97 | 1.9 | 1.97 | Pas |
| 517 | J XVII | Callirrhoe | S/1999 J 1 | Clh | 23.8 | 0.30 | 145 | 759 | 646 | 14.0 | 8.8 | 12 | 20.8 | 13.9 | 12.02 | 24.3 | 1.93 | Clh |
| 519 | J XIX | Megaclite | S/2000 J 8 | Meg | 23.6 | 0.42 | 150 | 753 | 641 | 15.1 | 5.3 | 7.5 | 21.7 | 14.1 | 5.36 | 22.5 | 1.95 | Meg |
| 528 | J XXVIII | Autonoe | S/2001 J 1 | Aut | 23.8 | 0.33 | 151 | 761 | 647 | 15.5 | 4.4 | 6.2 | 22.0 | 16.0 | 12.97 | 26.8 | 1.93 | Aut |
| 539 | J XXXIX | Hegemone | S/2003 J 8 | Heg | 23.3 | 0.36 | 153 | 740 | 632 | 15.9 | 3.7 | 5.2 | 22.8 | 16.0 | 12.30 | 3.4 | 1.97 | Heg |
| 532 | J XXXII | Eurydome | S/2001 J 4 | Eyd | 22.9 | 0.29 | 149 | 717 | 615 | 16.2 | 3.2 | 4.5 | 22.7 | 17.1 | 14.58 | 20.7 | 2.03 | Eyd |
| 548 | J XLVIII | Cyllene | S/2003 J 13 | Cyl | 23.7 | 0.42 | 147 | 752 | 641 | 16.3 | 3.1 | 4.3 | 23.2 | 16.6 | 12.53 | 29.8 | 1.95 | Cyl |
| 567 | J LXVII | | S/2017 J 6 | 1736 | 23.2 | 0.34 | 150 | 734 | 628 | 16.6 | 2.7 | 3.8 | 23.5 | 15.7 | 14.53 | 17.0 | 1.99 | 1736 |
| 549 | J XLIX | Kore | S/2003 J 14 | Kor | 24.2 | 0.33 | 142 | 777 | 659 | 16.6 | 2.7 | 3.8 | 23.6 | 16.2 | 11.55 | 24.2 | 1.89 | Kor |
| 558 | J LVIII | Philophrosyne | S/2003 J 15 | Phi | 22.6 | 0.23 | 146 | 703 | 605 | 16.7 | 2.5 | 3.6 | 23.5 | 15.0 | 2.55 | 8.6 | 2.06 | Phi |
| 55502 | | | S/2003 J 4 | 334 | 22.9 | 0.33 | 148 | 718 | 616 | 16.7 | 2.5 | 3.6 | 23.5 | 14.9 | 8.57 | 1.1 | 2.03 | 334 |
| 536 | J XXXVI | Sponde | S/2001 J 5 | Spo | 23.5 | 0.32 | 149 | 748 | 638 | 16.7 | 2.5 | 3.6 | 23.0 | 17.5 | 10.64 | 20.9 | 1.96 | Spo |
| 55507 | | | S/2003 J 23 | 3323 | 23.8 | 0.31 | 145 | 760 | 647 | 16.7 | 2.5 | 3.6 | 23.9 | 17.4 | 16.18 | 18.6 | 1.93 | 3323 |
| 556 | J LVI | | S/2011 J 2 | 1132 | 22.9 | 0.36 | 152 | 718 | 616 | 16.8 | 2.4 | 3.4 | 23.6 | 16.2 | 12.74 | 4.4 | 2.03 | 1132 |
| 559 | J LIX | | S/2017 J 1 | 1731 | 23.7 | 0.33 | 146 | 756 | 644 | 16.8 | 2.4 | 3.4 | 23.8 | 17.1 | 15.69 | 19.9 | 1.94 | 1731 |
| 55519 | | | S/2016 J 4 | 1634 | 23.1 | 0.29 | 147 | 727 | 623 | 17.3 | 1.9 | 2.7 | 24.0 | 16.3 | 12.14 | 2.6 | 2.00 | 1634 |
| 509 | J IX | Sinope | -- | Sin | 23.7 | 0.26 | 157 | 759 | 646 | 11.1 | 33 | 47 | 18.3 | 10.5 | 9.29 | 11.7 | 1.93 | Sin |
| 541 | J XLI | Aoede | S/2003 J 7 | Aoe | 23.8 | 0.44 | 156 | 761 | 648 | 15.6 | 4.2 | 6.0 | 22.5 | 14.9 | 10.08 | 0.5 | 1.93 | Aoe |

Most Irregular moons are small objects: For each giant planet system, one Irregular is larger than 100 km; about 30 to 40 objects have diameters >10 km (9 or 10 in the Jupiter system), and all others are <10 km. The smallest objects might even be smaller than the largest known ring moonlets of Saturn.[37] Because of their small sizes, low albedos, and large heliocentric distances, almost all Irregular moons are very faint objects as seen from Earth. With apparent magnitudes between ∼15 and ∼27 (Table 6), large telescopes are required to

[37] Dubbed "propellers" (Tiscareno et al. 2010, 2019; Spitale and Porco 2010); these objects have never been regarded as "individual moons".

**Table 6** (*Continued*)

*Column notes:*

- The table provides orbital and physical properties, and JUICE-related numbers (based on orbit tour CReMA_5_0). Objects are ordered by orbit-dynamical groups (see also Table 7); with the object that gives the group its name highlighted in gray
- JPL ID [¶] ... JPL/SPICE identity; 5 digits for objects with no official IAU designation yet
- IAU desig. ... Object designation (and Roman numbering) by the International Astronomical Union (IAU)
- Moon name ... Object name
- Prov. desig. ... Provisional designation by the Minor Planet Center at first announcement, before numbering
- Abbr. (TD) [#] ... Object 3- or 4-character abbreviation (T. Denk scheme)
- $a$; $e$; $i$ [¶] ... Semi-major axis; orbit eccentricity; orbit inclination w.r.t. ecliptic plane (mean eclipic orbital elements; epoch: 2000-01-01.5 TDB; ephemeris: JUP344 (objects 506-55508); JUP346 (55509-55523))
- $P_{sid}$ [¶] ... Sidereal orbit period ("from star to star")
- $P_{syn}$ ... Synodic orbit period ("from new moon to new moon")
- $H$ [§] ... Absolute magnitude ($V$ magnitude (brightness) of an object if located 1 au away from the Sun and observed at 0° solar phase angle)
- Size ... Mean diameter; calculated from $H$ and $p_v$ (albedo): $D = 1$ au $\cdot(2/\sqrt{p_v}) \cdot 10^{-0.2\cdot(H-M_\odot)}$. $M_\odot = -26.71$ mag (apparent $V$ magnitude of the Sun; from Pecaut and Mamajek 2013). Since $p_v$ is mostly unknown, two values are given for each object (for $p_v = 6\%$ and 3%; inspired by Grav et al. 2015).
- Apparent mag. from Earth ($R$) [$] ... Apparent $R$ magnitude of the object as seen from Earth
- Apparent mag. from JUICE ($V$) ... Best $V$ magnitude of the object during the JUICE Jupiter approach and Jupiter orbit mission phases (19 Jan 2031 to 20 Dec 2034)
- Closest to JUICE ... Closest range between object and spacecraft during this timespan
- Revs from JOI to GOI ... Number of synodic revolutions of the object between Jupiter orbit insertion (21 Jul 2031) and Ganymede orbit insertion (20 Dec 2034)

*External sources (URLs):*

[¶] JPL SSD: https://ssd.jpl.nasa.gov/sats/elem/sep.html

[♯] T. Denk: https://tilmanndenk.de/wp-content/uploads/Moons_TDAbbrevs_JPL-ID.txt

[§] Minor Planet Center: https://www.minorplanetcenter.net/iau/NatSats/NaturalSatellites.html

[$] S.S. Sheppard: https://sites.google.com/carnegiescience.edu/sheppard/moons/jupitermoons

observe them from Earth. The Irregular Moons are so numerous because they are likely the result of continuous collisional grinding in the orbit of the central planet, which started from progenitor objects ("parent bodies") that had originated elsewhere in the Solar System and had then been captured (e.g., Jewitt and Haghighipour 2007; Nicholson et al. 2008; Bottke et al. 2013; Denk et al. 2018; Nesvorný 2018).

Although exceeding by far the other groups of regular satellites by number, the total mass of the Jovian Irregulars compared to all Jovian satellites is less than $10^{-5}$. Interestingly, the mass of Jupiter's Irregulars might be even smaller than that of the small inner Jovian moons. If combined into one single object, the Irregulars would form a sphere of ∼150 km, which compares for the small inner moons to a diameter of ∼180 km. The equivalent volume of the inner moons is about twice the volume of the Irregulars. The two largest objects in each group – Amalthea and Himalia – would each account for ∼82% of the volume of their respective groups; Elara and Pasiphae, the second and third largest Irregulars, ∼8% and ∼5% of the Irregular's volume, respectively. The masses of the Irregulars are not known. If the densities of Himalia and Elara were similar to the density of Amalthea, the inner moons' total mass would be higher than the total mass of today's Irregulars.

The Irregular moons are of scientific interest for similar reasons as the comets, Trojans, Centaurs, or Kuiper-Belt objects: Understanding them could provide further constraints on the various hypotheses and models of the formation of the Solar System. In a far future,

the Irregular moons might also serve as bases for crewed expeditions to the giant planets. JUICE observations will help to determine fundamental physical properties of many of the Jovian Irregular moons, in particular by means of photometric lightcurves.

While orbiting Saturn, the observation campaign of the Saturnian Irregulars by *Cassini* marked the first utilization of an interplanetary spacecraft for a systematic photometric survey of Irregular moons (Denk and Mottola 2019). The strategies developed for this effort will be used as guides for a possible planning of JUICE JANUS observations of the Irregular moons in the Jovian system.

Note that the terms "regular" and "irregular" do not refer to the non-spherical (irregular) shapes of these moons, but to the presumed formation history of the parent bodies. Contrary to the regular moons – in the Jupiter system the small inner moons and the Galilean moons –, it is believed that the Irregular moons formed far away from the gravity influence of the planet. They have later been captured by Jupiter and are thus "irregular members" of the Jovian satellite system. Because the Jovian Irregulars are always much farther from Jupiter than the regular moons, the terms "outer moons" and "Irregular moons" can be used interchangeably. This synonymity is also found at Saturn and Uranus, but not at Neptune where satellite Triton is believed to be a captured object (e.g., Cruikshank 1995; Agnor and Hamilton 2006) and thus of "irregular origin" as well. Further, it is unclear if satellite Nereid is a former regular moon or indeed a captured object (e.g., Goldreich et al. 1989; Nogueira et al. 2011). Since the nomenclature seems in general not well consolidated yet – for example, the wording "outer moon" is also sometimes used for objects like Callisto, Iapetus, or Oberon that are the outermost of the large moons of their respective planet –, for the purpose of this paper, we consider captured objects orbiting far away (many million kilometers) from the host planet, as well as their collisional remnants, Irregular moons. To distinguish from the other possible meanings, we handle the word "Irregular" like a proper name, writing it with a capital "I", like the capital letters in "Main Belt Asteroids" or "Near Earth Objects".

## 4.1 Brief Review of Knowledge

### 4.1.1 Irregular-Moon Discoveries

The first discovery of an outer moon in the Solar System was Saturn's Phoebe in 1899 (Pickering 1899a,b), this was the first satellite discovered using the relatively new technique of dry-plate photography. Only a few years later, the first Irregular Jovian satellites were found: On 03 Dec 1904 and 02 Jan 1905, Charles Perrine at Lick Observatory discovered objects J VI (Himalia) and J VII (Elara), respectively (Campbell 1905a,b; Perrine 1905a,b). Just another three years later, Philibert Melotte at Greenwich Observatory discovered the first retrograde Jovian moon, J VIII (Pasiphae, in 1908) (Cowell 1908; Cowell et al. 1908).

The next four Jovian Irregulars were all found by Seth Nicholson at Lick and Wilson Observatories over a time span of 37 years: J IX (Sinope, in 1914; recovered in 1938 after an observation hiatus of ten years), J X (Lysithea, in 1938), J XI (Carme, also in 1938), and J XII (Ananke, in 1951) (Nicholson 1914, 1938, 1939a,b, 1951). Beyond the Jovian system, only Neptune's Nereid had been discovered among the Irregular moons during that time (Kuiper 1949). With a diameter of ∼340 km, Nereid is the largest Irregular moon in the Solar System (leaving Triton aside) and comprises about two-thirds of the volume of all Irregular/outer moons combined. Finally (and back at Jupiter), Charles Kowal at Palo-

mar Observatory detected J XIII (Leda) in 1974[38] (Kowal et al. 1975). A further satellite, Themisto (J XVIII), had been spotted by Kowal and Elizabeth Roemer one year later,[39] but since no follow-on observation succeeded, this moon remained elusive for another 25 years. With 10 known objects plus a suspicious one, the era of Irregular satellite discoveries by photography with plates ended in 1997 with the first discovery of Uranian Irregulars in CCD images (Gladman et al. 1998).

We refer to the eight Jovian moons discovered between 1904 and 1974 as the "classical Jovian Irregulars". They are presumably the only Jovian Irregulars with diameters exceeding ∼15 km (Table 6). Similarly to the Galilean satellites for centuries, they were distinguished over many decades only by their numbers, but were eventually named by the IAU (International Astronomical Union) in October 1975.[40] The names are selected from the large pool of liaisons or daughters of the Roman god Jupiter or his Greek counterpart Zeus. As a naming scheme, it was decided that all Jovian Irregular moons on retrograde orbits would get names ending with an 'e', while the prograde-moon names would end with 'a' (e.g., Blunck 2010). This convention is still followed for new names of retrograde moons, and for prograde objects that are part of the Himalia group. For all other prograde Irregulars, names ending with 'o' are now adopted.

With the advent of large CCD sensors in combination with increasing computer power in the late 1990s, an unprecedented boom of Irregular-moon discoveries began. While 61 planetary moons were known before 1997, with 10 of them or 16% being Irregular moons (again excluding Triton), the count grew to 167 by 2007 – with 108 or 65% of them Irregulars. By far the most successful discoverers were the research groups of Scott Sheppard and David Jewitt in Hawai'i, and of Brett Gladman in Nice (France) and Vancouver (Canada). After a slack of a decade with just two new reports, another wave of announcements starting in 2017 increased the total number of known planetary moons in the Solar System to 288 in 2023 and to 419 in August 2025 – of which 357 or 85% are Irregulars. Key to this success was combining new data with older images from the 2000s and 2010s. For the Jupiter system, Scott Sheppard (now in Washington, DC) continued to lead the discoveries of the newly reported Jovian moons (Sheppard et al. 2023). Table 6 gives basic properties of 87 of the 89 known Jovian Irregulars,[41] Fig. 2 shows a visual concept of the system.

### 4.1.2 Previous Spacecraft (Non-)observations of Jovian Irregulars

Another part of history are past robotic missions to Jupiter, and how they observed (or not) the Irregular moons. The *Galileo* spacecraft, orbiting Jupiter between 1995 and 2003, did not observe any Irregular moon. Before final shutdown of the SSI camera in January 2002, there have been some opportunities at phase angles $<70°$ for prograde moons Himalia,

[38] IAU circ. no. 2702 (20 Sep 1974): Probable new satellite of Jupiter (discovery of object later named Leda), http://www.cbat.eps.harvard.edu/iauc/02700/02702.html • IAU circ. no. 2703 (01 Oct 1974): Probable new satellite of Jupiter, http://www.cbat.eps.harvard.edu/iauc/02700/02703.html • IAU circ. no. 2711 (24 Oct 1974): Jupiter XIII, http://www.cbat.eps.harvard.edu/iauc/02700/02711.html.

[39] IAU circ. no. 2845 (03 Oct 1975): Probable new satellite of Jupiter (discovery of object later named Themisto (J XVIII)), http://www.cbat.eps.harvard.edu/iauc/02800/02845.html • IAU circ. no. 2855 (23 Oct 1975): Probable new satellite of Jupiter, http://www.cbat.eps.harvard.edu/iauc/02800/02855.html.

[40] IAU circ. no. 2846 (07 Oct 1975): Satellites of Jupiter (JV - JXIII) naming. http://www.cbat.eps.harvard.edu/iauc/02800/02846.html.

[41] S/2017 J 10 (JPL ID 55525; Ananke group member; https://minorplanetcenter.net/mpec/K25/K25HL0.html) and S/2017 J 11 (55526; Carme group; https://minorplanetcenter.net/mpec/K25/K25HL1.html) have been announced after peer review.

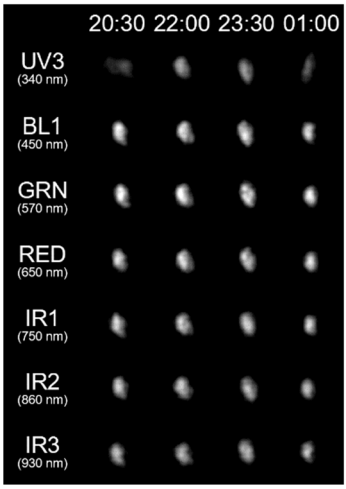


**Fig. 20** Four Himalia views in seven color filters, obtained with the *Cassini* ISS NAC from 18 to 19 Dec 2000, reveal a non-spherical shape of this moon. The complete observation campaign spanned ∼5 h. The images are calibrated, enlarged (with bicubic pixel interpolation); Himalia's disk size in the original images was ∼4 to 6 pixels. Some UV3 images are smeared because long exposures suffered from an attitude-control issue with the spacecraft (see text). Distance 4.44 Gm, pixel scale ∼27 km/px, solar phase angle ∼70°; the Sun illuminates Himalia from left. Exposure times: UV3 5.6 s; BL1 460 ms; GRN 120 ms; RED 90 ms; IR1 100 ms; IR2 320 ms; IR3 560 ms. Image IDs: N1355863292 (18 Dec 2000 20:30:01 UTC) to N1355880764 (19 Dec 2000 01:21:13 UTC)

Elara, and Lysithea where the objects would have appeared about two pixels in size for SSI. For example, the closest approach to any of the classical Jovian Irregulars occurred at Lysithea on 06 Apr 1999 (1.3 Gm range, 46° phase). However, due to the severe downlink limitations of the mission, observations had not been considered. Unresolved observations to obtain lightcurves, as was performed a decade later with *Cassini* at Saturn, were also not discussed. These would have been theoretically possible with the *Galileo* SSI camera, but not in practice under the limited tape-recorder space and downlink conditions. Furthermore, the pointing stability of the *Galileo* scan platform for long exposures appears questionable.

Opposite to *Galileo*, the ISS camera of the *Cassini* spacecraft observed Himalia from a distance of 4.4 Gm on 18 and 19 Dec 2000. The images show a tiny disk ∼4×6 pixels across (Denk et al. 2001; Porco et al. 2003) (Fig. 20). This corresponds to a visible cross-section of (150×120) ± 20 km. The geometric albedo was determined to be 0.05±0.01. No unambiguous bright or dark spots were obvious on the small disk. Due to a technical issue with the spacecraft at that time, attitude control was not on wheels, but on thrusters, which resulted in a reduced pointing accuracy with Himalia "bouncing around" from image to image. Nevertheless, since most of the observations had a short exposure time, almost all are of good quality.

*New Horizons*, while passing Jupiter, obtained images of Himalia and Elara between 27 Feb and 07 Mar 2007 at solar phase angles between 11° and 90° (Himalia; twelve observations) and between 21° and 91° (Elara; eight observations); these were taken from distances between 14.9 and 5.5 Gm (Himalia) and 11.8 and 5.8 Gm (Elara). In the data, the objects are barely resolved.

The two *Voyager* spacecraft passed Jupiter in March and July 1979. Closest approach to a classical Irregular moon was *Voyager-2* to Elara at 4.0 Gm distance and 111° phase angle

on 28 Jun 1979. The *Voyager Picture Catalog*[42] contains an Elara observation 10 h later, but it is unclear if the object has been hit. Among the numerous spots in the images, there is no "obvious dot" that might be attributed to Elara. However, this is not surprising: solar-phase angle during the observation was 116°, exposure time for the clear and color filter images 5.76 s – too short for a notable signal.

### 4.1.3 Basic Properties: Orbits

The orbits of the Jovian Irregular satellites are not closed in a Keplerian sense because of strong solar perturbations at such large distances from Jupiter. Based on semi-major axes and orbit inclinations averaged over a few thousand years (mean orbital elements),[43] the Jovian Irregulars can be divided relatively clearly into eight orbit-dynamical groups: four with retrograde orbits and four on prograde or "direct" orbits (with two of them containing just one single object; for a graphical representation of the $a$-$i$-space diagram, see also Fig. 1 in Palumbo et al. 2025, this collection). In the Solar System, such an unambiguous division for all known Irregulars is best observed at Jupiter.

The orbit-dynamical groups of the Jupiter system (Table 7) are designated after their largest member. Among the 13 known prograde objects, the Himalia group dominates with nine known members, including the two largest Jovian Irregulars (Himalia and Elara). With inclinations ∼28°, the orbit tilts are similar to the retrograde Ananke and Pasiphae group objects, except for the orbital direction. However, the distances of the Himalia group members to Jupiter are just half as large, with semi axes of ∼11.6 Gm. Themisto, so far the only object in its group, is even closer to Jupiter (7.4 Gm), but has a significantly higher inclination. Further out, but not as far from Jupiter as the retrograde moons, are the two known Carpo-group moons and the other standalone object, Valetudo.

Counting 76 objects, the four retrograde groups contain the majority of the Jovian Irregular moons: The *Carme group* has 31 known members; these are distinct from the other moons by their rather moderate orbital tilts against the ecliptic (∼165°) and by large semi-major axes (∼23 Gm). The *Ananke group* (27 objects) is slightly closer to Jupiter (∼21 Gm) and the members' orbit inclinations deviate more from the ecliptic (∼148°). The *Pasiphae group* contains 16 known moons; their semi-major axes (∼23.4 Gm) and orbit inclinations (also ∼148°) make some of these objects the outermost of the Jovian system. Their average orbit eccentricity of 0.34 is also higher than for the Ananke (0.23) and Carme (0.26) objects. Finally, Sheppard et al. (2023) noted that Sinope and small moon Aoede (J XLI) are somewhat dynamically unique with respect to their orbit inclinations and might thus be considered a separate sub group. Since a lack of togetherness is also supported by the very different spectral characteristics between Sinope and Pasiphae (e.g., Vilas and Hendrix 2024), we list Sinope and Aoede as a separate group here. They also belong to the outermost objects in the Jovian system. Other objects that might not belong to one of these groups because their semi-major axes or inclinations deviate noticeably from the group's average are the moons Euporie (J XXXIV) and S/2017 J 9 (J LXX; both Ananke group), and object Kore (J XLIX; Pasiphae group).

Because of the eccentric orbits and different semi-major axes, the velocities of the objects vary widely. Innermost prograde moon Themisto is fastest near periapsis passage when

[42] *Voyager* Picture Catalog, Jet Propulsion Laboratory (JPL) Regional Planetary Image Facility (RPIF), 08 Aug 1983.

[43] Mean elements (in this context) are the elements of a precessing ellipse which has been fit in a least squares sense to the numerically integrated orbit; https://ssd.jpl.nasa.gov/sats/elem/sep.html.

**Table 7** Orbit-dynamical grouping of the Jovian Irregular moons

| Largest object | Size [km] | # of obj. | End letter | Orbit dir. | $a$ [Gm] | [$R_J$] | [au] | [$R_{H,J}$] | $i$ [°] | $P_{sid}$ [d] | $P_{syn}$ [d] | $v_{Orb}$ [km/s] | Revs in tour | Abbr. (TD) |
|---|---|---|---|---|---|---|---|---|---|---|---|---|---|---|
| Themisto | 9 | 1 | o | pro | 7.4 | 103 | 0.049 | 0.14 | 44° | 130 | 134 | 4.14 | 9.3 | Thm |
| Himalia | 140 | 9 | a | pro | 11.6 | 162 | 0.077 | 0.22 | 28° | 255 | 272 | 3.31 | 4.6 | Him |
| Carpo | 3 | 2 | o | pro | 16.7 | 233 | 0.112 | 0.31 | 52° | 442 | 492 | 2.76 | 2.5 | Crp |
| Valetudo | 1 | 1 | o | pro | 18.7 | 261 | 0.125 | 0.35 | 35° | 528 | 601 | 2.60 | 2.17 | Val |
| Ananke | 29 | 27 | e | retro | 21.0 | 292 | 0.140 | 0.39 | 148° | 623 | 544 | 2.46 | 2.3 | Ana |
| Carme | 47 | 31 | e | retro | 23.1 | 323 | 0.154 | 0.43 | 165° | 733 | 627 | 2.34 | 2.0 | Car |
| Pasiphae | 58 | 16 | e | retro | 23.4 | 328 | 0.157 | 0.44 | 148° | 742 | 633 | 2.33 | 2.0 | Pas |
| Sinope | 35 | 2 | e | retro | 23.7 | 332 | 0.159 | 0.45 | 157° | 760 | 647 | 2.31 | 1.9 | Sin |

*Notes* (see also Table 1):

- Size – diameter of the largest group member. For objects >10 km, sizes are from Grav et al. (2015); for the smaller ones, they are estimated from their absolute magnitude $H$ and an albedo assumption of 0.05.
- # of obj. – number of known objects in this group (as of December 2025).
- End letter – ending letter of object names in this group: retrograde moons names end with 'e', progrades from Himalia group with 'a', others with 'o'.
- Orbit dir. – orbit movement direction (jovicentric); 'pro' = prograde or direct; 'retro' = retrograde.
- Orbital parameters are mean values of all group members; based on mean orbital elements from the JPL SSD website (https://ssd.jpl.nasa.gov/sats/elem/sep.html).
- $a$ – mean semi-major axis.
- $i$ – mean orbit inclination with respect to the ecliptic plane.
- $P_{sid}$ – mean sidereal orbit period ("star to star") in units of days.
- $P_{syn}$ – mean synodic orbit period ("full moon to full moon") in units of days.
- $v_{Orb}$ – mean orbit velocity.
- Revs in tour – average synodic revolutions around Jupiter during the 1248 days long orbit tour of JUICE (time span between JOI and GOI in tour CReMA 5_0).
- Abbr. (TD) – 3-character abbreviation used in this work (T. Denk scheme).

it reaches 5.9 km/s relative to Jupiter. At the outer edge, objects of the Pasiphae and Sinope groups may move as slow as ∼1.5 km/s near the apoapsis points of their orbits. The mean velocity of the Irregular moons is 2.5 km/s (see also Table 7). For comparison, the JUICE spacecraft's velocity relative to Jupiter near apojove of the first orbit is 0.72 km/s, and 17.5 km/s before start of JOI burn. The speed of Ganymede is 10.9 km/s.

The relatively well-defined orbit-dynamical grouping of the Jovian Irregulars leads to the hypothesis that the outer Jovian moons are collisional remnants of progenitor objects which were captured by Jupiter in the early days of the Solar System (e.g., Sheppard and Jewitt 2003; Jewitt and Haghighipour 2007; Nesvorný et al. 2007; Nicholson et al. 2008; Bottke et al. 2010; Nesvorný et al. 2014; Nesvorný 2018). If true, this would mean that the individual members of each group are part of a so-called "collisional family" and should share similar surface properties like colors, composition, or regolith characteristics. For example, these parent bodies could have originated in the outer parts of the Solar System and their collisional remnants could have subsequently filled a special dynamical niche to survive. In such a scenario, it is well possible that especially the smaller objects are not solid bodies, but rubble piles; i.e., they might be conglomerates of gravel, sand, and rubble, loosely bound by gravity. During the violent phase of the early Jovian system, Bottke et al. (2010) and Bottke et al. (2013) suggest that potentially up to 99% of the original material that made up the progenitor objects of the Jovian Irregulars was lost inward, being collected preferentially by Callisto with a possible thickness of several dozen to more than 100 meters.

Chen et al. (2024) modeled dust transport from the Jovian Irregulars inwards in detail. They were interested to learn about transport, final fate, and spatial distribution of these dust grains, especially the distributions and mass accretion rates on the Galilean satellites which act as particle sinks. They found that the mass production rate of the prograde Irregulars is higher than for the retrogrades because of the stronger effect of Jovian gravitational focusing on the impacting micrometeoroids and because of their larger overall cross-section. Among the ejecta particles controlled by Poynting-Robertson drag, about 50% of those originating from prograde Irregulars end on Callisto, about 20% on Ganymede, with the impact areas on the surfaces being nearly uniformly distributed. From the retrograde dust, almost all particles collide with Callisto's leading hemisphere. Chen et al. (2024) also calculated total mass influx densities for Callisto's leading ($2.8\times10^{-8}$ kg m$^{-2}$ yr$^{-1}$) and trailing hemispheres ($1.7\times10^{-8}$ kg m$^{-2}$ yr$^{-1}$).

### 4.1.4 Basic Properties: Bodies

Rather little is known about the physical properties of the Jovian Irregulars, and the majority of the publications so far concentrated on color or spectral measurements. First observations of Himalia by use of photoelectric photometers have been made in April 1970; they had the goal to collect photometric data for many Solar-System satellites in a standard system (UBV), and to seek for possible brightness variations which might indicate if an object rotates synchronously or not (Andersson and Burkhead 1970; Andersson 1974). In 1975, Cruikshank (1977) measured Himalia and Elara with the radiometer of the University of Hawai'i 2.2-m telescope on Mauna Kea in the thermal infrared at 20 μm. He found pitch-black bodies with extremely low albedos of 0.03 and determined their diameters to 170 ± 10 km (Himalia) and 80 ± 10 km (Elara).

**Colors** of the largest Jovian Irregulars from near-UV to near-IR wavelengths (UBVRI and VJHK) were studied by various groups also since the 1970s (Degewij et al. 1980a,b; Luu 1991; Sykes et al. 2000; Rettig et al. 2001; Grav and Holman 2004). Progradely orbiting Himalia has a "neutral" ("grayish") color that looks similar to C-type asteroids. Elara, Lysithea, and Leda, as the other large members of the Himalia group, were found to be spectrally similar to Himalia, suggesting a common progenitor object that was homogeneous in composition. On the other hand, Themisto, the innermost Jovian Irregular, resembles P-type objects and should not be related. For the five largest retrograde moons, a quite large diversity in color was measured. While Pasiphae appears only slightly redder than the prograde moons of the Himalia group and also resembles C-types, Ananke looks analogous to P-types, and Carme, Callirrhoe, and Sinope to D-types. With a spectral slope of $\sim 12\ ^{\%}/_{100\,\mathrm{nm}}$, Sinope appeared reddest among the observed Jovian Irregulars. Interestingly, Grav and Holman (2004) measured for Sinope a significantly different color than Sykes et al. (2000). They speculated that this moon might show color differences on its surface. JUICE JANUS observations will have the potential to confirm or deny this hypothesis.

In more recent times, Graykowski and Jewitt (2018) performed an optical color survey of 43 Irregular moons, 20 among them orbiting Jupiter. They measured absolute $R$ magnitudes ($H_R$) as well as B-, V-, and R-band colors, and found that the colors of the objects do not correlate with $H_R$. Differently to what is common in the Kuiper Belt, no ultrared matter ($B-R \geq 1.6$) was found among the Irregulars, leading to the conclusion that if the Irregulars were originating from the Kuiper Belt, some kind of color modification must have happened. The lack of ultrared Irregulars even at Neptune suggests that such a process should not be of thermal nature.

Visible and near-infrared narrowband **spectrophotometry** of the prograde objects Himalia, Elara and Lysithea and of the retrograde moons Pasiphae, Sinope, Carme, Ananke

and Callirrhoe has been obtained between 2006 and 2010 by Vilas and Hendrix (2024) using the MMT Observatory Red Channel spectrograph. The data again show the diversity between the objects and might suggest different origin regions in the Solar System, with Sinope significantly differing in composition from Pasiphae, seemingly arguing against a common parent body. The largest bodies of the Ananke and Pasiphae groups are suggested to have formed in the same region where C-type asteroids formed that populate the outer Main Belt today. Subtle spectral differences between the measured prograde moons of the Himalia group are interpreted by Vilas and Hendrix (2024) as different stages in aqueous alteration at the moment of breakup of the progenitor. They suggest that Himalia might have been the former core, Elara at a transition position between the core and an outer layer, and Lysithea farther from the center of the parent body, possibly at the surface (Fig. 10 in their paper shows a sketch). For the size of the progenitor body, Vilas and Hendrix (2024) speculate ∼300 km.

**Spectra** of nine Jovian Irregulars were presented by Bhatt et al. (2017) and Sharkey et al. (2023). SpeX/IRTF data from 0.8 to 2.4 μm were obtained of objects Himalia, Elara, and Carme (by Bhatt et al.; taken in 2012 and 2013), and of Pasiphae, Sinope, Lysithea, and Ananke (by Sharkey et al.; taken in 2018 and 2021); and MODS/Large Binocular Telescope data from 0.4 to 0.9 μm were obtained of Leda and Themisto (by Sharkey et al.; taken in 2018 and 2019). These works extend the spectral inventory of Jovian Irregulars down to a size of ∼10 km. In agreement with earlier work, all observed objects of the prograde Himalia group (Himalia, Elara, Lysithea, Leda) show more or less flat (C-type) spectra and might have retained their spectral similarity even after the presumed breakup event from a parent body. The reddish color of Themisto has been confirmed. For retrograde moons Pasiphae, Ananke, Lysithea and Sinope, a close spectral match with Jupiter Trojans, including targets of the *Lucy* mission (Levison et al. 2021) (3548) Eurybates (C-type), (617) Patroclus (P-type), and (11351) Leucus (D-type), was found. Furthermore, Sharkey et al. (2023) see reasonable near-IR spectral analogs between Pasiphae and Sinope on the one hand and Murchison CM chondrite meteorite material on the other hand, leading them to suggest that these objects might have been formed from similar material.

Based on measurements from NEOWISE data at IR wavelengths, Grav et al. (2015) published thermal model fits for the 11 objects Himalia, Elara, Lysithea, Leda, Ananke, Praxidike, Carme, Kalyke, Pasiphae, Callirrhoe, and Sinope, and determined **diameter and albedo** values. In agreement with previous work, they again established that the Jovian Irregulars are very dark; the albedos range from ∼0.06 down to ∼0.03. For Table 6, these two albedo values were selected for the object diameter calculations based on absolute magnitudes $H$. Table 8 shows a comparison of the Grav et al. (2015) results with size calculations based on $H$. The numbers appear in quite good agreement.

The (non-)existence of **$H_2O$ on the surfaces and inside** the Irregular moons is an important question because this has major implications for their formation history. For example, Hartmann (1987) argued for C-type asteroids to be the progenitor objects of the Jovian Irregulars (which implies them being dry), while more recently, Nesvorný et al. (2007) considered an origin from the trans-Neptunian area of the Solar System as a part of the Nice-model framework most likely (which implies water ice). Near-infrared spectra of Irregular satellites and Centaurs were taken by Brown (2000). While several objects, including Phoebe and Nereid, showed 1.5 and 2.0 μm absorption bands indicative of water ice, Himalia, Elara, and Pasiphae appeared spectrally featureless. A conclusion of that paper was that the Jovian Irregular moons are consistent with asteroidal origins, while the water ice on Phoebe is consistent with a formation as an icy planetesimal. Brown et al. (2003) and Chamberlain and Brown (2004) compiled a near-IR spectrum of Himalia from the *Cassini* VIMS data taken

**Table 8** Sizes of Jovian Irregular moons

| JPL ID | Name | Visible albedo $p_v$ Grav et al. (2015) (NEOWISE) | Size [km] Grav et al. (2015) (NEOWISE) | Size [km] from NEOWISE albedo and $H$ | Size range [km] for $p_v = 0.06 \ldots 0.03$ |
|---|---|---|---|---|---|
| 506 | Himalia | $0.057 \pm 0.008$ | $139.6 \pm 1.7$ | 143 | 140 ... 197 |
| 507 | Elara | $0.046 \pm 0.007$ | $79.9 \pm 1.7$ | 73 | 64 ... 90 |
| 510 | Lysithea | $0.036 \pm 0.006$ | $42.2 \pm 0.7$ | 41 | 32 ... 45 |
| 513 | Leda | $0.034 \pm 0.006$ | $21.5 \pm 1.7$ | 21 | 16 ... 23 |
| 512 | Ananke | $0.038 \pm 0.006$ | $29.1 \pm 0.6$ | 32 | 25 ... 36 |
| 527 | Praxidike | $0.029 \pm 0.006$ | $7.0 \pm 0.7$ | 8.4 | 5.8 ... 8.2 |
| 511 | Carme | $0.035 \pm 0.006$ | $46.7 \pm 0.9$ | 55 | 42 ... 60 |
| 523 | Kalyke | $0.029 \pm 0.014$ | $6.9 \pm 1.3$ | 6.6 | 4.6 ... 6.5 |
| 508 | Pasiphae | $0.044 \pm 0.006$ | $57.8 \pm 0.8$ | 62 | 53 ... 75 |
| 517 | Callirrhoe | $0.052 \pm 0.016$ | $9.6 \pm 1.3$ | 9.5 | 8.8 ... 12 |
| 509 | Sinope | $0.042 \pm 0.006$ | $35.0 \pm 0.6$ | 40 | 33 ... 47 |

*Notes:* Compared are (4th column) diameters from thermal modelling of NEOWISE data (from Table 3 in Grav et al. 2015) with (5th column) diameters calculated from absolute magnitudes $H$ as described in Table 6, but for the NEOWISE albedos (3rd column). The right column gives the diameter range calculated from $H$ for the albedo range 0.06 to 0.03, as given in Table 6 for all Jovian Irregulars. Objects are ordered by orbit dynamic groups.

in December 2000. Between 1 and 5 μm, the data show a slightly reddish spectrum with a possible absorption near 3 μm. This is suggestive of the presence of $H_2O$ or OH, and could also be due to hydrate minerals. The absence of water absorption features at 1.5 and 2.0 μm has been explained by a small grain size and by the presence of the dark non-water component. In 2013, Brown and Rhoden (2014) obtained a high-resolution Himalia spectrum from 2 to 4 μm with the NIRSPEC spectrograph of the Keck Observatory (Mauna Kea). This spectrum shows unambiguous evidence of an absorption at 3 μm and is very similar to the spectrum of asteroid (52) Europa. This asteroid is the main representative of a class of asteroids spectrally intermediate between asteroids showing evidence for aqueous alteration and (further away from the Sun) asteroids showing evidence for water ice (Takir and Emery 2012).

Even if the Jovian Irregulars appear as black as fresh asphalt, it may well be possible that they are mainly composed of water ice. Their upper crusts or regolith blankets might simply have lost all volatiles, with the consequence that the remaining refractory material, perhaps carbon-bearing, now dominates the colors and spectra of the surfaces. This is not surprising because dark material at Jupiter's distance from the Sun can be heated to above −110 °C (e.g., Cartwright et al. 2024 measured ∼170 K as the peak surface temperature on Callisto; see also Orton et al. 1996 for temperature measurements in the Jupiter system with the *Galileo* spacecraft, or Morrison 1977 for early radiometric observations). Such temperatures are too high to keep water ice stable over billions of years. Analogous to the process that formed the dark leading side on Iapetus (Spencer and Denk 2010), micrometeorite impact gardening of the upper decimeters of Jovian Irregular-satellite regolith and subsequent sublimation could have completely depleted the upper crusts from water. As a variation of this hypothesis, it might be speculated that some or all of the small Irregulars lost a signif-

icant fraction of their water ice and other volatiles during the re-assembly process after the putative destruction of the parent bodies.

A **rotation period** of an Irregular moon was first determined by Degewij (1978) and Degewij et al. (1980a). For Himalia, they determined a spurious period of 9.5 ± 0.3 h, recognizing this as a value "typical" for asteroids. The result was obtained by phasing lightcurves taken with a polarimeter during two consecutive nights of "variable, but generally poor, seeing" in November 1976 through 2.5 rotational cycles (Fig. 4 in Degewij et al. 1980a). Unluckily, the correct phasing of three cycles in that interval was discarded presumably because the lightcurves from the two nights looked too different to each other for the assumption of covering the same hemisphere of the object. Therefore, an incorrect Himalia period was established for more than 30 years. The correct value is 7.7819 h ± 2 s, with a lightcurve amplitude of 0.20 ± 0.01 mag (Pilcher et al. 2012) — still "typical" for asteroids.

From her CCD measurements of the classical Jovian Irregulars, Luu (1991) also deduced rotation periods for other Jovian Irregular moons. The data of Elara and Pasiphae did not reveal any periodicity, and no lightcurve compilation was attempted for Himalia and Leda. For Sinope, Lysithea, Carme, and Ananke, periods were found between ∼8.3 and ∼13.2 h; these are also "typical". The lightcurve amplitudes did not exceed 0.3 mag. Since this work compiled the lightcurves from rather short observations spanning over just one to three nights, and because all single-night lightcurves were shorter than the deduced periods, these rotation periods must be considered uncertain.

### 4.2 Irregular-Moons Observations of Saturn by Cassini ISS as the Role Model

The NASA *Cassini* spacecraft was the first mission that performed an extensive observation campaign of Irregular satellites from a vantage point inside the system of the moons' host planet (Denk and Mottola 2019). Especially during the second half of the mission (named "*Cassini* Solstice Mission"; from 2010 to 2017), the Irregular moons of Saturn (Denk et al. 2018)[44] were observed regularly with the ISS-NAC camera (Imaging Science Subsystem, Narrow Angle Camera; Porco et al. 2004) from quite large distances between ∼5 and ∼31 Gm. Observations of the Irregulars, which from those distances appear smaller than a pixel of the CCD sensor of the NAC, were performed for many hours at a time with a cadence of a couple of minutes to derive lightcurves. The good photometric quality of the NAC CCD – in particular its 100% fill factor, which enables accurate imaging of undersampled sources – helped achieving excellent results.

Collecting photometric lightcurves of Solar System objects to derive their physical and rotational properties has been a standard procedure in astronomy for more than a century (e.g., Müller 1897; von Oppolzer 1901),[45] with CCDs being used for this purpose for about four decades (e.g., Kristian and Blouke 1982; Wisniewski and McMillan 1987). It therefore makes sense as well to carry out such observations from spacecraft. Interestingly, there are similarities between the techniques used for spacecraft observations to those used by

[44] For Saturn's Irregular moons, see also T. Denk's website: https://tilmanndenk.de/outersaturnianmoons/.

[45] Egon von Oppolzer's short note in the *Astronomische Nachrichten* dated 09 Feb 1901 about brightness fluctuations of asteroid (433) Eros of more than 1 mag within a few hours acted as an unintentional kick-off for the first, admittedly still completely uncoordinated, lightcurve campaign of a minor body in the Solar System; it prompted no less than 15 reports on observations in professional journals within less than three months. Before that, brightness changes of minor bodies have mainly been attributed to varying solar phase angles. Alternatively, in the case of variable trails on photographic plates, clouds or other weather phenomena have been assumed (Wolf 1901), but rotation effects of the objects themselves were considered unlikely (e.g., Müller 1897, p. 375 ff.) – except for the long-known brightness dichotomy on Iapetus (Cassini 1677).

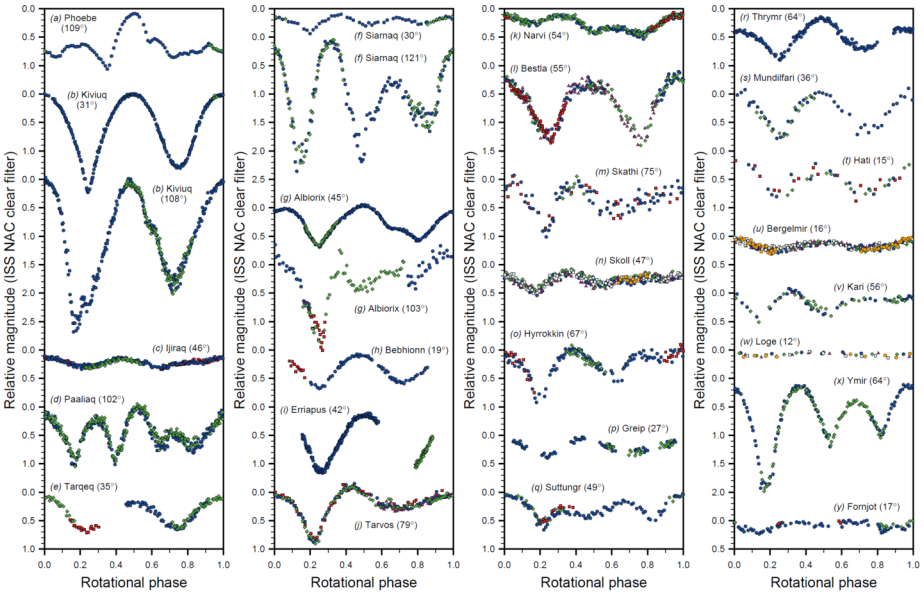


**Fig. 21** Lightcurves of 25 Irregular moons of Saturn from *Cassini* ISS NAC data. Observation phase angles are noted in brackets. Different symbols and colors indicate different rotational cycles from the same observation or from another observation close in time. Adapted from Fig. 2 in Denk et al. (2018)

amateur astronomers who also track individual minor bodies of the Solar System over long periods of time with small telescopes (e.g., Warner 2016). Of course, for the Irregular moons that are inaccessible to small telescopes from Earth, a spacecraft has the crucial advantage of its close-by location.

At the time of the *Cassini* mission, 38 Irregular moons of Saturn were known.[46] Most of them reached a maximum apparent brightness below ∼16 mag for at least a short period of time (a few weeks) during the mission. Because this brightness was above the ISS-NAC detection limit with a reasonable SNR, almost all could have been observed in principle by the spacecraft, allowing for an almost complete census of the rotation periods. However, 13 objects were not imaged because of inaccurate knowledge of their orbits at that point in time (Jacobson et al. 2012).

From the *Cassini*-NAC lightcurves, many physical properties of the Saturnian Irregulars could be derived. From just one single observation, if long enough (i.e., at least one lightcurve extremum can unambiguously be identified twice and correctly phased), the synodic rotation period can be deduced with an accuracy of a few percent. From the *Cassini* campaign (Denk and Mottola 2019), rotation periods of 25 objects have been determined (Fig. 21), of which just one (Phoebe) was previously known. The measured periods range from ∼5.5 h to ∼76 h (objects Hati and Tarqeq, respectively). Occasionally, color-filter observations were interspersed, allowing for simultaneous lightcurves at different wavelengths.

[46]This number increased to 122 in May 2023 (Ashton et al. 2023) and then further to 250 in Mar 2025 (Ashton et al. 2025). Announcements in the Minor Planet Center Newsletter: https://www.minorplanetcenter.net/media/newsletters/MPC_Newsletter_Jun2023.pdf (2023) and https://www.minorplanetcenter.net/media/newsletters/MPC_Newsletter_Mar2025.pdf (2025).

These measurements allowed searches for possible color variations on the surfaces, although none have been uniquely identified so far.

When observed multiple times under different viewing geometries, additional basic physical properties of the Irregular moons can be deduced. These include pole-axis orientations (to within a few degrees), sidereal periods, low-order convex-shape models, solar-phase curves (to constrain physical surface properties), semi-axes ratios ($a/b$, $b/c$), and object sizes, if an absolute calibration is available and if the albedo is known or can be estimated. From the *Cassini* data, 13 convex-shape models, pole solutions, sidereal periods, object shapes, object sizes, and phase curves have been calculated.[47] These Saturnian Irregulars were observed between 6 times (Hati; ∼200 images; ∼43 h of spacecraft activity time) and 26 times (Kiviuq; ∼2800; ∼393 h). The lowest phase angle for a lightcurve observation was 1° (Tarvos), the highest 143° (Siarnaq).

The *Cassini* data have shown that the Irregular Saturnian moons are very diverse with respect to their rotation periods and shapes (Denk et al. 2018), and the lightcurve amplitudes of different objects show enormous variations. The tendency of amplitude increase with increasing solar-phase angle known for asteroids was also found to hold for the Saturnian Irregulars. The lowest amplitude of 0.1 mag occurred during an observation of moon Loge at 12° phase, the largest was 2.6 mag, observed for Kiviuq at 108° phase angle (Denk and Mottola 2019). There are also numerous lightcurves departing from the common four extrema scheme (two maxima and two minima), and showing – especially at high solar phases – six or even eight extrema.[48] The high irregularities of the lightcurves seem to indicate that these bodies are not simple equilibrium figures whose shape is driven by spin, but rather by their formation mechanism and by their collisional evolution.

Because the technique of convex-shape lightcurve inversion (Kaasalainen et al. 2002b) mentioned above provides only an approximation of the convex hull of the bodies, i.e., a representation of the true shape as if "wrapped in foil", the derived models do not capture concavities like craters, saddles or constrictions. To retrieve such non-convex features, complementary observation techniques like stellar occultations or low-resolution disk-resolved imaging would be necessary. Lacking those measurements, the lightcurves and shape models of some Saturnian Irregulars might even be compatible with contact-binary configurations like Selam, the satellite of asteroid (152830) Dinkinesh (Levison et al. 2024), or even with binary moons (Denk et al. 2018).

### 4.3 Observations and Science of the Irregular Moons with JUICE

The final section on the Jovian Irregulars provides an overview of JUICE's scientific goals and the details of how to achieve them. It begins with a compilation of the benefits of observations with a spacecraft located inside the system. This is followed by a brief summary of the scientific objectives that can be pursued with JUICE. The following two sections describe in detail how the scientific instruments (especially JANUS) will perform their measurements and how the specific measurements might address the science questions. The potentials of an object search campaign are then briefly outlined. Finally, the potentials of a targeted flyby of a small Irregular moon are presented.

[47] Papers in preparation by S. Mottola and T. Denk.

[48] Six extrema show objects Ymir, Siarnaq, Hyrrokkin, Skoll, Kari, Suttungr, Narvi, and possibly Fornjot; eight shows Paaliaq.

### 4.3.1 Spacecraft Versus Earth-Based Observations

There are multiple advantages for using a "nearby" spacecraft for Irregular-moon research even if the objects remain unresolved. These advantages are not limited to JUICE, but apply in principle to any spacecraft in the vicinity of any planet with a system of Irregular moons.

• *Solar phase:* In principle, all values between 0° and 180° are possible from spacecraft, although in practice this range is smaller and depends on the orbit orientation of the moon. Table 6 lists the lowest phase angles for each Jovian Irregular as seen from JUICE; the range is from ∼30° down to almost zero phase. On the high-phase side, the apparent brightness poses a major limit, but straylight as well as instrumental and spacecraft constraints and flight rules may also become important. About 130° to ∼150° might be realistic for the largest objects. From Earth, the maximum phase angles are 12° at Jupiter, 6° at Saturn, 3° at Uranus, and 2° at Neptune.

• *Apparent brightness:* As seen from the spacecraft orbiting the host planet, the Irregular moons may appear >10 mag brighter than from Earth, and the Jovian Irregulars are on average ∼8 mag brighter for JUICE. This is a consequence of the closer range; which is for JUICE in the Jupiter system ∼35 to ∼700 times, and even more for spacecraft visiting the other giant planets. Of course, the Irregulars will also appear occasionally much fainter for the spacecraft than from Earth, sometimes >30 mag, when the phase angle is very high.

• *Reachable magnitudes:* Large telescopes with apertures of many meters on Earth might reach apparent magnitudes down to ∼24 (Jovian Irregulars; Table 6) or even ∼27 (at Uranus and Neptune where straylight is less severe) for low SNR detections, and observations useful for lightcurve measurements might work down to ∼22 mag. For telescopes of interplanetary spacecraft with modest apertures of ∼0.1 to 0.2 m, ∼20 mag objects can be detected, and sufficient SNR for lightcurves can be reached down to ∼17 mag. Because the gain from closer distance is ∼8 mag at Jupiter, especially the smaller Irregulars are easier to observe at high SNR from a small spacecraft telescope than from a large observatory on Earth.

• *180°-longitude ambiguity:* The Earth, the Sun, and the target object are usually located in one plane (approximately the ecliptic) for all ground-based observations. This leads to an ambiguity for the pole-shape solution, resulting in two pole directions ∼180° apart in ecliptic longitude (Kaasalainen and Lamberg 2006) that cannot be distinguished without other information like disk-resolved images or stellar occultations. As seen from a spacecraft, an Irregular moon may be imaged while far away from the ecliptic equator. Already a deviation of ∼10° for one observation might help to resolve this ambiguity (Kaasalainen and Ďurech 2007).

• *Weather:* Obviously, no weather phenomena hamper a spacecraft, and no clouds interfere with taking data. The observations are only limited by the intrinsic photometric stability of the instrument. This is particularly helpful for relative comparisons between objects, like relative sizes of shape models. If one absolute size is known, and if the effects of different albedos and colors of the moons can be estimated, then absolute sizes of all shape models can be determined.

• *Straylight:* From the ground, the host planet (Jupiter) is usually less than 3° away from the Irregular moons, which is a big issue while observing objects apparently ∼25 magnitudes or ∼10 billion times fainter than the planet. From the perspective of the orbiting spacecraft, the primary planet, a large moon or the Sun are mostly not located close in the sky while observing the Irregular moons.

• *Tracking duration:* Possible uninterrupted object tracking by spacecraft is in principle only limited by engineering requirements. For *Cassini*, the longest Irregular-moon targeting lasted more than 38 h. On Earth, the day/night cycle as well as the proximity of the objects

to the horizon while setting or rising sets a much shorter time span of ∼8 h or less for continuous observations.

• *Available observation time:* Suitable Earth-based telescopes or observatories in space like *HST*, *JWST* or the planned *Roman Space Telescope* are used for various research fields in astronomy and thus notoriously overbooked. A smaller spacecraft camera orbiting a planet is almost exclusively focused on the planet's system. Especially during apoapsis phases of the mission, there are often diminished spacecraft pointing requests, and the camera can therefore be pointed towards Irregular moons for long periods of time. For example, summing the *Cassini* observation times of the Saturnian Irregulars adds up to ∼19 weeks, a time allocation completely unrealistic for large telescopes on Earth and absolutely hopeless for space telescopes.

• *Viewing geometry:* Different viewing geometries at different ecliptic longitudes and latitudes are essential for accurate lightcurve inversion (Kaasalainen et al. 2002a). From the spacecraft, the geometry can sufficiently change within months or even weeks, while this takes years from Earth, or even more than a decade for Irregulars orbiting Uranus or Neptune. For a spacecraft observer revolving with the planet around the Sun, it is the orbital period of the object around the host planet that matters, while for ground-based observations, it is the orbital period of the planet around the Sun.

• *Appulses with stars:* Occasional apparent close encounters of the target with background stars (appulses) as the object travels across the star field, hamper the photometric measurements. Since an Irregular moon moves much faster over the sky when seen from the spacecraft than from Earth, possible appulses are much shorter. While such a geometry can make ground-based observations problematic over hours, for the spacecraft, appulses with stars are rather short, usually lasting at the order of several minutes.

• *Astrometry:* The operational lifetime of a spacecraft is rather short (years) compared to ground-based measurements (years to decades). Thus, the spacecraft does not contribute much to the determination of orbital periods, but rather to the shape and orientation of the orbits. For example, *Cassini* data of Saturn's Irregular moons increased the measurement accuracy to ∼500 km and even occasionally down to a few kilometers, while the Earth-based precision at Saturn is ∼2000 to ∼3000 km (Jacobson et al. 2022).

### 4.3.2 Science Objectives for the Irregular Moons Addressable with JUICE

The science objectives for the Jovian Irregulars for JUICE are very similar to those of *Cassini* for the Saturnian Irregular moons: determination of fundamental physical properties mainly through lightcurves. Each lightcurve provides a piece of the puzzle that helps to complete our picture of the giant planets and their moons, its physical processes and its history. The more rotational data we have, the better models can be built for the formation, evolution, internal structure and external forces on Irregular moons in the Solar system.

The JUICE mission Definition Study Report (ESA 2014) also notes the Irregular moons, in particular with the goal to obtain disk-resolved data. Most of the Cassini work was performed after publication of this report, thus its goals and methods to be used by an orbiting spacecraft were added later to the science activities of JUICE and JANUS.

As for *Cassini*, the emphasis of the JUICE observations lies on properties difficult or impossible to study from Earth, and the objects remain unresolved (sub-pixel) in almost all observations for all instruments.[49] For the JANUS camera (Palumbo et al. 2025, this

[49] Example for JANUS: Object diameter 5 km; range 10 Gm → apparent viewing angle 0.1"; geometrically, this target fills less than 1/1000 of the area of one JANUS pixel.

collection), these physical properties include rotation periods (synodic/ sidereal), colors (longitude-resolved), spin states (pole-axis directions), object shapes (convex-shape models), object sizes (relative between the objects, and if possible absolute), and absolute magnitudes $H$, surface roughnesses, particle sizes, etc. (solar-phase curves). JANUS images will also improve the orbital elements of the Irregular moons (astrometry), and could identify so far unknown objects within the population (moon search). Shape models and orbital parameters may also be refined if UVS (Retherford et al. 2026, this collection) might observe a stellar occultation in which an Irregular satellite passes in front of a UV-bright star.

Obtaining these properties for the individual objects is not only interesting per se, but also for allowing comparative studies between the Jovian Irregular moons. Furthermore, the JUICE observations will enable the Irregular-moon properties to be compared to those of other minor-body groups in the Solar System, including Main Belt and Trojan asteroids, Centaurs, Irregular moons of the other giant planets, Trans-Neptunian Objects, and comets. Color comparisons between Jovian Irregulars might reveal patterns between or within the dynamical groups.

The surface composition of Jupiter's Irregular satellites is also still largely unknown. For example, in the UV range of the electromagnetic spectrum, the most prominent feature of Phoebe and other Saturnian satellites is a sharp water-ice absorption edge near 160 nm (e.g., Hendrix and Hansen 2008a,b; Hendrix et al. 2010), which might be detected by UVS for the largest Jovian Irregulars.

Of very high interest is the science question of a possible contamination of the surfaces of the Galilean satellites by exogeneous material (e.g., ESA 2014), similar to what happens for Iapetus and Phoebe in the Saturn system (e.g., Denk et al. 2010; Tosi et al. 2010). Being the outermost and darkest Galilean satellite, Callisto is naturally suspected of being the most exposed to this type of contamination (Bottke et al. 2010, 2013; Chen et al. 2024; Cartwright et al. 2024). Close investigation of the surface composition of Callisto (Poulet et al. 2024, this collection), combined with observations of several Irregular satellites, could shed light on the question how compositional asymmetries between the leading and trailing hemispheres of Callisto might be related to contamination by retrograde and prograde Irregular satellites, respectively.

Science from a targeted flyby could in addition provide unique information on the surface composition, size, shape, and detailed surface characteristics (geological structures, craters, texture, etc.). Such a flyby with a minimum range of 5000 km is not scheduled at the time of this writing, but under investigation by the JUICE project (see Sect. 4.3.6 for a short discussion).

### 4.3.3 Observing the Jovian Irregulars with JUICE

For the JUICE mission, it is intended to perform a similar campaign for the Jovian Irregular moons with the JANUS camera as has been done with the *Cassini* ISS-NAC. The lessons learned with *Cassini* are of great benefit for JUICE (Sect. 4.2). Observations of the Jovian system by JUICE are currently planned to start on 19 Jan 2031, i.e., about six months prior to JOI (Boutonnet et al. 2024, this collection). Except for very limited early observations during cruise checkouts, this date may be considered as the potential start for the observation campaign of the Irregular moons. In the baseline orbit tour trajectory from 2025, JOI is planned for 21 Jul 2031, followed by the first and largest orbit of the spacecraft around Jupiter. The first return to the inner Jovian system (perijove 2) would then occur in early February 2032, with perijove 3 planned for no later than mid-April 2032. These first two orbits are likely most suitable for Irregular moon observations because the larger distances

to Jupiter and to the Galilean moons make this time frame generally less in demand for other remote-sensing requests. The remainder of the orbit tour until GOI in late 2034 is also well suited for potential Irregular-moon observations, but observation time in that phase of the mission will be more subject to competition. In principle, Irregular moon observations might be performed anytime during the orbit tour, but in practice, they will not happen while the spacecraft is near perijove or in the vicinity of an icy Galilean moon due to competition with the prime mission goals. Furthermore, the Jovian radiation belts would cause big problems for the envisioned long-duration exposures near JUICE's perijove passages. No observation will be considered after GOI.

For the **sub-pixel lightcurve observations** of Jupiter's Irregular moons **with JANUS**, the basic plan is to use the panchromatic (PAN) filter for all shutters except for dedicated color images. Observation duration might be several hours to more than 1.5 days. Image cadence will depend on the available data volume and might be on the order of several minutes. To keep data volume as low as possible, lossless compression and sub-frame recording appear particularly promising. The smallest possible sub-frame, with a size of $376 \times 128$ pixels (Fig. 22), has the potential to reduce the data volume by a factor of 64. The accuracy of the lightcurve data depends on object brightness. It is expected to be $\lesssim$0.1 mag for objects of apparent magnitude 16 or brighter. Background stars are not expected to interfere significantly unless the field is very crowded, like near the center of the Milky Way.

All but a few of the known Jovian Irregular moons are occasionally bright enough (brighter than the tentatively adopted limit of $\sim$17 mag; see Table 6) for being potential lightcurve observation targets for JANUS, with the very brightest ones — Himalia and maybe Elara, Themisto, Lysithea, Pasiphae — being potentially at reach even for UVS and MAJIS. Differently to the Saturnian moons for *Cassini*, it is expected that the target orbits will be sufficiently well known and that target aiming will not be an issue for JUICE even when recording the smallest possible sub-frames (Fig. 22). Final target selection may thus be based on considerations like visibility during the first two (least contested) orbits, object brightness, and scientific interest especially based on orbit groups. It appears very likely that more Irregular moon discoveries will be announced until JUICE arrival, but that some of their orbits will remain uncertain even until 2031. Because the current number of potential targets is already beyond what can be scheduled for JUICE, most of the newcomers might not be included in the plan. However, should a new object have intriguing properties – like inaugurating a new orbital group or experiencing an unusually close approach to JUICE – adding it to the observation list would be considered.

**Lightcurves** from photometric time series of sub-pixel sized objects by JANUS can provide numerous information on the objects themselves. First, a simple comparison between the shapes of lightcurves of different objects shows if they have a similar or a diverse appearance. Examples for moons looking very similar to each other are Saturn's Pallene and Methone. Their ellipsoidal shapes are consistent with fluid equilibrium shapes, and fluid-like behavior on geological time scales is considered a valid option for them (Thomas et al. 2013). Contrary to this, very diverse lightcurves have been found for the Irregular moons of the giant planets (e.g., Luu 1991; Denk and Mottola 2019; Farkas-Takács et al. 2017), implying that they must have very different and likely irregular shapes and that fluid-like behavior should not play a dominant role. This is also expected for the JANUS lightcurves, but we cannot be sure for the small objects which are likely collisional remnants and possibly rubble piles. Object appearances can be driven by surface albedo patterns or by object shape, or both; the lightcurves are indicators for this. For example, Phoebe's lightcurves are albedo-dominated, while the smaller Saturnian Irregulars show lightcurves with 2-maxima/2-minima or even 3-max/3-min patterns and are likely dominated by shape

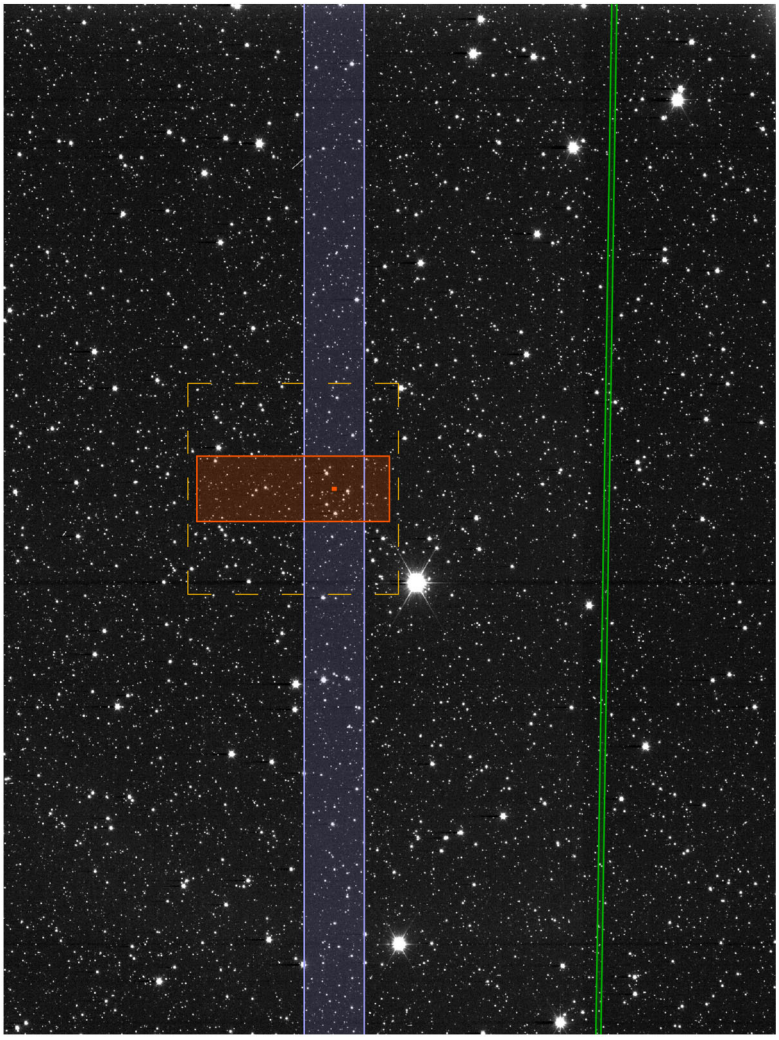

**Fig. 22** JANUS pointing for Irregular moons (illustration).
*Red frame:* Size of a 376×128-pixels sub-frame of JANUS (∼19×7 arcmin). *Blue lines:* Approximate position of the UVS slit. *Green lines:* Approximate position of the MAJIS slit at zero position. Through an internal scanning mirror, the potential field-of-view is larger than the complete JANUS FOV (see also Fig. 8). *Red dot:* Position of the aimed moon. *Dashed orange frame:* Size of the *Cassini* ISS NAC Field-of-View (21×21 arcmin; for comparison).
*Background:* JANUS PAN filter image acquired on 18 Jul 2023. RA/Dec = 299°/+59° (J2000; northern part of constellation Cygnus); the bright star near image center is HD 189276 ($V = 4.98$).
*Frames and instruments kernels* used for this illustration: juice_v39.tf, juice_janus_v08.ti, juice_majis_v08.ti, juice_uvs_v06.ti. See also ESA's JUICE operational SPICE kernel dataset: https://www.cosmos.esa.int/web/spice/spice-for-juice

(Denk and Mottola 2019). Comparing the amplitudes of numerous lightcurves (at similar phase angles) of Jupiter's Irregular moons to other groups of objects might indicate if there are fundamental shape differences between the objects. For example, for the Saturnian Irregulars (of sizes $\gtrsim$5 km), the mean lightcurve amplitude of 0.34 mag (for phase $<30°$) is

comparable to asteroids of similar sizes, implying that there is no fundamental difference between these groups with respect to their equatorial elongations (ratios of equatorial body axes; Denk and Mottola 2019). An important hint provided by lightcurves is which objects are the unusual ones. Extreme amplitudes, very complex lightcurve shapes, 3-max/3-min lightcurves at low phase, or unusual details like kinks might identify candidates for preferred follow-up observations from Earth, for example for stellar occultations for sub-satellite search. Among Saturn's moons, a prominent example is Kiviuq ($P_{Kiv} \sim 22$ h) which appears between 5 and 10 times brighter or darker every ∼5.5 h (Denk and Mottola 2019). Finally, **lightcurves in** different **color** filters can be intermingled with the regular lightcurve observations in the PAN filter to support composition determination, potentially revealing strong hemispheric color differences on the objects, if present. Furthermore, JANUS might obtain color data from smaller Irregulars, which are very difficult or impossible to be observed from Earth. Comparison of data of many objects within an orbital group might reveal insight on possible heterogeneities of the progenitors, or on objects that might not belong to the group despite similar orbital elements.

For the determination of **synodic rotation periods**, it is envisioned that as many objects as possible will be observed with JANUS at least once over a long time period, ideally for >1.5 d. Although JUICE is a solar-powered spacecraft, such long observations should be possible because the solar arrays have a large rotation flexibility around their axis (> 180°) so that they can adjust their orientation w.r.t the Sun direction. The observations for rotation period determination may be carried out in one go or with a few interruptions. The proposed duration of 1.5 d is rather arbitrarily chosen for practical reasons. Lightcurves for objects with a period $\gtrapprox$34 h will not or will just barely be completely covered, and such an observation would not lead to an unambiguous result. For context, among the Saturnian Irregulars two out of 25 objects have periods >1.5 d (Denk and Mottola 2019). The accuracy of the rotation periods should be a few minutes in most cases.

For the observation time selection, four criteria are of major importance:

• First is the apparent brightness (Fig. 23): The brighter the object, the better the SNR. Because brightness correlates well with solar phase angle, the moons are brightest when phase is lowest. The only, but rare exception is when object distance and phase angle are anti-correlated, and orbit eccentricity of the moon is high. In this case, the apparent magnitude might remain more or less constant, with the effects of phase and distance on apparent brightness canceling out each other. (This was, for example, the case for Saturnian moon Erriapus as seen from *Cassini*, see Fig. 2c in Denk and Mottola 2019.) However, *Cassini* data have shown that observations at higher phase in most cases exhibit larger lightcurve amplitudes, and these data often allowed an easier determination of the rotation period than flat lightcurves taken at low phase – the ANR (amplitude-to-noise ratio) is a more relevant quantity than the SNR. On the other hand, many objects are so small and dark that there might be only little flexibility in scheduling.

• Second criterion is that the observation should take place as early as possible in the mission. The smaller retrograde moons, in particular, have at most only two observation windows during the tour (Table 6; Fig. 23b). If at all possible, observations will be carried out during the first window.

• The third criterion involves avoidance of crowded star fields, as is the case when the object moves through the galactic plane. *Cassini* experience has shown that this point is not so critical for the brighter targets even close to the galactic center, but significant for the fainter ones; this constraint must thus be verified on a case by case basis. Early in the mission, including the Jupiter approach phase in early 2031, the low-phase opportunities fall near the direction of the Galactic center (right ascension ∼250° to ∼290°). Later in the

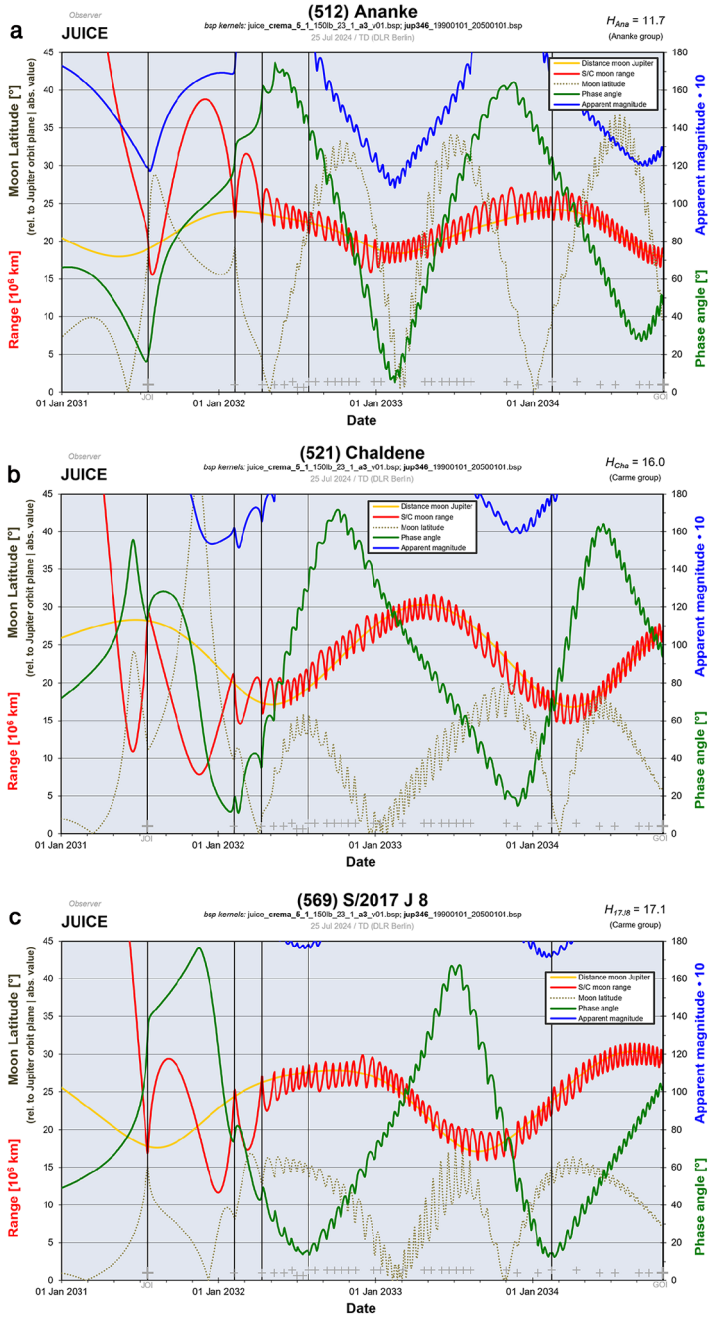


**Fig. 23** Visibility of Irregular moons (a) (512) Ananke ($H = 11.7$ mag), (b) (521) Chaldene ($H = 16.0$ mag), and (c) (569) S/2017 J 8 ($H = 17.1$ mag) from JUICE. Shown over time are the ranges of the objects to Jupiter (orange lines, scales on left axes) and to JUICE (red lines; left axes), the phase angles (green lines; scales on right axes), the predicted apparent magnitudes (blue lines; right axes), and the latitude of the objects relative to Jupiter's orbit plane as seen by JUICE (absolute values; gray dashed line; left axes). The magnitude scale ends at 18 because objects are unlikely to be suitable for JANUS lightcurve observations at times when they appear darker than 18 mag

mission, the zero-phase point shifts further west, and the Milky Way will almost never be an issue.

• Fourth and final, no engineering and other science activity that requires spacecraft pointing should take place at the chosen observation epoch. If so, an alternative time must be found.

Synodic rotation periods can be derived from lightcurves by determination of repetitive patterns and have the potential for lots of information. For example, if a spin barrier is seen in a sample, it might point to an object density limit. Or, there might be patterns like very fast or very slow rotators within a particular group. Although not expected, there might be resonances to other periods in the system. Among slow rotators, even tumblers might exist; this might give hints on the time frame of the last major collision. Finally, a statistical comparison to other minor-body classes like Saturn's Irregulars or the asteroids might be of interest, for example with respect to the significance of the YORP effect.

To achieve **pole/shape solutions and sidereal periods** for an object, the *Cassini* experience shows that at least six well-placed observations – better more – are required, ideally each covering a full rotation cycle. These should sample non-redundant topocentric Ecliptic longitudes to allow the unambiguous determination of the object's pole axis. Also, the observations should span at least 15° in topocentric Ecliptic latitude to provide a good constraint on the extension of the object in the z-direction (Kaasalainen and Ďurech 2007). Ideally, pole/shape solutions will be obtained for about one third to half of the objects which will be observed for synodic period purposes. The accuracies that might be achieved depend on the data sets and the individual objects' properties. Ideally, they can be accurate to within a few degrees and a few milliseconds. The method of retrieval of rotation states (sidereal periods), spin-axis directions, and convex approximations of the shapes of the objects is described by Mottola et al. (2023).

For multiple targets, possible patterns of non-random spin directions might be detected; for example, for asteroids, Hanuš et al. (2011) found relations of ecliptic latitudes to object sizes. The object shapes might tell something about the formation process. The shapes might resemble each other very much or might be diverse, or diverse but with patterns (as found for Saturn's Irregulars).[50] They might be smooth or complex, might show extreme object elongations, might show signs for binarity, might look similar for objects of similar sizes or not, etc. Finally, the shape solutions provide relative sizes between the objects; if one absolute size is known, all sizes can be determined as long as the influence of albedos and colors can be estimated.

For the determination of **phase curves** to obtain information on physical surface properties, JANUS observations at phase angles $>12°$ should be included because these phases are not accessible from Earth. Ideally, the covered phase range should be as large as possible with $\sim 20°$ to $\sim 30°$ increments, with the highest phase angles limited by an apparent magnitude of $\sim 17$. Observations near zero phase are also of high priority for determination of absolute magnitudes and thus object sizes as a function of albedos, or of albedo values if an absolute size is known. Many Irregular moons will not be visible at very low ($<3°$) or very high ($>60°$) phase angles due to geometric constraints by the orbit of the spacecraft with respect to the orbit of the moon, or because the objects will become too faint to be observable. A general goal is to get the broadest possible phase range for the objects. In most cases, the observation times selected for pole/shape should also provide a good data base for the phase curve. On the other hand, there might be some objects where observation scheduling is insufficient for pole/shape, but may be adequate for a phase curve.

[50] Paper in preparation by T. Denk and S. Mottola.

Observations with the **MAJIS** imaging spectrometer (Poulet et al. 2024, this collection) to investigate surface compositions of the Jovian Irregular moons will be challenging (but not impossible) because its IFOV of 150 μrad will not make it possible to spatially resolve the objects from the current baseline spacecraft trajectory. In this regard, the two main parameters driving the best opportunities for MAJIS are basically distance and phase angle. The phase angle must be $<90°$ to increase the dayside fraction and therefore the measurable signal. Potential MAJIS targets are thus the largest objects, and observations can be scheduled simultaneously to the JANUS lightcurve observations (Fig. 22). A close flyby of an Irregular moon would be of great benefit for MAJIS (see also Sect. 4.3.6).

For the Ultraviolet Spectrograph (**UVS**; Retherford et al. 2026, this collection), the low far-UV solar flux and small, dark nature of the satellites will also likely make observations difficult. The best prospect for UV reflectance measurements will involve long stares at large spacecraft distances from Jupiter, where the instrumental background from charged particle radiation is low. As for all remote-sensing instruments onboard JUICE, the Irregular moons will be considerably smaller than the $\sim 0.16° \times 0.1°$ UVS resolution element. However, the photon-counting ability of the instrument makes it possible that some UV spectral information may be obtainable for the largest objects using long stares, particularly since the spacecraft will be at a large distance from Jupiter during the observations, minimizing the instrument background from charged particles trapped within Jupiter's magnetosphere. As for MAJIS, UVS data can be sampled simultaneously to JANUS observations as well (Fig. 22).

To determine the feasibility of detecting a possible sharp water-ice absorption edge near 160 nm on Jupiter's Irregular satellites (see brief discussion in Sect. 4.3.2), we estimated the expected UVS count rate for observations of Himalia assuming either a constant 2% albedo across the UVS spectral range (consistent with the UV reflectance of various meteorite and lunar samples, e.g., Wagner et al. 1987), or an albedo of 2% at $<160$ nm and 4% at $>160$ nm to model the steep increase in reflectance at the $H_2O$ absorption edge. Assuming an angular diameter of 7", which Himalia exceeds in the current baseline trajectory in Jan-Feb 2032, and binning the spectrum to 10 nm spectral resolution, we find that the models with and without surface $H_2O$ (Fig. 24) should be distinguishable with a 2-h integration. Equivalent models of the next largest moon, Elara, suggest that stares longer than 6 h would be required to achieve similar spectral quality, assuming an angular diameter $>3.6$ "(potentially achievable in July 2031 and Feb-Mar 2032). Such stares do not need to be performed as single continuous observations but may be broken down into smaller sub-exposures as necessary. The other Irregular moons might be too small for UV observations to be practical, potentially requiring hundreds of hours of staring to build up significant UVS counts.

Additionally, UVS may contribute to studies of the shapes and orbits of the Irregular satellites using stellar occultation measurements, if suitable opportunities can be identified. During occultation events, UVS stares at a UV-bright star as it passes behind a target of interest. By measuring the precise times of ingress (when the star is first fully occulted by the satellite) and egress (when the star is detectable again following the occultation), UVS can determine the size of the target along the occultation path, refining shape models, while a comparison between the predicted and observed time of the occultation can be used to refine the orbital solution. A new catalog of almost 90,000 UV-bright stars has been produced to facilitate future searches for occultation opportunities (Velez et al. 2024). The distance between the observer and the target is not an important factor for stellar occultations, so in principle these measurements could be performed in the tour phase of the mission as well as during cruise.

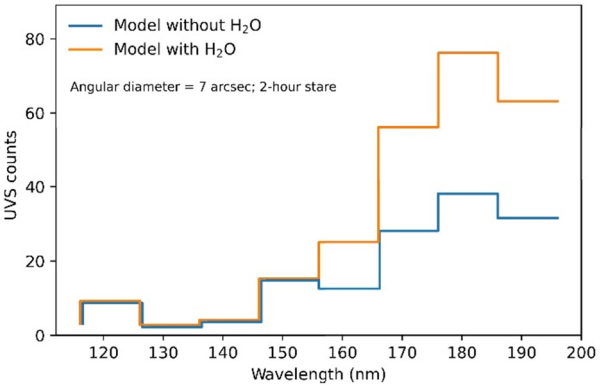


**Fig. 24** Modelled UVS spectra of sunlight reflected by Himalia, binned to 10 nm spectral resolution and assuming two spectral models: one (without $H_2O$) for which the albedo is 2% across the full UVS bandpass, and one in which the presence of $H_2O$ increases the albedo to 4% at wavelengths >160 nm

### 4.3.4 Astrometry of the Irregular Moons

Like for the inner moons, astrometric measurements of the Irregular moons of Jupiter will be performed with the JANUS instrument (ESA 2014). Here, the major difference for some of the Irregulars will be the availability of *Gaia* data (Tanga et al. 2023; Emelyanov et al. 2023), which are currently already providing high accuracy observations for the ten largest outer Jovian moons (Themisto, Leda, Himalia, Lysithea, Elara, Ananke, Carme, Pasiphae, Sinope, and Callirrhoe are within the *Gaia* limit of 20.9 mag; see also Table 6). The quality of the data depends on the apparent magnitude of the moon, but the typical Gaia astrometric precision is about 1 mas along scan direction, which is equivalent to 3 km at Jovian distance during opposition (Fig. 25). Because the *Gaia* mission has ended in 2025, the JANUS data will extend the time period of highly accurate positional measurements by seven to nine years. It is noteworthy that the high accuracy of *Gaia* data shows the need for a better computation of the correction between the photocenter and the center of figure (assumed to be identical with the center of mass) of these moons. Such calculations require a knowledge of the moons' 3D-shapes and ideally of the scattering laws of their surface. Hence, the photometric JANUS observation campaign of the Jovian outer moons will be necessary for reaching the ultimate JANUS astrometric precision, while benefiting from former data sets like *Gaia*.

An additional factor that will determine the precision of astrometric measurements by the JUICE onboard instruments is the accuracy of the JUICE spacecraft state vector. It is expected that its accuracy, as provided by the nominal mission trajectory determination means, will define the instrument (e.g., JANUS) positional contribution in the astrometry error budget. In addition to nominal mission operational assets of trajectory determination, contributions to the determination of the state vector will be provided by the radio science 3GM instrument (Iess et al. 2026, this collection) and PRIDE experiment (Gurvits et al. 2023). As demonstrated by the analysis conducted by Dirkx et al. (2017) and Fayolle et al. (2023; the latter specifically for the stellar occultation observed by JUICE), depending on the trajectory configuration 3GM and PRIDE will improve the accuracy of Jovian moons' ephemerides to a several tens of meters level in the 2030s. While the latter studies focused on the Galilean moons, their applicability to the improvements of ephemerides of the minor Jovian moons will be a subject of a separate investigation.

For the other Jovian Irregular moons fainter than 20.9 mag, JANUS data will be the best source of astrometric data to constrain their orbital motion. Following what has been experienced with the *Gaia* data, the ephemeris of the Irregulars will then drift very slowly

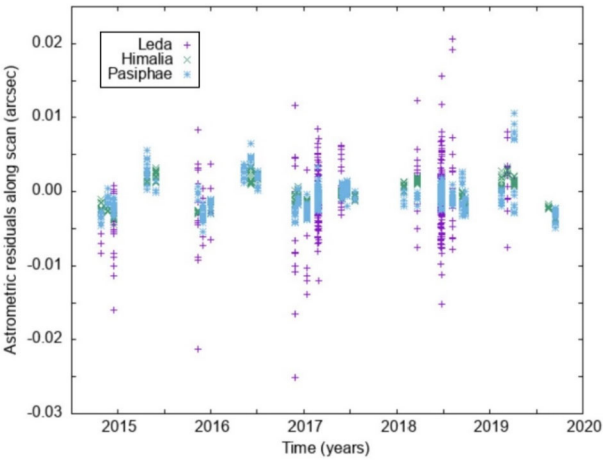


**Fig. 25** Astrometric residuals of three Jovian Irregular moons from the *Gaia* FPR catalogue (David et al. 2023). Such high accuracy is close to what JANUS will do. The combination of both datasets will provide a never achieved dynamical constraints on such kind of Solar-System objects

over time, if at least one orbital period is covered by JANUS data (which is equal to ∼0.4 to ∼1.8 years; Table 6).

Residing at more than ten million kilometers from Jupiter (Table 7),[51] the Irregular moons are hardly sensitive to the physics at play within the inner moons and Galilean systems. Still, two specific orbital features will be investigated. Following Emelyanov (2005), it will be possible to look for the determination of the mass of few of the outer moons, thanks to orbital modifications at the time of close encounters. The second feature will be to look for orbital wobbling, possibly associated with putative moonlets. Such an endeavor will rely on an analysis similar to the one used for discovering asteroid moons with *Gaia* data. While never discovered so far, the existence of moons of moons is well possible (Denk et al. 2018 argue in this direction for the Saturnian Irregulars), and its discovery would be a tremendous result for the JUICE mission.

On the practical side, JANUS sub-frame images (Fig. 22) shall be sufficient for astrometry, because the large number of images expected will certainly allow for numerous pictures with useful stars inside the field of view. In particular, astrometry does not require large series of images at a specific epoch, but a large time span. A bigger issue will be the accuracy of the photocenter on the images. Here again, lessons learned from *Cassini* are beneficial to JUICE. In particular, it has been shown that even with an under-sampled Point Spread Function, specific algorithms can still provide an accuracy of 0.2 pixel (Zhang et al. 2021). Such a technique of photocenter determination shall be applied to both the stars in the background and the Irregular moons. Finally, the accuracy of the spacecraft position itself will be important to guarantee the accuracy of the whole measurement. If for the inner system, the observation of mutual events may mitigate such error, it is extremely unlikely that mutual events will occur with outer moons. Because no specific radio-tracking will be planned at the time of the astrometric observations, one shall rely on the overall expected precision of the JUICE orbit which is estimated to be of several kilometers.

### 4.3.5 Potentials of a Search Campaign for Very Faint Irregular Moons

On approach to Jupiter and once within the Jovian system, it might be possible to conduct a search for additional small, faint Irregular moons with the JANUS camera. However, the

[51] The only exception being Themisto revolving at 5 to 10 Gm from Jupiter.

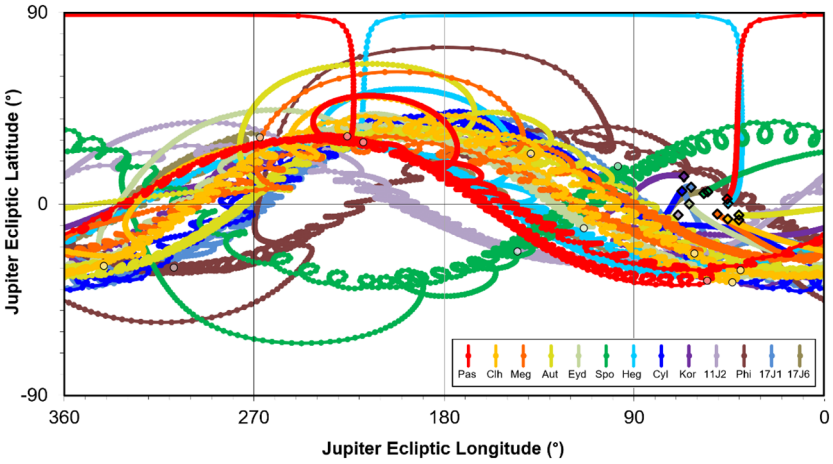


**Fig. 26** Sky map of the positions of 13 Pasiphae-group Irregulars as seen from JUICE in coordinates defined by Jupiter's orbit around the Sun. Time frame: 19 Jan 2031 (diamonds) to 18 Dec 2034 (open circles). Colors mark individual objects (see Table 6), the dots 00:00 UTC on each day. Primary movement direction of the objects is from left to right, the smaller loops are caused by the JUICE orbits. The almost polar locations of moons Pasiphae and Hegemone will be reached about five weeks before JOI when JUICE will be ∼24 Gm away from Jupiter during final approach

search strategy would differ from those performed from Earth, because of the much larger search area involved; remember that the spacecraft orbits inside the Irregular moon system.[52] Therefore, only search campaigns with specific goals seem appropriate. Fig. 26 shows the sky-projected positions of 13 Pasiphae-group objects from 2031 to 2034 as a proxy for potential locations of unknown objects.

Within the system, several long exposure images or image mosaics by JANUS, pointing towards the anti-Sun direction (the zero-phase point), could provide very deep imaging power, allowing the discovery of objects that would have an apparent magnitude of ∼29 if seen from Earth. The best that can in principle be expected with other devices from Earth or near Earth is $V$ ∼27.7 with the *Nancy Grace Roman Space Telescope* (Holler et al. 2018). Such a search might give a hint on the size-frequency distribution of sub-kilometer sized Jovian Irregulars. To this end, it is important to adopt an observation configuration in which Jupiter and the Galilean satellites are located behind the camera to minimize potential stray-light.

During Jupiter approach of the spacecraft in spring 2031, scanning the area of the orbit of innermost Irregular moon Themisto might reveal objects that reside too close to Jupiter to be detectable with Earthbased telescopes. However, the solar phase angle of this area during approach is >60°, resulting in a reduction of apparent Irregular-moon brightness of almost three magnitudes and thus making such a search less efficient, but likely still worthwhile.

### 4.3.6 Potentials of a Targeted Flyby

The JUICE mission might have the potential to enable a close (targeted) flyby of an Irregular satellite of Jupiter (ESA 2014), although none is in the current mission plan. In the past,

[52] From Earth near Jupiter opposition, the Hill sphere of Jupiter covers ∼73 deg$^2$, of which less than one fourth is occupied by satellites. The full sky (every sphere) has 41,253 deg$^2$, the JANUS FOV 2.2 deg$^2$.

**Table 9** First closeup (disk-resolved) views of minor bodies in the Solar System (selection)

| Object type | Date | Name | Size | Spacecraft |
|---|---|---|---|---|
| Near-Earth Asteroid | 14 Feb 2000 | (433) Eros | 17 km | *NEAR Shoemaker* |
| Martian moon | 01 Dec 1971 | Phobos | 22 km | *Mariner 9* |
| Main Belt Asteroid | 29 Oct 1991 | (951) Gaspra | 12 km | *Galileo* |
| Jupiter Trojan | 12 Aug 2027 | (3548) Eurybates | 69 km | *Lucy* |
| Giant planet small moon | 12 Nov 1980 | Janus, Epimetheus | 90 km | *Voyager 1* |
| Large Irregular moon | 11 Jun 2004 | Phoebe | 213 km | *Cassini* |
| Comet nucleus | 14 Mar 1986 | 1/P Halley | 11 km | *Giotto, Vega* |
| Kuiper-belt object | 01 Jan 2019 | (486958) Arrokoth | 18 km | *New Horizons* |

among all outer moons in the Solar System, only Phoebe, the largest Irregular moon of Saturn, has been visited by a spacecraft. During Saturn approach in June 2004, *Cassini* came within ∼2070 km of Phoebe's surface and obtained data with most onboard instruments; the best NAC images have a spatial resolution (pixel scale) of 13 m/px. During the following 13.2-year orbital tour, *Cassini* never again came close to an Irregular moon.[53] Other, just barely disk-resolved, observations of Irregular moons include *Voyager 2* imaging of Phoebe (1981) and Nereid (1989), *Cassini* imaging of Himalia (2000) and again Phoebe during the orbit tour (2004-2006 and 2015), and *New Horizons* imaging of Himalia and Elara (2007). However, since the spacecraft were more than two million kilometers away in all cases, the object disks only fill a few or a few dozens of pixels in the images. Furthermore, the four observed objects are among the five largest Irregular moons of the Solar System. The numerous small ones were never within reach of a closeup view.

Performing a close flyby of a small Irregular moon of Jupiter would be a first, and might be as scientifically revealing as the first close flybys and disk-resolved imaging of representatives of other groups of minor bodies in the Solar System (Table 9). Besides those visits, numerous additional small asteroids and comets have been visited and imaged by spacecraft,[54] but no small Irregular moon.

The science rationale for a nearby visit of a small Irregular moon would be very similar to the case for close encounters with asteroids and comets: Characterize an example of a unique and previously un-encountered class of objects. What does it look like? Is it a rubble pile, monolithic, or composed of multiple large monolithic shards? What is the albedo, surface composition, detailed shape, inner structure, mass, density?[55] Is it somehow magnetized? Might we see impact craters and possibly tell something about the formation epoch? Are there examples of contact-binary objects or even double moons within the population? Might differences in appearance (compared to inner Solar system objects) be directly attributed to a much weaker YORP effect at Jupiter distance? Is the object possibly accompanied by a dust ring or a rubble ring?

[53] As far as we know, the closest approach of the Cassini spacecraft to any Saturnian Irregular moon after Phoebe has been ∼420,000 km to object S/2019 S 24 on 01 Aug 2004. However, this ∼4-km sized object was unknown at the time; its discovery has been publicly announced more than 20 years later.

[54] https://en.wikipedia.org/wiki/List_of_minor_planets_and_comets_visited_by_spacecraft.

[55] With an ∼100-km altitude flyby at 3.7 km/s, a rough mass estimate (∼ ±30%) might be obtained from the JUICE 3GM gravity experiment for an ∼4-km sized and ∼1.4 g/cm$^3$ density object (Paolo Cappuccio, Sapienza Univ., *priv. comm.*).

One close flyby will likely be able to answer only a fraction of these questions, but even then, such encounter data would likely have the potential to directly influence hypotheses for the formation history of these objects, and how that history can be put into the context of the history of the Solar System. The latter is particularly interesting with respect to the question if or to what extent the dark refractory material on their surfaces is the source of the dark material covering the outer Galilean satellite Callisto and possibly Ganymede, as was suggested by Pollack et al. (1978), Bottke et al. (2013), and others, and was modeled in detail by Chen et al. (2024) (see Sect. 4.1.3). This question could be addressed in particular by the MAJIS spectrometer – but not from tens of thousands to millions of kilometers range because the sub-pixel appearance of Irregular moons would prevent reliable measurements of all but the very largest objects. JANUS, through high-resolution multi-color imaging of dark-material patches on the surface unaffected by possible water-ice contamination, could also provide impactful data. UVS measurements at $\leq$2 nm spectral resolution would be possible, showing water-ice and other volatiles absorption features (like $CO_2$, $SO_2$, $NH_3$), or revealing some carbonaceous and organic materials that exhibit broad absorption features or reflectance peaks in the 100-200 nm region (Hendrix et al. 2016), or constraining surface grain sizes of silicates through measuring gradual spectral slopes from UV to visible spectral regions (e.g., Cloutis et al. 2008). SWI would provide inputs to the thermophysical properties of the surface material and highly sensitive observations of spectral features of cold gases, like, e.g., water vapor.

In JUICE's reference trajectory CReMA_5_1, the closest approach to an Irregular moon is Kallichore (J XLIV; S/2003 J 11; member of the Carme group of retrograde moons)[56] during the first orbit on 07 Oct 2031 at a distance of 0.96 Gm (Table 6; Fig. 27; Fig. 28). With an estimated diameter of ~3 km and a suspected intense collisional history, Kallichore might be an object similar in structure to (162173) Ryugu (diameter 0.9 km), (152830) Dinkinesh (0.7 km), or (101955) Bennu (0.5 km). But the composition might be much different, as Kallichore may contain much more water ice and possibly have a much lower density. To appear larger than one pixel, Kallichore must be brought closer than ~0.1 Gm to the JANUS camera, and <10,000 km to MAJIS. At the time of the publication of this paper, the possibility of a minor moon flyby is being studied, Kallichore being the sole potential candidate target (Palumbo et al. 2025). The baseline trajectory for JUICE will be frozen in 2028 (Boutonnet et al. 2024).

## 5 Summary

This paper provides an overview of our current knowledge about Io, the four small inner moons of Jupiter, and the planet's numerous Irregular satellites. Furthermore, it describes in some detail the prospects for the JUICE mission while approaching Jupiter and while orbiting the planet over the four-year period from January 2031 to late 2034. There is currently no close flyby planned for any of the objects discussed here, although the option of a targeted flyby of one specific small Irregular moon (JXLIV Kallichore) is under investigation. The closest approaches to the objects discussed in our paper (for orbit tour CReMA_5_1) will be ~400,000 km to Io, ~450,000 km to one of the small inner moons (Thebe), and less than one million km to one of the Irregular moons (Kallichore). While the average observation range for Io and the small inner moons will be below one million kilometers during

[56]Discovery announcement in MPEC 2003-E29 (07 Mar 2003): https://www.minorplanetcenter.net/mpec/K03/K03E29.html; official designation and naming by the IAU WGPSN in IAU circ. no. 8502 (30 Mar 2005): http://www.cbat.eps.harvard.edu/iauc/08500/08502.html.

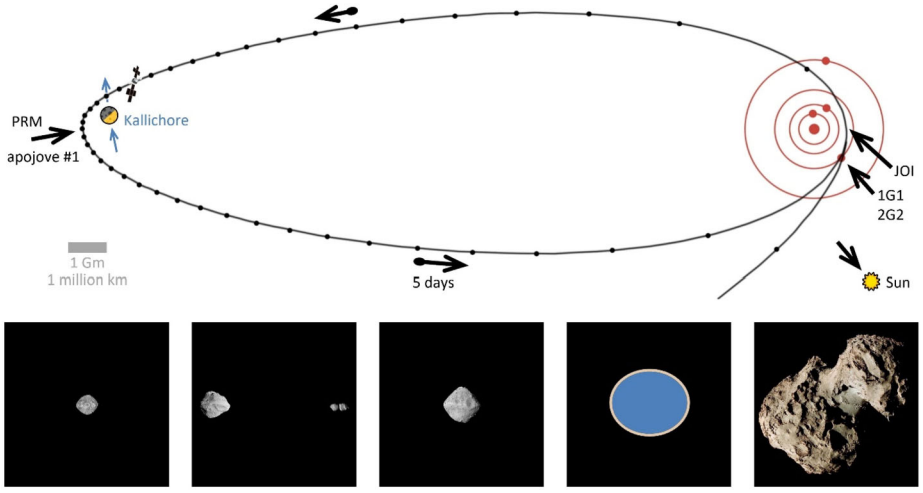


**Fig. 27** Sketch of first orbit of JUICE from about a week before Jupiter arrival until second Ganymede flyby (CReMA_5_1; with Ganymede and JUICE in a 29:1 resonance during first orbit). The approximate position of Irregular moon Kallichore on 07 Oct 2031 is indicated, the closest distance in the reference trajectory is 960,000 km. The approach of the spacecraft takes place over the unlit side of retrograde Kallichore, departure over the lit side. JOI and PRM (Perijove Raise Manoeuvre) are major trajectory corrections by the engine, 1G1 and 2G2 are the first and second Ganymede flybys. *Insets at bottom* (from left, to scale; the edge length of each box is 4 km): asteroids (101955) Bennu, (152830) Dinkinesh with contact-binary satellite Selam, (162173) Ryugu, small Jovian Irregular moon Kallichore (ellipse sketch), comet 67P/Churyumov-Gerasimenko

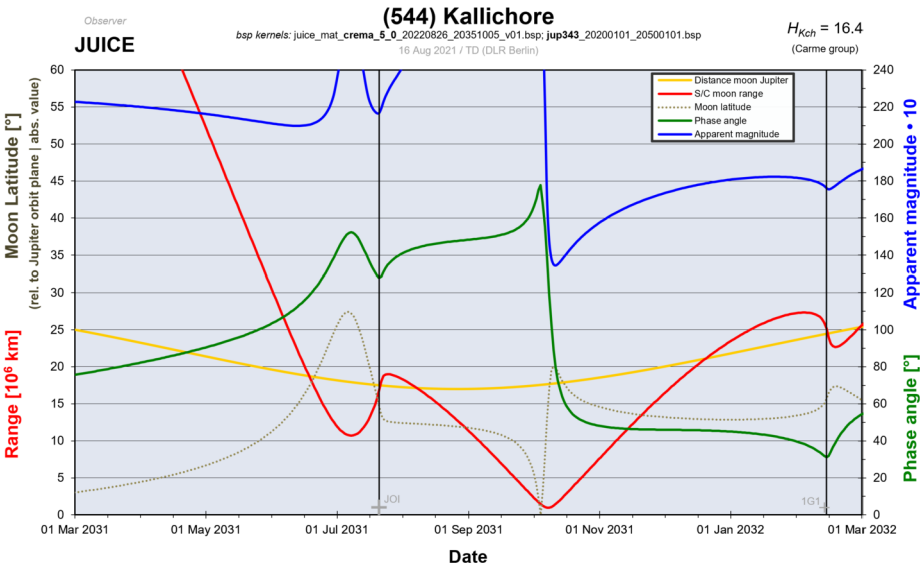


**Fig. 28** Visibility diagram for Irregular moon Kallichore (SPICE ID 544) from April 2031 to April 2032 (JUICE orbit tour CReMA_5_0). See Fig. 23 for meanings of the different curves. During the first orbit, JUICE comes closer than 1 Gm to this object. Note the rapid change in phase angle and apparent brightness. Approach is over the unlit side, departure over the lit side. The spacecraft will be more than 600 times closer to Kallichore and this moon will appear ∼10,000 times brighter than achievable from Earth. Before the October 2031 opportunity, Kallichore is brightest during Jupiter approach between 06 and 18 Jun 2031 when it reaches 21.0 mag (phase angle 107° to 118°; distance 27 to 19 Gm)

perijove passages of JUICE, the Irregulars will mainly be observed from more than 10 Gm, occasionally even at >20 Gm distance while the spacecraft is far away from Jupiter.

For the innermost **Galilean satellite Io** (Fig. 3, Table 2), the prime duty for JUICE will be distant monitoring of volcanoes, especially for the polar areas which are very hard to observe from Earth. In images of the JANUS camera, Io will appear with a size between ∼300 and ∼640 pixels – in data from the spectrometer MAJIS one tenth of this. Imaging Io while in eclipse (in Jupiter's shadow) will be performed from larger distances.

The JANUS tasks are to characterize the thermal activity, to determine the composition, surface changes and geological features, and to detect and monitor volcanic eruptions including hot spots and plumes at spatial scales down to ∼6 km/px and in the wavelength range from ∼0.4 to ∼1 μm. Furthermore, JANUS will monitor Io's sodium cloud, the aurora, and the interactions with Jupiter's magnetosphere.

MAJIS is planned to observe Io at spatial scales between ∼60 and ∼100 km/px and in the spectral range of 0.49-5.56 μm. It will be able to identify species like $SO_2$ frost, $S_2$, SO, $SO_2$ gas, NaCl, KCl, Fe-bearing salts, silicates, $FeS_2$, or iron sulfides. The sensitivity to monitor cooler volcanic features will be a major strength of the observations.

The Ultraviolet Imaging Spectrograph (UVS) will measure emission and absorption features of atomic and molecular species in Io's atmosphere, will observe time-variable auroral and airglow emissions of S, O, and Cl, and will map the $SO_2$ atmosphere. The Io surface will be monitored in reflected UV light to search for large-scale variations. The Io neutral cloud and plasma torus will also be monitored for composition and variability. Although the spatial resolution of *HST*/STIS is better than UVS, the JUICE UV spectrometer has the advantage to observe the nightside of Io, and the polar areas from more favorable emission angles.

The Submillimetre Wave Instrument (SWI) has its own pointing mechanism, which allows daily monitoring operations. The instrument measures at the two wavelengths of 250 and 500 μm and is thus sensitive to low-temperature thermal emissions. The spatial resolutions are ∼800 and ∼1600 km, respectively. The tasks are to explore Io's nightside atmosphere, to investigate the atmospheric chemistry, to determine and map the mean gas temperature and, if possible, the vertical structure (thermal profile, plume compared to hydrostatic structure), and to measure atmospheric dynamics. The detectable species include NaCl, KCl, isotopic ratios of oxygen, sulfur and chlorine, and yet undetected atmospheric species such as $O_2$, SiO, $S_2O$, CO, $H_2O$, $O_3$ and $H_2O_2$.

PEP (Particle Environment Package) will investigate plasma ions and electrons, energetic particles, and thermal and energetic neutral particles. From the JNA (Jupiter Neutrals Analyzer) observations, several characteristic quantities of the Io plasma torus will be derived. PEP-JENI could also detect ENAs directly emitted from Io's atmosphere.

The **small inner Jovian moons Metis** (mean diameter ∼43 km), **Adrastea** (∼16 km), **Amalthea** (∼167 km), and **Thebe** (∼99 km) (Fig. 1, Fig. 10, Table 3) reside in a very peculiar location of the Solar System. Their distances to Jupiter's cloud deck are very small (0.8 to 2.1 $R_J$), their orbital velocities are very fast (24 to 31.5 km/s, jovicentric), and fictitious forces act on the surfaces with the possibility that there are areas of negative acceleration, especially on Metis. Adrastea and Metis have orbits with very similar semi-major axes. They encounter each other every $25\frac{1}{4}$ days after $84\frac{2}{3}$ (Adrastea) and $85\frac{2}{3}$ Jupiter orbits (Metis) at a distance of just ∼1000 km. All four moons have shapes that deviate considerably from a sphere. Except for bright spots on the surfaces, the albedos are <0.1 and the colors are reddish.

JUICE observations will take place from altitudes of 500,000 km or larger. At this distance, the JANUS spatial sampling is ∼7.5 km/px, while MAJIS' is ∼75 km/px. As general

science goals can be stated the characterization of the objects (global properties), the characterization of the surfaces (local properties), formation history and evolution (as the overarching goal of most science activities), and high-accuracy astrometry. In the vicinity of the inner moons, a search for unknown objects within the orbit of Io is possible; this includes checking for the strange objects near Amalthea discovered by the Galileo spacecraft's star scanner (Fieseler et al. 2004).

In comparison to images of the small inner moons from previous missions, especially *Galileo*, the spatial resolutions will be roughly the same. In all other aspects, JUICE will be much superior because complete surveys with respect to solar phase (much wider range; constrain the surface regolith properties), colors and spectra (UV to IR; determine surface components), surface (geographic) longitude coverage (0° to 360°; geologic and albedo mapping), and polar views (sub-spacecraft latitudes north and south >20°; map polar areas) will be possible, plus astrometric observations at unprecedented spatial accuracies to refine the target's orbits.

With regard to the small inner moons, the JANUS observations are the main activities of JUICE. Among the other remote sensing instruments, UVS will search for characteristic signatures of water ice near 160 nm. MAJIS will observe Amalthea and Thebe tentatively at spatial scales <100 km/px; it is very advantageous for the quality of the data if the apparent size of the object exceeds one pixel. The higher-level goal is to find clues for the formation history – "circumjovian nebula (in situ)" versus "further away". SWI will likely observe Amalthea, seeking to reveal the thermal inertia of the upper few centimeters and the production rate of water vapor.

Astrometry (JANUS imaging) will also provide various information. It contributes to the determination of the shapes and orientations of the orbits of these four moons. Furthermore, masses and (from shape models) densities will be determined – are all small inner moons as "lightweight" as Amalthea? Even the internal mass distribution and homogeneity of the objects might be determined from the amplitudes of physical librations. Mutual event observations offer the possibility of performing an intersatellite astrometric adjustment, significantly reducing the impact of JUICE's position error.

The 89 **Irregular moons** make up the vast majority of the Jovian moons (Fig. 2, Table 6), with 85% of the known objects revolving on retrograde orbits. An orbit-dynamical subdivision into six groups and two single objects is summarized in Table 7. Their distances to Jupiter vary between ∼5 and ∼34 Gm.[57] The largest Jovian Irregular is Himalia with a size of ∼140 km (Fig. 20). About nine or ten objects are larger than 10 km, all others are smaller, with the smallest having diameters of less than 2 km. The surfaces are as black as fresh asphalt. The colors of the large objects vary between "grayish" ("neutral") and "reddish" (Sinope's spectral slope was measured to ∼12 $^{\%}/_{100\,\mathrm{nm}}$). Observations in the near-IR indicate the presence of $H_2O$ on Himalia. Eight objects have been observed by JWST in January 2024, revealing significant differences between each other.

The closest approaches of JUICE (baseline trajectory from 2023) will be ∼1 Gm (Kallichore) and ∼2.5 Gm (S/2003 J 12 and Philophrosyne). As far as the largest closest distances are concerned, JUICE will never come closer than ∼17 Gm to object Arche.

JUICE's primary observing instrument for the Irregulars will be the JANUS camera. The observation strategy will be similar to *Cassini*'s for the Irregular moons of Saturn (Denk and Mottola 2019): Repeated imaging over a long time span (potentially tens of hours) of the unresolved objects to compile lightcurves using time windows when the spacecraft has

[57] Themisto at perijove: ∼5 Gm or ∼70 $R_J$; Aoede at apojove: ∼34 Gm or ∼480 $R_J$ or ∼0.64 $R_{H,J}$ or ∼0.23 au.

no other strict primary attitude requirements. Best, but not exclusive observation times for JUICE with respect to scheduling will be early in the mission during the large first and second orbits when the spacecraft will be far from perijove passages for many weeks or even months.

The science objectives for JUICE are part of the overarching fundamental question on planetary system formation and evolution, and will in particular address the determination of basic physical properties of Jovian Irregular moons with emphasis on properties difficult or impossible to study from Earth. For JANUS, lightcurves might reveal rotation periods (synodic or sidereal), spin states (pole-axis directions), object shapes (convex-shape models), and object sizes (relative between the objects; absolute if albedos are known, or if other size constraints are available for some objects). The observations might also address to a certain extent the quest for contact-binary or binary moons. Solar-phase curves over a wide range of phase angles (surface regolith properties), absolute visual magnitudes $H$, and surface colors (longitude-resolved) will also be obtained. Almost all known Jovian Irregulars will in principle be within reach of JANUS (Table 6). Observing numerous different targets allows building up statistics and searching for patterns like a possible fast-spin barrier, like possible non-random distributions of rotation periods or pole directions, and like color-correlations or non-correlations (or outliers of individual objects) within orbit-dynamical groups, and so on. Color comparisons to the dark material on the surfaces of Callisto and Ganymede are also very important. For the spectrometers MAJIS and UVS, the largest object Himalia and maybe Elara and Pasiphae will be within reach (and Kallichore, if the close flyby option will be chosen), providing information on surface water, the surface composition in general, and will allow for an even higher level comparison to the dark materials on the outer Galilean satellites than possible with JANUS alone. Finally, all the results can be compared to those of the other populations of minor bodies in the Solar System, namely Trojans, Hildas, Centaurs, KBOs, comets, Main Belt Asteroids, and other giant-planet Irregular moons.

JANUS images will also improve the orbital elements of the Jovian Irregulars. Here, the data do not contribute much to the orbital periods, but significantly to shape and orientation of the orbits. There might be a chance to determine the masses of the largest objects. For a search for hitherto undetected objects, the geometric conditions are not favorable because JUICE will be inside the system of the Irregular satellites which distributes them over half of the sky as seen from the spacecraft. Nevertheless, there might be opportunities to search for members of a possible group of innermost satellite Themisto, or to do a "deep search" on a small area in the sky near the anti-Sun point to get a size-frequency statistics of sub-kilometer sized moons. Finally, a targeted flyby at Kallichore in early October 2031 is under investigation. Should this encounter be added in 2028 to the final baseline orbit trajectory, it would open access to a trove of new information.

Especially due to its close proximity to the Jovian moons, the unique viewing perspective from outside the ecliptic plane and at Solar-phase angles $>12°$, and the relatively good availability of observation time compared to ground-based or near-Earth space-based telescopes, JUICE will take a key role in the early 2030s for observations of Io, the small inner moons of Jupiter, and the Jovian Irregulars. The expected data set is likely to remain unique for a long time to come.

**Acknowledgements** JUICE is a mission under ESA leadership with contributions from its Member States, NASA, JAXA and the Israel Space Agency. It is the first Large-class mission in ESA's Cosmic Vision programme. Part of this work was carried out at the Jet Propulsion Laboratory, California Institute of Technology, under contract with NASA. Co-authors from Italian institutes acknowledge support from Italian Space Agency under ASI-INAF agreement n. 2023-6-HH.0. V. Lainey, E. Lellouch, B. Cecconi, and R. Moreno acknowledge support from CNES (Centre National d'Etudes Spatiales). P.M. Molyneux, K.D. Retherford, G.R.

Gladstone, and T.K. Greathouse acknowledge NASA funding supporting the UVS team for ESA's JUICE mission. A. Solomonidou acknowledges support from the Hellenic Space Center. H. Huybrighs' work at DIAS was supported by a DIAS Research Fellowship in Astrophysics and by Taighde Éireann – Research Ireland award 22/FFP-P/11545; he also gratefully acknowledges financial support from Khalifa University's Space and Planetary Science Center (Abu Dhabi, UAE) under Grant no. KU-SPSC-8474000336. L. Roth acknowledges support from the Swedish National Space Agency through grant 2024-00112. F. Tsuchiya is supported by the JSPS KAKENHI (grant number 20KK0074). T. Van Hoolst acknowledges support by the BRAIN-be 2.0 programme of the Belgian Federal Science Policy Office and by the Belgian PRODEX program managed by the European Space Agency in collaboration with the Belgian Federal Science Policy Office. P. Thomas thanks Brian T. Carcich (Latchmoor Services, INC) for assistance in generating shape model products shown in Fig. 13 and 14. We gratefully thank two anonymous reviewers and the editor Frank Schulz for their very valuable help in improving the manuscript.

**Funding Information** Open Access funding enabled and organized by Projekt DEAL.

## Declarations

**Competing Interests** The authors declare that they have no competing financial or non-financial interests to declare that are relevant to the content of this article. C. Tubiana, C. Vallat, and O. Witasse are Guest Editors of the collection "ESA's Jupiter Icy Moons Explorer (JUICE): Science, Payload, and Mission", but were not involved in the peer review of this article.



## References

Adriani A, et al (2017) JIRAM, the Jovian infrared auroral mapper. Space Sci Rev 213:393–446. https://doi.org/10.1007/s11214-014-0094-y

Agnor CB, Hamilton DP (2006) Neptune's capture of its moon Triton in a binary-planet gravitational encounter. Nature 441:192–194

Anderson JD, Johnson TV, Schubert G, Asmar S, Jacobson RA, Johnston D, Lau EL, Lewis G, Moore WB, Taylor A, Thomas PC, Weinwurm G (2005) Amalthea's density is less than that of water. Science 308:1291–1293

Andersson LE (1974) A photometric study of Pluto and satellites of the outer planets. Ph.D. thesis, University of Indiana, Bloomington, IN. https://core.ac.uk/download/pdf/213846436.pdf

Andersson LE, Burkhead MS (1970) Observations of the satellite Jupiter VI. Astron J 75:734

Archinal BA, Acton CH, A'Hearn MF, Conrad A, Consolmagno GJ, Duxbury T, Hestroffer D, Hilton JL, Kirk RL, Klioner SA, McCarthy D, Meech K, Oberst J, Ping J, Seidelmann PK, Tholen DJ, Thomas PC, Williams IP (2018) Report of the IAU working group on cartographic coordinates and rotational elements: 2015. Celest Mech Dyn Astron 130:22

Ashton E, Beaudoin M, Gladman BJ (2020) Jovian irregulars the population of kilometer-scale retrograde Jovian irregular moons. Planet Sci J 1:52. 7pp

Ashton E, Gladman B, Alexandersen M, Petit JM (2023) Piecing together the collisional history of the irregular moons of Saturn with the help of 64 new discoveries. In: DPS meeting #55, San Antonio, TX. Program Number: 316.01

Ashton E, Gladman B, Alexandersen M, Petit JM (2025) Discovery of 128 new saturnian irregular moons. Res Notes AAS 9:57. 3pp

Auclair-Desrotour P, Mathis S, Le Poncin-Lafitte C (2015) Scaling laws to understand tidal dissipation in fluid planetary regions and stars. I. Rotation, stratification and thermal diffusivity. Astron Astrophys 581:A118

Bagenal F (1997) The ionization source near Io from Galileo wake data. Geophys Res Lett 24(17):2111–2114

Bagenal F, Dols V (2020) The space environment of Io and Europa. J Geophys Res Space Phys 125:e27485. https://doi.org/10.1029/2019JA027485
Barabash S, et al (2026) PEP for JUICE. Space Sci Rev in prep.
Barnard EE (1892) Discovery and observations of a fifth satellite to Jupiter. Astron J 12:81–85
Barnard EE (1894) On the dark poles and bright equatorial belt of the first satellite of Jupiter. Mon Not R Astron Soc 54:134–136. https://doi.org/10.1093/mnras/54.3.134
Barnard EE (1897) A micrometrical determination of the dimensions of the planets and satellites of the Solar System made with the 36-inch refractor of the Lick Observatory. Pop Astron 5:285–302
Barnard EE (1909) Observations of the fifth satellite of Jupiter in the years 1908 and 1909, with a new determination of its period. Miscellaneous observations of Jupiter and his belts and moons. Astron Nachr 181:301–310
Bellucci G, D'Aversa E, Formisano V, Cruikshank D, Nelson RM, Clark RN, Baines KH, Matson D, Brown RH, McCord TB, Buratti BJ, Nicholson PD (Cassini VIMS Team) (2004) Cassini/VIMS observation of an Io post-eclipse brightening event. Icarus 172:141–148. https://doi.org/10.1016/j.icarus.2004.05.012
Belton MJS, Klaasen KP, Clary MC, Anderson JL, Anger CD, Carr MH, Chapman CR, Davies ME, Greeley R, Anderson D, Bolef LK, Townsend TE, Greenberg R, Head JW, Neukum G, Pilcher CB, Veverka J, Gierasch PJ, Fanale FP, Ingersoll AP, Masursky H, Morrison D, Pollack JB (1992) The Galileo solid-state imaging experiment. Space Sci Rev 60:413–455
Bhatt M, Reddy V, Schindler K, Cloutis E, Bhardwaj A, Le Corre L, Mann P (2017) Composition of Jupiter irregular satellites sheds light on their origin. Astron Astrophys 608:A67. https://doi.org/10.1051/0004-6361/201630361
Binder AB, Cruikshank DP (1964) Evidence for an atmosphere on Io. Icarus 3:299–305. https://doi.org/10.1016/0019-1035(64)90038-7
Bindschadler DL, Theilig EE, Schimmels KA, Vandermey N (2003) Project Galileo: final mission status. 54th AIAA. Bremen. https://doi.org/10.2514/6.iac-03-q.2.01
Birnbaum MM, Bunker RL, Tavolacci JT (1983) A radiation-hardened star scanner for spacecraft guidance and control. J Guid Control Dyn 6:39–46. https://doi.org/10.2514/3.19800
Blöcker A, Saur J, Roth L, Strobel DF (2018) MHD modeling of the plasma interaction with Io's asymmetric atmosphere. J Geophys Res Space Phys 123:9286–9311. https://doi.org/10.1029/2018JA025747
Blunck J (2010) Solar System moons — discovery and mythology. Springer, Berlin. https://doi.org/10.1007/978-3-540-68853-2
Bolton SJ, Lunine JI, Stevenson D, Connerney JEP, Levin S, Owen TC, Bagenal F, Gautier D, Ingersoll AP, Orton GS, Guillot T, Hubbard W, Bloxham J, Coradini A, Stephens SK, Mokashi P, Thorne R, Thorpe R (2017) The Juno mission. Space Sci Rev 213:5–37. https://doi.org/10.1007/s11214-017-0429-6
Borderies N, Yoder CF (1990) Phobos' gravity field and its influence on its orbit and physical librations. Astron Astrophys 233:235–251
Bottke WF, Nesvorný D, Vokrouhlický D, Morbidelli A (2010) The irregular satellites: the most collisionally evolved populations in the Solar System. Astron J 139:994–1014. https://doi.org/10.1088/0004-6256/139/3/994
Bottke WF, Vokrouhlický D, Nesvorný D, Moore JM (2013) Black rain: the burial of the Galilean satellites in irregular satellite debris. Icarus 223:775–795. https://doi.org/10.1016/j.icarus.2013.01.008
Bouchez AH, Brown ME, Schneider NM (2000) Eclipse spectroscopy of Io's atmosphere. Icarus 148:316–319. https://doi.org/10.1006/icar.2000.6518
Boutonnet A, Langevin Y, Erd C (2024) Designing the JUICE trajectory. Space Sci Rev 220(6):67. https://doi.org/10.1007/s11214-024-01093-y
Broadfoot AL, Belton MJS, Takacs PZ, Sandel BR, Shemansky DE, Holberg JB, McElroy MB (1979) Extreme ultraviolet observations from Voyager 1 encounter with Jupiter. Science 204:979–982
Brown ME (2000) Near-infrared spectroscopy of centaurs and irregular satellites. Astron J 119:977–983
Brown ME, Rhoden AR (2014) The 3 μm spectrum of Jupiter's irregular satellite Himalia. Astrophys J Lett 793:L44. https://doi.org/10.1088/2041-8205/793/2/L44
Brown RH, Baines KH, Bellucci G, Bibring JP, Buratti BJ, Capaccioni F, Cerroni P, Clark RN, Coradini A, Cruikshank DP, Drossart P, Formisano V, Jaumann R, Langevin Y, Matson DL, McCord TB, Mennella V, Nelson RM, Nicholson PD, Sicardy B, Sotin C, Amici S, Chamberlain MA, Filacchione G, Hansen G, Hibbitts K, Showalter M (2003) Observations with the Visual and Infrared Mapping Spectrometer (VIMS) during Cassini's flyby of Jupiter. Icarus 164:461–470. https://doi.org/10.1016/S0019-1035(03)00134-9
Burns JA (1977) Planetary satellites. University of Arizona Press, Tucson, p 598
Burns JA (1986) Some background about satellites. In: Burns JA, Matthews MS (eds) Satellites. University of Arizona Press, Tucson, pp 1–38. Chap. 1
Burns JA, Simonelli DP, Showalter MR, Hamilton DP, Porco CC, Esposito LW, Throop H (2004) Jupiter's ring-moon system. In: Bagenal F, Dowling TE, McKinnon WB (eds) Jupiter: the planet, satellites

and magnetosphere, Cambridge planetary science, vol 1. Cambridge University Press, Cambridge, pp 241–262
Campbell WW (1905a) Harvard Coll Obs Bull 173 (6 Jan 1905)
Campbell WW (1905b) Harvard Coll Obs Bull 178 (27 Feb 1905)
Carlson RW, Smythe WD, Lopes-Gautier RMC, Davies AG, Kamp LW, Mosher JA, Soderblom LA, Leader FE, Mehlman R, Clark RN, Fanale FP (1997) Distribution of sulfur dioxide and other infrared absorbers on the surface of Io. Geophys Res Lett 24:2479–2490. https://doi.org/10.1029/97GL02609
Carlson RW, Kargel JS, Douté S, Soderblom LA, Dalton JB (2007) Io's surface composition. In: Lopes R, Spencer JR (eds) Io after Galileo: a new view of Jupiter's volcanic moon. Springer, Berlin, pp 193–229. https://doi.org/10.1007/978-3-540-48841-5_9
Carr MH, Belton MJS, Bender K, Breneman H, Greeley R, Head JW, Klaasen KP, McEwen AS, Moore JM, Murchie S, Pappalardo RT, Plutchak J, Sullivan R, Thornhill G, Veverka J (1995) The Galileo imaging team plan for observing the satellites of Jupiter. J Geophys Res 100(E9):18935–18956. https://doi.org/10.1029/95JE00971
Carr MH, McEwen AS, Howard KA, Chuang FC, Thomas PC, Schuster P, Oberst J, Neukum G, Schubert G (Galileo Imaging Team) (1998) Mountains and calderas on Io: possible implications for lithosphere structure and magma generation. Icarus 135:146–165. https://doi.org/10.1006/icar.1998.5979
Cartwright RJ, Villanueva GL, Holler BJ, Camarca M, Faggi S, Neveu M, Roth L, Raut U, Glein CR, Castillo-Rogez JC, Malaska MJ, Bockelée-Morvan D, Nordheim TA, Hand KP, Strazzulla G, Pendleton YJ, de Kleer K, Beddingfield CB, de Pater I, Cruikshank DP, Protopapa S (2024) Revealing Callisto's carbon-rich surface and $CO_2$ atmosphere with JWST. Planet Sci J 5:60
Cassini JD (1677) Histoire de la Découverte de deux Planetes autour de Saturne, faite à l'Observatoire Royal par M. Cassini. J Savants No. VI:70–72. (15. Mars 1677). https://books.google.de/books?id=AgJWqf8lvnoC
Cassini JD (1694) Monsieur Cassini his new and exact tables for the eclipses of the first satellite of Jupiter, reduced to the Julian stile, and meridian of London. Philos Trans R Soc 18:237–256. http://www.jstor.org/stable/102468
Chamberlain MA, Brown RH (2004) Near-infrared spectroscopy of Himalia. Icarus 172:163–169. https://doi.org/10.1016/j.icarus.2003.12.016
Charnoz S, Salmon J, Crida A (2010) The recent formation of Saturn's moonlets from viscous spreading of the main rings. Nature 465:752–754. https://doi.org/10.1038/nature09096
Chen Z, Yang K, Liu X (2024) 'Life' of dust originating from the irregular satellites of Jupiter. Mon Not R Astron Soc 527:11327–11337. https://doi.org/10.1093/mnras/stad3829
Cheng AF, Weaver HA, Conard SJ, Morgan MF, Barnouin-Jha O, Boldt JD, Cooper KA, Darlington EH, Grey MP, Hayes JR, Kosakowski KE, Magee T, Rossano E, Sampath D, Schlemm C, Taylor HW (2008) Long-Range Reconnaissance Imager on new horizons. Space Sci Rev 140:189–215. https://doi.org/10.1007/s11214-007-9271-6
Cloutis EA, McCormack KA, Bell JF, Hendrix AR, Bailey DT, Craig MA, Mertzmand SA, Robinson MS, Riner MA (2008) Ultraviolet spectral reflectance properties of common planetary materials. Icarus 197:321–347
Comstock RL, Bills BG (2003) A Solar System survey of forced librations in longitude. J Geophys Res 108:E9. https://doi.org/10.1029/2003JE002100
Conrad A, Pedichini F, Li Causi G, Antoniucci S, de Pater I, Davies AG, de Kleer K, Piazzesi R, Testa V, Vaccari P, Vicinanza M, Power J, Ertel S, Shields J, Ragland S, Giorgi F, Jeffries SM, Hope D, Perry J, Williams DA, Nelson DM (2024) Observation of Io's resurfacing via plume deposition using ground-based adaptive optics at visible wavelengths with LBT SHARK-VIS. Geophys Res Lett 51:e2024GL108609. https://doi.org/10.1029/2024GL108609
Cooper NJ, Murray CD, Porco CC, Spitale JN (2006) Cassini ISS astrometric observations of the inner Jovian satellites, Amalthea and Thebe. Icarus 181:223–234
Cooper NJ, Renner S, Murray CD, Evans MW (2015) Saturn's inner satellites: orbits, masses, and the chaotic motion of atlas from new Cassini imaging observations. Astron J 149:27. 18pp
Cooper NJ, Lainey V, Meunier LE, Murray CD, Zhang QF, Baillie K, Evans MW, Thuillot W, Vienne A (2018) The Caviar software package for the astrometric reduction of Cassini ISS images: description and examples. Astron Astrophys 610:A2. https://doi.org/10.1051/0004-6361/201731713
Cowell PH (1908) Note on the discovery of a moving object near Jupiter. Mon Not R Astron Soc 68:373
Cowell PH, Melotte PJ, Crommelin ACD (1908) Newly discovered eighth satellite of Jupiter. Mon Not R Astron Soc 68:456–458
Cruikshank DP (1977) Radii and albedos of four Trojan asteroids and Jovian satellites 6 and 7. Icarus 30:224–230
Cruikshank DP (1982) Barnard's satellite of Jupiter. Sky Telesc 64:220–224
Cruikshank DP (ed) (1995) Neptune and Triton. The University of Arizona Press, Tucson

Cruikshank DP, Nelson RM (2007) A history of the exploration of Io. In: Lopes RMC, Spencer JR (eds) Io after Galileo: a new view of Jupiter's volcanic moon, Springer Praxis Books. Springer, Berlin, pp 5–33. https://doi.org/10.1007/978-3-540-48841-5_2

Cruikshank DP, Emery JP, Kornei KA, Bellucci G, D'Aversa E (2010) Eclipse reappearances of Io: time-resolved spectroscopy (1.9-4.2 μm). Icarus 205:516–527. https://doi.org/10.1016/j.icarus.2009.05.035

David P, et al (2023) Gaia focused product release: asteroid orbital solution. Properties and assessment. Astron Astrophys 680:A37

Davies AG, Perry JE, Williams DA, Nelson DM (2024) Io's polar volcanic thermal emission indicative of magma ocean and shallow tidal heating models. Nat Astron 8:94–100. https://doi.org/10.1038/s41550-023-02123-5

Davis MW, Gladstone GR, Retherford KD, Persyn SC (2021) The JUICE ultraviolet spectrograph: a next-generation compact UVS for ESA's JUICE mission. In: Proc. SPIE 11852, International Conference on Space Optics — ICSO 2020, 1185226 (11 June 2021). https://doi.org/10.1117/12.2599357

de Kleer K, Rathbun JA (2023) Io's thermal emission and heat flow. In: Lopes RMC, de Kleer K, Keane JT (eds) Io: a new view of Jupiter's moon. Astrophysics and Space Science Library, vol 468. Springer, Cham, pp 173–209. https://doi.org/10.1007/978-3-031-25670-7_6

de Kleer K, Hughes EC, Nimmo F, Eiler J, Hofmann AE, Luszcz-Cook S, Mandt K (2024) Isotopic evidence of long-lived volcanism on Io. Science. https://doi.org/10.1126/science.adj0625

de Pater I, Lissauer J (2015) Planetary sciences, 2nd edn. Cambridge University Press, Cambridge. https://doi.org/10.1017/CBO9781316165270

de Pater I, Showalter MR, Burns JA, Nicholson PD, Liu MC, Hamilton DP, Graham JR (1999) Keck infrared observations of Jupiter's ring system near Earth's 1997 ring plane crossing. Icarus 138:214–223. https://doi.org/10.1006/icar.1998.6068

de Pater I, Hamilton DP, Showalter MR, Throop HB, Burns JA (2018) The rings of Jupiter. In: Tiscareno MS, Murray CD (eds) Planetary ring systems. Cambridge University Press, Cambridge, pp 125–134. https://doi.org/10.1017/9781316286791.006. Chap. 6

de Pater I, Luszcz-Cook S, Rojo P, Redwing E, de Kleer K, Moullet A (2020) ALMA observations of Io going into and coming out of eclipse. Planet Sci J 1:60. https://doi.org/10.3847/PSJ/abb93d

de Pater I, Keane JT, de Kleer K, Davies AG (2021) A 2020 observational perspective of Io. Annu Rev Earth Planet Sci 49:643–678. https://doi.org/10.1146/annurev-earth-082420-095244

de Pater I, Goldstein D, Lellouch E (2023a) The plumes and atmosphere of Io. In: Lopes RMC, de Kleer K, Keane JT (eds) Io: a new view of Jupiter's moon. Astrophysics and Space Science Library, vol 468. Springer, Cham, pp 233–290. https://doi.org/10.1007/978-3-031-25670-7_8

de Pater I, Lellouch E, Strobel DF, de Kleer K, Fouchet T, Wong MH, Holler BJ, Stansberry J, Fry PM, Brown ME, Bockelée-Morvan D, Trumbo SK, Fletcher LN, Hedman MM, Molter EM, Showalter M, Tiscareno MS, Cazaux S, Hueso R, Luszcz-Cook S, Melin H, Moeckel C, Mura A, Orton G, Roth L, Saur J, Tosi F (2023b) An energetic eruption with associated SO 1.707 micron emissions at Io's kanehekili fluctus and a brightening event at loki patera observed by JWST. J Geophys Res Planets 128:e2023JE007872. https://doi.org/10.1029/2023JE007872

de Pater I, Strobel DF, Davies AG, Saur J, Roth L, de Kleer K, Lellouch E, Milby Z, Schmidt C, Fouchet T, Wong MH, Fletcher LN, Harkett J, Roman M, Cartwright RJ, Perry JE, Renaud-Kim J, Jordan C, Schlegel S, Williams DA, Nelson DM (2025) First detection of [SI] in near-IR JWST observations of Io in eclipse, and comparison with SO emissions, evolving volcanic eruptions, and prior UV HST-STIS [SI] emissions. J Geophys Res Planets 130(11):e2024JE008850. https://doi.org/10.1029/2024JE008850

de Sitter W (1931) Jupiter's Galilean satellites (George Darwin lecture). Mon Not R Astron Soc 91:706–738. https://doi.org/10.1093/mnras/91.7.706

Degewij J (1978) Photometry of Faint Asteroids and Satellites. Ph.D. thesis (proefschrift ter verkrijging van de graad van Doctor in de Wiskunde en Natuurwetenschappen). Chapter IV: Faint Satellites pp 94–100. https://inis.iaea.org/collection/NCLCollectionStore/_Public/10/450/10450788.pdf

Degewij J, Andersson LE, Zellner B (1980a) Photometric properties of outer planetary satellites. Icarus 44:520–540

Degewij J, Cruikshank DP, Hartmann WK (1980b) Near-infrared colorimetry of J6 Himalia and S9 Phoebe: a summary of 0.3- to 2.2- μm reflectances. Icarus 44:541–547

Denk T, Mottola S (2019) Studies of irregular satellites: I. Lightcurves and rotation periods of 25 Saturnian moons from Cassini observations. Icarus 322:80–103

Denk T, Helfenstein P, Roatsch T, Thomas PC, Squyres SW, Porco CC, Neukum G (2001) Himalia — first disk-resolved observations of an outer Jovian satellite. Conference on Jupiter (planet, satellites & magnetosphere). In: Jupiter conference abstracts book, Boulder, CO, 25–30 Jun 2001, pp 30–31

Denk T, Neukum G, Roatsch T, Porco CC, Burns JA, Galuba GG, Schmedemann N, Helfenstein P, Thomas PC, Wagner RJ, West RA (2010) Iapetus: unique surface properties and a global color dichotomy from Cassini imaging. Science 327:435–439

Denk T, Mottola S, Tosi F, Bottke WF, Hamilton DP (2018) The irregular satellites of Saturn. In: Schenk PM, Clark RN, Howett CJA, Verbiscer AJ, Waite JH (eds) Enceladus and the Icy Moons of Saturn. Space science series. University of Arizona Press, Tucson, pp 409–434
Dessler AJ (1980) Mass-injection rate from Io into the Io plasma torus. Icarus 44:291–295
Dirkx D, Gurvits LI, Lainey V, Lari G, Milani A, Cimò G, Bocanegra-Bahamon TM, Visser PNAM (2017) On the contribution of PRIDE-JUICE to Jovian system ephemerides. Planet Space Sci 147:14–27
Dols V, Delamere PA, Bagenal F (2008) A multispecies chemistry model of Io's local interaction with the plasma torus. J Geophys Res 113:A09208. https://doi.org/10.1029/2007JA012805
Emelyanov NV (2005) The mass of Himalia from the perturbations on other satellites. Astron Astrophys 438:L33–L36
Emelyanov NV, Kovalev MY, Varfolomeev MI (2023) The orbits of outer planetary satellites using the Gaia data. Mon Not R Astron Soc 522:165–172. https://doi.org/10.1093/mnras/stad958
Engelmann R (1871) Über die Helligkeitsverhältnisse der Jupitertrabanten. Habilitation thesis, Leipzig, 1871
ESA (2014) JUICE (JUpiter ICy moons Explorer): Exploring the emergence of habitable worlds around gas giants. Definition Study Report. ESA/SRE(2014)1, September 2014. https://sci.esa.int/documents/33960/35865/1567260128466-JUICE_Red_Book_i1.0.pdf
Estrada PR, Durisen RH (2023) Constraints on the initial mass, age and lifetime of Saturn's rings from viscous evolutions that include pollution and transport due to micrometeoroid bombardment. Icarus 400:115296. https://doi.org/10.1016/j.icarus.2022.115296
Farkas-Takács A, Kiss C, Pál A, Molnár L, Szabó GM, Hanyecz O, Sárneczky K, Szabó R, Marton G, Mommert M, Szakáts R, Müller T, Kiss LL (2017) Properties of the irregular satellite system around Uranus inferred from $K2$, Herschel, and spitzer observations. Astron J 154:119. https://doi.org/10.3847/1538-3881/aa8365
Fayolle M, Lainey V, Dirkx D, Gurvits LI, Cimò G, Bolton SJ (2023) Spacecraft VLBI tracking to enhance stellar occultations astrometry of planetary satellites. Astron Astrophys 676:L6
Feaga LM, McGrath M, Feldman PD (2009) Io's dayside $SO_2$ atmosphere. Icarus 201:570–584
Feldman PD, Strobel DF, Moos HW, Retherford KD, Wolven BC, McGrath MA, Roesler FL, Woodward RC, Oliversen RJ, Ballester GE (2000) Lyman-$\alpha$ imaging of the $SO_2$ distribution on Io. Geophys Res Lett 27:1787–1790
Fieseler PD, Adams OW, Vandermey N, Theilig EE, Schimmels KA, Lewis GD, Ardalan SM, Alexander CJ (2004) The Galileo star scanner observations at Amalthea. Icarus 169:390–401
Flammarion C (1893) Le Nouveau Satellite de Jupiter. L'Astronomie 12:91–94
Fletcher LN, Cavalié T, et al (2023) Jupiter science enabled by ESA's Jupiter ICy Moons Explorer. Space Sci Rev 219(7):53. https://doi.org/10.1007/s11214-023-00996-6
Fuller J, Luan J, Quataert E (2016) Resonance locking as the source of rapid tidal migration in the Jupiter and Saturn moon systems. Mon Not R Astron Soc 458:3867–3879
Futaana Y, Barabash S, Wang XD, Wieser M, Wieser GS, Wurz P, Krupp N, Brandt PC (2015) Low-energy energetic neutral atom imaging of Io plasma and neutral tori. Planet Space Sci 108:41–53. https://doi.org/10.1016/j.pss.2014.12.022
Galilei G (1610) Sidereus Nuncius. Thomas Baglioni, Venezia. https://doi.org/10.3931/e-rara-695. https://library.si.edu/digital-library/book/sidereusnuncius00gali
Galilei G (1612) Discorso Intorno alle cose, che Stanno in sù l'acqua, ò che in quella si muovono. Cosimo Giunti, Firenze. https://bibdig.museogalileo.it/tecanew/opera?bid=354797&seq=77
Galilei G (1931) Le Opere di Galileo Galilei (Barbèra, G, ed.), Volume III, parte 2 (I Pianeti Medicei), Firenze. https://bibdig.museogalileo.it/tecanew/opera?bid=354795
Geissler PE, McMillan MT (2008) Galileo observations of volcanic plumes on Io. Icarus 197:505–518
Geissler PE, McEwen AS, Keszthelyi L, Lopes-Gautier RMC, Granahan J, Simonelli DP (1999) Global color variations on Io. Icarus 140:265–282. https://doi.org/10.1006/icar.1999.6128
Giles RS, Spencer JR, Tsang CCC, Greathouse TK, Lellouch E, López-Valverde MA (2024) Seasonal and longitudinal variability in Io's $SO_2$atmosphere from 22 years of IRTF/TEXES observations. Icarus 418:116151. https://doi.org/10.1016/j.icarus.2024.116151
Gingerich O, Van Helden A (2003) From occhiale to printed page: the making of Galileo's sidereus nuncius. J Hist Astron 34:251–267. https://doi.org/10.1177/002182860303400301
Gingerich O, Van Helden A (2011) How Galileo constructed the moons of Jupiter. J Hist Astron 42:259–264. https://doi.org/10.1177/002182861104200208
Giono G, Roth L (2021) Io's $SO_2$atmosphere from HST Lyman-$\alpha$ images: 1997 to 2018. Icarus 359:114212
Gladman B, Nicholson PD, Burns JA, Kavelaars JJ, Marsden BG, Williams GV, Offutt WB (1998) Discovery of two distant irregular moons of Uranus. Nature 392:897–899
Gladstone GR, Persyn SC, Eterno JS, et al (2017) The ultraviolet spectrograph on NASA's Juno mission. Space Sci Rev 213:447–473. https://doi.org/10.1007/s11214-014-0040-z
Goldreich P, Murray N, Longaretti PY, Banfield D (1989) Neptune's story. Science 245:500–504

Gradie J, Thomas PC, Veverka J (1980) The surface composition of Amalthea. Icarus 44:373–387
Grav T, Holman MJ (2004) Near-infrared photometry of the irregular satellites of Jupiter and Saturn. Astrophys J Lett 605:L141–L144
Grav T, Bauer JM, Mainzer AK, Masiero JR, Nugent CR, Cutri RM, Sonnett S, Kramer E (2015) NEOWISE: observations of the Irregular satellites of Jupiter and Saturn. Astrophys J 809:3
Graykowski A, Jewitt D (2018) Colors and shapes of the irregular planetary satellites. Astron J 155:184
Greco V, Molesini G, Quercioli F (1993) Telescopes of Galileo. Appl Opt 32:6219–6226. https://doi.org/10.1364/AO.32.006219
Gurvits LI, Cimò G, Dirkx D, Pallichadath V, Akins A, Altobelli N, Bocanegra-Bahamon TM, Cazaux SM, Charlot P, Duev DA, Fayolle MS, Fogasy J, Frey S, Lainey V, Molera Calvés G, Perger K, Pogrebenko SV, Md Said NM, Vallat C, Vermeersen LLA, Visser PNAM, Wang KN, Willner K (2023) Planetary Radio Interferometry and Doppler Experiment (PRIDE) of the JUICE mission. Space Sci Rev 219(8):79. https://doi.org/10.1007/s11214-023-01026-1
Hamilton DP, Burns JA (1991) Orbital stability zones about asteroids. Icarus 92:118–131. https://doi.org/10.1016/0019-1035(91)90039-V
Hamilton DP, Krüger H (2008) The sculpting of Jupiter's gossamer rings by its shadow. Nature 453:72–75. https://doi.org/10.1038/nature06886
Hamilton DP, Proctor AL, Rauch KP (2001) An explanation for the high inclinations of Thebe and Amalthea. DPS Meeting #33, id. 25.04, BAAS 33:1085
Hansen CJ, Caplinger MA, Ingersoll A, Ravine MA, Jensen E, Bolton S, Orton G (2017) Junocam: Juno's outreach camera. Space Sci Rev 213:475–506. https://doi.org/10.1007/s11214-014-0079-x
Hanuš J, Ďurech J, Brož M, Warner BD, Pilcher F, Stephens R, Oey J, Bernasconi L, Casulli S, Behrend R, Polishook D, Henych T, Lehký M, Yoshida F, Ito T (2011) A study of asteroid pole-latitude distribution based on an extended set of shape models derived by the lightcurve inversion method. Astron Astrophys 530:A134. https://doi.org/10.1051/0004-6361/201116738. 16pp
Harris DL (1961) Photometry and colorimetry of planets and satellites. In: Kuiper GP, Middlehurst BM (eds) Planets and satellites. University Chicago Press, Chicago, pp 272–342
Hartmann WK (1987) A satellite-asteroid mystery and a possible early flux of scattered C-class asteroids. Icarus 71:57–68
Hartogh P, et al (2026) The SWI instrument for JUICE. Space Sci Rev in prep.
Hendrix AR, Hansen CJ (2008a) Ultraviolet observations of Phoebe from the Cassini UVIS. Icarus 193:323–333
Hendrix AR, Hansen CJ (2008b) The albedo dichotomy of Iapetus measured at UV wavelengths. Icarus 193:344–351
Hendrix AR, Hansen CJ, Holsclaw GM (2010) The ultraviolet reflectance of Enceladus: implications for surface composition. Icarus 206:608–617
Hendrix AR, Vilas F, Li JY (2016) The UV signature of carbon in the Solar System. Meteorit Planet Sci 51(1):105–115
Herschel W (1797) Observations of the changeable brightness of the satellites of Jupiter. Philos Trans R Soc 87:332–351
Hikida R, Yoshioka K, Tsuchiya F, Kagitani M, Kimura T, Bagenal F, Schneider N, Murakami G, Yamazaki A, Kita H, Nerney E, Yoshikawa I (2020) Spatially asymmetric increase in hot electron fraction in the Io plasma torus during volcanically active period revealed by observations by Hisaki/EXCEED from November 2014 to may 2015. J Geophys Res: Space Phys 125:e2019JA027100. https://doi.org/10.1029/2019JA027100
Holler BJ, Milam SN, Bauer JM, Alcock C, Bannister MT, Bjoraker GL, Bodewits D, Bosh AS, Buie MW, Farnham TL, Haghighipour N, Hardersen PS, Harris AW, Hirata CM, Hsieh HH, Kelley MSP, Knight MW, Kramer EA, Longobardo A, Nixon CA, Palomba E, Protopapa S, Quick LC, Ragozzine D, Reddy V, Rhodes JD, Rivkin AS, Sarid G, Sickafoose AA, Simon AA, Thomas CA, Trilling DE, West RA (2018) Solar System science with the wide-field infrared survey telescope. J Astron Telesc Instrum Syst 4:034003. https://doi.org/10.1117/1.JATIS.4.3.034003
Huybrighs HLF, van Buchem CPA, Blöcker A, Dols V, Bowers CF, Jackman CM (2024) J Geophys Res, Atmos 129:e2023JA032371. https://doi.org/10.1029/2023JA032371
Iess L, et al (2026) 3GM for JUICE. Space Sci Rev in prep.
Jacobson RA (2010) The orbits and masses of the Martian satellites and the libration of Phobos. Astron J 139:668–679. https://doi.org/10.1088/0004-6256/139/2/668
Jacobson R, Brozović M, Gladman B, Alexandersen M, Nicholson PD, Veillet C (2012) Irregular satellites of the outer planets: orbital uncertainties and astrometric recoveries in 2009–2011. Astron J 144:132
Jacobson R, Brozović M, Mastrodemos N, Riedel JE, Sheppard SS (2022) Ephemerides of the irregular Saturnian satellites from Earth-based astrometry and Cassini imaging. Astron J 164:240

Jaeger WL, Turtle EP, Keszthelyi LP, Radebaugh J, McEwen AS, Pappalardo RT (2003) Orogenic tectonism on Io. J Geophys Res 108:E8. https://doi.org/10.1029/2002JE001946
Jewitt D, Haghighipour N (2007) Irregular satellites of the planets: products of capture in the Early Solar System. Annu Rev Astron Astrophys 45:261–295
Jewitt DC, Danielson GE, Synnott SP (1979) Discovery of a new Jupiter satellite. Science 206:951
Johnson TV, McCord TB (1970) Galilean satellites: the spectral reflectivity 0.30-1.10 micron. Icarus 13:37–42. https://doi.org/10.1016/0019-1035(70)90115-6
Johnson TV, Matson DL, Blaney DL, Veeder GJ, Davies A (1995) Stealth plumes on Io. Geophys Res Lett 22:3293–3296
Kaasalainen M, Ďurech J (2007) Inverse problems of NEO photometry: imaging the NEO population. In: Milani A, Valsecchi G, Vokrouhlický D (eds) Proceedings IAU Symposium 236. 16 pp.
Kaasalainen M, Lamberg L (2006) Inverse problems of generalized projection operators. Inverse Probl 22:749–769
Kaasalainen M, Mottola S, Fulchignoni M (2002b) Asteroid models from disk-integrated data. In: Bottke WF, Cellino A, Paolicchi P, Binzel RP (eds) Asteroids III. University of Arizona Press, Tucson, pp 139–150
Kaasalainen M, Torppa J, Piironen J (2002a) Models of twenty asteroids from photometric data. Icarus 159:369–395
Keane JT, et al (2021) The science case for Io exploration: a white paper to the 2023–2032 Planetary Science and Astrobiology Decadal Survey. Bull AAS 53(4). https://doi.org/10.3847/25c2cfeb.f844ca0e
Keane JT, Matsuyama I, Bierson CJ, Trinh A (2023) Tidal heating and the interior structure of Io. In: Lopes RMC, de Kleer K, Keane JT (eds) Io: a new view of Jupiter's moon. Astrophysics and Space Science Library, vol 468. Springer, Cham, pp 95–146. https://doi.org/10.1007/978-3-031-25670-7_4
Keszthelyi L, McEwen AS, Phillips CB, Milazzo M, Geissler P, Turtle EP, Radebaugh J, Williams DA, Simonelli DP, Breneman HH, Klaasen KP, Levanas G, Denk T (Galileo SSI Team) (2001) Imaging of volcanic activity on Jupiter's moon Io by Galileo during the Galileo Europa mission and the Galileo millennium mission. J Geophys Res 106(E12):33025–33052. https://doi.org/10.1029/2000JE001383
Keszthelyi L, Jaeger WL, Milazzo M, Radebaugh J, Davies AG, Mitchell KL (2007) New estimates for Io eruption temperatures: implications for the interior. Icarus 192:491–502. https://doi.org/10.1016/j.icarus.2007.07.008
Kivelson MG, Bagenal F, Kurth WS, Neubauer FM, Paranicas C, Saur J (2004) Magnetospheric interactions with satellites. In: Bagenal F, Dowling TE, McKinnon WB (eds) Jupiter: the planet, satellites and magnetosphere. Cambridge planetary science, vol 1. Cambridge University Press, Cambridge, pp 513–536. Ch. 21
Klaasen KP, Breneman HH, Cunningham WF, Kaufman JM, Klemaszewski JE, Magee KP, McEwen AS, Mortensen HB, Pappalardo RT, Senske DA, Sullivan RJ, Vasavada AR (1999) Calibration and performance of the Galileo solid-state imaging system in Jupiter orbit. Opt Eng 38(7):1178–1199. https://doi.org/10.1117/1.602168
Koga R, Tsuchiya F, Kagitani M, Sakanoi T, Yoneda M, Yoshioka K, et al (2018) Spatial distribution of Io's neutral oxygen cloud observed by Hisaki. J Geophys Res Space Phys 123:3764–3776. https://doi.org/10.1029/2018JA025328
Koga R, Tsuchiya F, Kagitani M, Sakanoi T, Yoshioka K, Yoshikawa I, et al (2019) Transient change of Io's neutral oxygen cloud and plasma torus observed by Hisaki. J Geophys Res Space Phys 124:10318–10331. https://doi.org/10.1029/2019JA026877
Kowal CT, Aksnes K, Marsden BG, Roemer E (1975) Thirteenth satellite of Jupiter. Astron J 80:460–464
Kristian J, Blouke M (1982) Charge-coupled devices in astronomy. Sci Am 247(10):48–56
Kuiper GP (1949) The second satellite of Neptune. Publ Astron Soc Pac 61(361):175–176
Lainey V, Van Hoolst T (2009) Jovian tidal dissipation from inner satellite dynamics. European Planetary Science Congress, EPSC2009-392
Lainey V, Rambaux N, Cooper N, Dahoumane R, Zhang Q (2023) Characterising the interior of five inner Saturnian moons using Cassini ISS data. Astron Astrophys 670:L25. https://doi.org/10.1051/0004-6361/202244757
Laplace PS (1805) Traité de Mécanique Céleste. In: Œuvres complètes, tome 4, livre VIII. https://www.digitale-sammlungen.de/de/view/bsb10049391. See p. 16 (page 62 in the scan) for the resonance formula; p.126 (page 172) for the masses of the Galilean satellites
Lellouch E, Paubert G, Moses JI, Schneider NM, Strobel DF (2003) Volcanically emitted sodium chloride as a source for Io's neutral clouds and plasma torus. Nature 421:45–47. https://doi.org/10.1038/nature01292
Levison HF, et al (2024) A contact binary satellite of the asteroid (152830) Dinkinesh. Nature 629:1015–1020. https://doi.org/10.1038/s41586-024-07378-0
Levison HF, Olkin CB, Noll KS, Marchi S, Bell JF III, Bierhaus E, Binzel R, Bottke WF, Britt D, Brown M, Buie M, Christensen P, Emery J, Grundy W, Hamilton VE, Howett C, Mottola S, Pätzold M, Reuter D, Spencer J, Statler TS, Stern SA, Sunshine J, Weaver H, Wong I (2021) Lucy Mission to the Trojan asteroids: science goals. Planet Sci J 2:171. https://doi.org/10.3847/PSJ/abf840

Lopes RMC, Spencer JR (eds) (2007) Io after Galileo: a new view of Jupiter's volcanic moon, Springer praxis books / geophysical sciences Springer, Berlin, pp 37. https://doi.org/10.1007/978-3-540-48841-5
Lopes RMC, Williams DA (2005) Io after Galileo. Rep Prog Phys 68:303–340. https://doi.org/10.1088/0034-4885/68/2/R02
Lopes RMC, Kamp LW, Smythe WD, Mouginis-Mark P, Kargel J, Radebaugh J, Turtle EP, Perry J, Williams DA, Carlson RW, Douté S (Galileo NIMS Team Galileo SSI Team) (2004) Lava lakes on Io: observations of Io's volcanic activity from Galileo NIMS during the 2001 fly-bys. Icarus 169:140–174. https://doi.org/10.1016/j.icarus.2003.11.013
Lopes RM, de Kleer K, Keane JT (eds) (2023) Io: A New View of Jupiter's Volcanic Moon. Astrophysics and Space Science Library, vol 468. Springer, Cham. https://doi.org/10.1007/978-3-031-25670-7.
Luu JX (1991) CCD photometry and spectroscopy of the outer Jovian satellites. Astron J 102:1213–1225
Mamajek EE, Prsa A, Torres G, Harmanec P, Asplund M, Bennett PD, Capitaine N, Christensen-Dalsgaard J, Depagne E, Folkner WM, Haberreiter M, Hekker S, Hilton JL, Kostov V, Kurtz DW, Laskar J, Mason BD, Milone EF, Montgomery MM, Richards MT, Schou J, Stewart SG (2015) IAU 2015 Resolution B3 on Recommended Nominal Conversion Constants for Selected Solar and Planetary Properties. https://doi.org/10.48550/arXiv.1510.07674. See also https://web.archive.org/web/20160128180606/https://www.iau.org/static/resolutions/IAU2015_English.pdf
Marius S (1611) Prognosticon Astrologicum auf das Jahr M.DC.XII. In: Vom Sommer. Nürnberg: Johann Lauer. https://www.simon-marius.net/index.php?lang=en&menu=25&id=1612, https://www.simon-marius.net/pix/content/25/Marius_1612-23000_StaatsarchivNbg.pdf (see sheet Ciii/ pdf file pages 12-13 therein)
Marius S (1612) Prognosticon Astrologicum auf das Jahr M.DC.XIII. In introduction part. Nürnberg: Johann Lauer. https://www.simon-marius.net/index.php?lang=en&menu=25&id=1613, https://www.simon-marius.net/pix/content/25/Marius_1613-23000_StaatsarchivNbg_253.pdf (see sheet Aiv/ pdf file page 5 therein)
Marius S (1614) Mundus Iovialis. Johann Lauer, Nürnberg. https://www.simon-marius.net/index.php?lang=en&menu=3&id=1
Masters A, Modolo R, et al (2025) Magnetosphere and plasma science with the Jupiter ICy Moons Explorer. Space Sci Rev 221(2):24. https://doi.org/10.1007/s11214-025-01148-8
Matz KD, Roatsch T (2018) CKVIEW – a multi-mission planning tool. SpaceOps Conference, Marseille, AIAA 2018-2392. https://doi.org/10.2514/6.2018-2392
McEwen AS, Keszthelyi L, Geissler P, Simonelli DP, Carr MH, Johnson TV, Klaasen KP, Breneman HH, Jones TJ, Kaufman JM, Magee KP, Senske DA, Belton MJS, Schubert G (1998) Active volcanism on Io as seen by Galileo SSI. Icarus 135:181–219. https://doi.org/10.1006/icar.1998.5972
Michelson AA (1891) Measurement of Jupiter's satellites by interference. Publ Astron Soc Pac 3:274–278
Millis RL (1978) Photoelectric photometry of J V. Icarus 33:319–321
Morabito LA (2012) Discovery of Volcanic Activity on Io. A Historical Review. eprint arXiv:1211.2554. https://doi.org/10.48550/arXiv.1211.2554
Morabito LA, Synnott SP, Kupferman PN, Collins SA (1979) Discovery of currently active extraterrestrial volcanism. Science 204:972. https://doi.org/10.1126/science.204.4396.972
Morrison D (1977) Radiometry of satellites and of the rings of Saturn. In: Burns J (ed) Planetary satellites. University of Arizona Press, Tucson, pp 269–301
Morrison D (1982) The satellites of Jupiter and Saturn. Annu Rev Astron Astrophys 20:469–495
Morrison D, Morrison ND (1977) Photometry of the Galilean satellites. In: Burns J (ed) Planetary satellites. University of Arizona Press, Tucson, pp 363–378
Mottola S, Hellmich S, Buie MW, Zangari AM, Stephens RD, Di Martino M, Proffe G, Marchi S, Olkin CB, Levison HF (2023) Shape models of Lucy targets (3548) Eurybates and (21900) orus from disk-integrated photometry. Planet Sci J 4:18. https://doi.org/10.3847/PSJ/acaf79
Moullet A, Lellouch E, Moreno R, Gurwell M, Black JH, Butler B (2013) Exploring Io's atmospheric composition with APEX: first measurement of 34SO2 and tentative detection of KCl. Astrophys J 776:32
Müller G (1897) Die Photometrie der Gestirne. Verlag von Wilhelm Engelmann, Leipzig. https://ia800901.us.archive.org/0/items/diephotometriede00mluoft/diephotometriede00mluoft.pdf
Mura A, Adriani A, Tosi F, Lopes RMC, Sindoni G, Filacchione G, Williams DA, Davies AG, Plainaki C, Bolton S, Altieri F, Cicchetti A, Grassi D, Migliorini A, Moriconi ML, Noschese R, Olivieri A, Piccioni G, Sordini R (2020) Infrared observations of Io from Juno. Icarus 341:113607. https://doi.org/10.1016/j.icarus.2019.113607
Mura A, Zambon F, Tosi F, Lopes RMC, Rathbun J, Pettine M, Adriani A, Altieri F, Ciarniello M, Cicchetti A, Filacchione G, Grassi D, Noschese R, Migliorini A, Piccioni G, Plainaki C, Sordini R, Sindoni G, Turrini D (2024) The temporal variability of Io's hot spots. Front Astron Space Sci 11:1369472. https://doi.org/10.3389/fspas.2024.1369472. Corrigendum: id. 1503779, https://doi.org/10.3389/fspas.2024.1503779

N. N (1676) Demonstration touchant le mouvement de la lumiere trouvé par M. Rømer de l'Academie Royale des Sciences. J Savants No. XX:233–236. (7. Decembre M. DC. LXXVI)
N. N (1677) A demonstration concerning the motion of light, communicated from Paris, in the journal des scavans, and here made English. Philos Trans R Soc 12(136):893–894. https://doi.org/10.1098/rstl.1677.0024. https://www.jstor.org/stable/101779
Nash DB, Betts BH (1995) Laboratory infrared spectra (2.3-23 μm) of $SO_2$phases: applications to Io surface analysis. Icarus 117:402–419. https://doi.org/10.1006/icar.1995.1165
Nash DB, Betts BH (1998) Ices on Io — composition and texture. In: Schmitt B, de Bergh C, Festou M (eds) Solar System ices. Kluwer, Dordrecht, pp 607–638. https://doi.org/10.1007/978-94-011-5252-5_25
Nesvorný D (2018) Dynamical evolution of the early Solar System. Annu Rev Astron Astrophys 56:137–174. https://doi.org/10.1146/annurev-astro-081817-052028
Nesvorný D, Vokrouhlický D, Morbidelli A (2007) Capture of irregular satellites during planetary encounters. Astron J 133:1962–1976
Nesvorný D, Vokrouhlický D, Deienno R (2014) Capture of irregular satellites at Jupiter. Astrophys J 784:22
Neugebauer G, Becklin EE, Jewitt DC, Terrile RJ, Danielson GE (1981) Spectra of the Jovian ring and Amalthea. Astron J 86:607–610. https://doi.org/10.1086/112922
Nicholson SB (1914) Discovery of the ninth satellite of Jupiter. Publ Astron Soc Pac 26(155):197–198
Nicholson SB (1938) Two new satellites of Jupiter. Publ Astron Soc Pac 50(297):292–293
Nicholson SB (1939a) The satellites of Jupiter. Publ Astron Soc Pac 51(300):85–94
Nicholson SB (1939b) Discovery of the tenth and eleventh satellites of Jupiter and observations of these and other satellites. Astron J 48:129–132
Nicholson SB (1951) An unidentified object near Jupiter, probably a new satellite. Publ Astron Soc Pac 63:297–299
Nicholson PD, Matthews K (1991) Near-infrared observations of the Jovian ring and small satellites. Icarus 93:331–346
Nicholson PD, Ćuk M, Sheppard SS, Nesvorný D, Johnson TV (2008) Irregular satellites of the giant planets. In: Barucci MA, Boehnhardt H, Cruikshank DP, Morbidelli A (eds) The Solar System beyond Neptune. University of Arizona Press, Tucson, pp 411–424
Nogueira E, Brasser R, Gomes R (2011) Reassessing the origin of Triton. Icarus 214:113–130
Oberst J, Schuster P (2004) Vertical control point network and global shape of Io. J Geophys Res 109:E4. E04003. https://doi.org/10.1029/2003JE002159
Ockert-Bell ME, Burns JA, Daubar IJ, Thomas PC, Veverka J, Belton MJS, Klaasen KP (1999) The structure of Jupiter's ring system as revealed by the Galileo imaging experiment. Icarus 138:188–213
Ogilvie GI, Lin DNC (2004) Tidal dissipation in rotating giant planets. Astrophys J 610:477–509
O'Neil WJ, Ausman NE, Johnson TV, Landano MR, Marr JC (1993) Performing the Galileo Jupiter Mission with the Low-Gain Antenna (LGA) and an Enroute Progress Report. 44th Congress of the International Astronautical Federation, Oct 16-22, 1993, Graz, Austria, IAF-93.Q.5.411
Orton GS, Spencer JR, Travis LD, Martin TZ, Tamppari LK (1996) Galileo photopolarimeter-radiometer observations of Jupiter and the Galilean satellites. Science 274:389–391
Pagnini P (1931) J Br Astron Assoc 41:415–422. Galileo and Mayer, Simon
Palumbo P, Roatsch T, et al (2025) The JANUS (Jovis Amorum ac Natorum Undique Scrutator) VIS-NIR multi-band imager for the JUICE mission. Space Sci Rev 221(3):32. https://doi.org/10.1007/s11214-025-01158-6
Park RS, Jacobson RA, Gomez Casajus L, Nimmo F, Ermakov AI, Keane JT, McKinnon WB, Stevenson DJ, Akiba R, Idini B, Buccino DR, Magnanini A, Parisi M, Tortora P, Zannoni M, Mura A, Durante D, Iess L, Connerney JEP, Levin SM, Bolton SJ (2025) Io's tidal response precludes a shallow magma ocean. Nature 638:69–73. https://doi.org/10.1038/s41586-024-08442-5
Peale SJ, Cassen P, Reynolds RT (1979) Melting of Io by tidal dissipation. Science 203:892–894. https://doi.org/10.1126/science.203.4383.892
Pecaut MJ, Mamajek EE (2013) Intrinsic colors, temperatures, and bolometric corrections of pre-main-sequence stars. Astrophys J Suppl Ser 208:9. https://doi.org/10.1088/0067-0049/208/1/9. (22pp)
Perrine CD (1905a) Discovery, observations and approximate orbits of two new satellites of Jupiter. Lick Obs Bull 3:129–133
Perrine CD (1905b) Orbits of the sixth and seventh satellites of Jupiter. Astron Nachr 169(4035):43–44
Pickering EC (1899a) A new satellite of Saturn. Bull Harv Coll Obs 49:17. 1899. https://ui.adsabs.harvard.edu/abs/1899BHarO..49....1P
Pickering EC (1899b) A new satellite of Saturn. Harvard Coll Obs Circ 43. (Also reprinted in Astron Nachr 3562, 189-192; Astrophys J 9(4), 274-276; Nature 60, 21-22; Pop Astron 7, 233-235.)
Pilcher CB, Ridgway ST, McCord TB (1972) Galilean satellites: identification of water frost. Science 178:1087–1089. https://doi.org/10.1126/science.178.4065.1087

Pilcher F, Mottola S, Denk T (2012) Photometric lightcurve and rotation period of Himalia (Jupiter VI). Icarus 219:741–742

Pollack JB, Fanale F (1982) Origin and evolution of the Jupiter satellite system. In: Morrison D (ed) Satellites of Jupiter. University of Arizona Press, Tucson, pp 872–910

Pollack JB, Witteborn FC, Erickson EF, Strecker DW, Baldwin BJ, Bunch TE (1978) Near-infrared spectra of the Galilean satellites: observations and compositional implications. Icarus 36:271–303

Pommier A, McEwen AS (eds) (2022) Exploring Jupiter's moon Io. Elements 18(6):368–404. https://www.elementsmagazine.org/exploring-jupiters-moon-io/

Porco CC, West RA, McEwen A, Del Genio AD, Ingersoll AP, Thomas PC, Squyres S, Dones L, Murray CD, Johnson TV, Burns JA, Brahic A, Neukum G, Veverka J, Barbara JM, Denk T, Evans MW, Ferrier JJ, Geissler P, Helfenstein P, Roatsch T, Throop H, Tiscareno M, Vasavada AR (2003) Cassini imaging of Jupiter's atmosphere, satellites, and rings. Science 299:1541–1547

Porco CC, West RA, Squyres SW, McEwen AS, Thomas PC, Murray CD, Del Genio A, Ingersoll AP, Johnson TV, Neukum G, Veverka J, Dones L, Brahic A, Burns JA, Haemmerle V, Knowles B, Dawson D, Roatsch T, Beurle K, Owen W (2004) Cassini imaging science: instrument characteristics and capabilities and anticipated scientific investigations at Saturn. Space Sci Rev 115:363–497. https://doi.org/10.1007/s11214-004-1456-7

Porco CC, Baker E, Barbara J, Beurle K, Brahic A, Burns JA, Charnoz S, Cooper N, Dawson DD, DelGenio AD, Denk T, Dones L, Dyudina U, Evans MW, Giese B, Grazier K, Helfenstein P, Ingersoll AP, Jacobson RA, Johnson TV, McEwen AS, Murray CD, Neukum G, Owen WM, Perry J, Roatsch T, Spitale J, Squyres SW, Thomas PC, Tiscareno M, Turtle EP, Vasavada AR, Veverka J, Wagner R, West R (2005) Cassini imaging science: initial results on Phoebe And Iapetus. Science 307:1237–1242. https://doi.org/10.1126/science.1107981

Poulet F, Piccioni G, Langevin Y, Dumesnil C, Tommasi L, Carlier V, Filacchione G, et al (2024) Moons And Jupiter Imaging Spectrometer (MAJIS) on Jupiter ICy Moons Explorer (JUICE). Space Sci Rev 220(3):27. https://doi.org/10.1007/s11214-024-01057-2

Radebaugh J, Keszthelyi LP, McEwen AS, Turtle EP, Jaeger W, Milazzo M (2001) Paterae on Io: a new type of volcanic caldera? J Geophys Res 106(E12):33005–33020. https://doi.org/10.1029/2000JE001406

Rambaux N, Lainey V, Cooper N, Auzemery L, Zhang QF (2022) Spherical harmonic decomposition and interpretation of the shapes of the small saturnian inner moons. Astron Astrophys 667:A78. https://doi.org/10.1051/0004-6361/202243355

Rathbun JA, Spencer JR, Davies AG, Howell RR, Wilson L (2002) Loki, Io: a periodic volcano. Geophys Res Lett 29:citeID 1443. https://doi.org/10.1029/2002GL014747

Redwing E, de Pater I, Luszcz-Cook S, de Kleer K, Moullet A, Rojo PM (2022) NaCl and KCl in Io's atmosphere. Planet Sci J 3:238. https://doi.org/10.3847/PSJ/ac9784. (11pp)

Retherford KD, Gladstone GR, Persyn SC, Davis MW, Greathouse TK, Molyneux PM, et al (2026) The Ultraviolet Spectrograph on ESA's Jupiter ICy Moons Explorer Mission (JUICE-UVS). Space Sci Rev in prep.

Rettig TW, Walsh K, Consolmagno G (2001) Implied evolutionary differences of the Jovian irregular satellites from a BVR color survey. Icarus 154:313–320

Rieke GH (1975) The temperature of Amalthea. Icarus 25:333–334

Roesler FL, Moos HW, Oliversen RJ, Woodward RC, Retherford D, Scherb F, McGrath MA, Smyth WH, Feldman PD, Strobel DF (1999) Far-ultraviolet imaging spectroscopy of Io's atmosphere with HST/STIS. Science 283:353–357

Roth L, Saur J, Retherford KD, Feldman PD, Strobel DF (2014) A phenomenological model of Io's UV aurora based on HST/STIS observations. Icarus 228:386–406

Roth L, Blöcker A, de Kleer K, Goldstein D, Lellouch E, Saur J, Schmidt C, Strobel DF, Tao C, Tsuchiya F, Dols V, Huybrighs H, Mura A, Szalay JR, Badman SV, de Pater I, Dott AC, Kagitani M, Klaiber L, Koga R, McEwen A, Milby Z, Retherford KD, Schlegel S, Thomas N, Tseng WL, Vorburger A (2025) Mass supply from Io to Jupiter's magnetosphere. Space Sci Rev 220(3):27. https://doi.org/10.1007/s11214-025-01137-x

Salama F, Allamandola LJ, Witteborn FC, Cruikshank DP, Sandford SA, Bregman JD (1990) The 2.5-5.0 micron spectra of Io - evidence for $H_2S$ and $H_2O$ frozen in $SO_2$. Icarus 83:66–82. https://doi.org/10.1016/0019-1035(90)90006-U

Sandford SA, Geballe TR, Salama F, Goorvitch D (1994) New narrow infrared absorption features in the spectrum of Io between 3600 and 3100 $cm^{-1}$ (2.8-3.2 μm). Icarus 110:292–302. https://doi.org/10.1006/icar.1994.1123

Schenk PM, Bulmer MH (1998) Origin of mountains on Io by thrust faulting and large-scale mass movements. Science 279:1514–1517. https://doi.org/10.1126/science.279.5356.1514

Schenk DM, Williams DA (2004) A potential thermal erosion lava channel on Io. Geophys Res Lett 31:L23702. https://doi.org/10.1029/2004GL021378

Schmidt C, Spencer JR, Roth L, Ganesh A, Moye C, Saur J, Retherford KD, Grodent DC (2023) Io's Far Ultraviolet Emissions Surrounding its Passage Through Jupiter's Shadow. AGU Fall, Poster P31E-3133
Schmitt B, Rodriguez S (2003) Possible identification of local deposits of $Cl_2SO_2$ on Io from NIMS/Galileo spectra. J Geophys Res 108:E9. https://doi.org/10.1029/2002JE001988
Schneider NM, Spencer JR (2023) Understanding Io: four centuries of study and surprise. In: Lopes RMC, de Kleer K, Keane JT (eds) Io: a new view of Jupiter's moon. Astrophysics and Space Science Library, vol 468. Springer, Cham, pp 9–39. https://doi.org/10.1007/978-3-031-25670-7_2
Schubert G, Anderson JD, Spohn T, McKinnon WB (2004) Interior composition, structure and dynamics of the Galilean satellites. In: Bagenal F, Dowling TE, McKinnon WB (eds) Jupiter. The planet, satellites and magnetosphere. Cambridge planetary science, vol 1. Cambridge University Press, Cambridge, pp 281–306
See TJJ (1902) Observations of the diameters of the satellites of Jupiter, and of Titan, the principal satellite of Saturn. Astron Nachr 157:325–336
Sharkey BNL, Reddy V, Kuhn O, Sanchez JA, Bottke WF (2023) Spectroscopic links among giant planet irregular satellites and Trojans. Planet Sci J 4:223. https://doi.org/10.3847/PSJ/ad0845. (20pp)
Sheehan W (1995) The immortal fire within: the life and work of Edward Emerson Barnard. Cambridge University Press, Cambridge, UK. ISBN 978-0-521-04601-5
Shen Y, Tremaine S (2008) Stability of the distant satellites of the giant planets in the Solar System. Astron J 136:2453–2467. https://doi.org/10.1088/0004-6256/136/6/2453
Sheppard SS, Jewitt DC (2003) An abundant population of small irregular satellites around Jupiter. Nature 423:61–263. https://doi.org/10.1038/nature01584
Sheppard SS, Tholen DJ, Alexandersen M, Trujillo CA (2023) New Jupiter and Saturn satellites reveal new moon dynamical families. Res Notes AAS 7:100. https://doi.org/10.3847/2515-5172/acd766
Showalter MR, Burns JA, de Pater I, Hamilton DP, Horanyi M (2003) Recent Hubble Observations of Jupiter's Ring System. DPS meeting #35, Monterey, CA, id.11.08
Showalter MR, Cheng AF, Weaver HA, Stern SA, Spencer JR, Throop HB, Birath EM, Rose D, Moore JM (2007) Clump detections and limits on moons in Jupiter's ring system. Science 318:232–234. https://doi.org/10.1126/science.1147647
Showalter MR, de Pater I, Verbanac G, Hamilton DP, Burns JA (2008) Properties and dynamics of Jupiter's gossamer rings from Galileo, Voyager, Hubble and Keck images. Icarus 195:361–377
Simonelli DP, Rossier L, Thomas PC, Veverka J, Burns JA, Belton MJS (2000) Leading/trailing albedo asymmetries of Thebe, Amalthea, and Metis. Icarus 147:353–365
Smith BA, Briggs GA, Danielson GE, Cook AF, Davies ME, Hunt GE, Masursky H, Soderblom LA, Owen TC, Sagan C, Suomi VE (1977) Voyager imaging experiment. Space Sci Rev 21:103–127. https://doi.org/10.1007/BF00200847
Smith BA, Soderblom LA, Beebe RF, Boyce J, Briggs GA, Carr MH, Collins SA, Cook AF, Danielson GE, Davies ME, Hunt GE, Ingersoll AP, Johnson TV, Masursky H, McCauley J, Morrison D, Owen T, Sagan C, Shoemaker EM, Strom R, Suomi VE, Veverka J (1979b) The Galilean satellites and Jupiter: Voyager 2 imaging science results. Science 206:927–950
Smith BA, Soderblom LA, Johnson TV, Ingersoll AP, Collins SA, Shoemaker EM, Hunt GE, Masursky H, Carr MH, Davies ME, Cook AF, Boyce J, Danielson GE, Owen T, Sagan C, Beebe RF, Veverka J, Strom RG, McCauley JF, Morrison D, Briggs GA, Suomi VE (1979a) The Jupiter system through the eyes of Voyager 1. Science 204:951–972
Smythe WD, Nelson RM, Nash DB (1979) Spectral evidence for $SO_2$ frost or adsorbate on Io's surface. Nature 280:766. https://doi.org/10.1038/280766a0
Spencer JR, Denk T (2010) Formation of iapetus's extreme albedo dichotomy by exogenically-triggered thermal migration of water ice. Science 327:432–435
Spencer JR, Jessup KL, McGrath MA, Ballester GE, Yelle R (2000) Discovery of Gaseous $S_2$ in Io's Pele Plume. Science 288:1208–1210. https://doi.org/10.1126/science.288.5469.1208
Spencer JR, Stern SA, Cheng AF, Weaver HA, Reuter DC, Retherford K, Lunsford A, Moore JM, Abramov O, Lopes RMC, Perry JE, Kamp L, Showalter M, Jessup KL, Marchis F, Schenk PM, Dumas C (2007) Io volcanism during the new horizons Jupiter flyby: a major eruption of the Tvashtar volcano. Science 318:240–243. https://doi.org/10.1126/science.1147621
Spitale JN, Porco CC (2010) Free unstable modes and massive bodies in Saturn's outer B ring. Astron J 140:1747–1757
Standish EM, Williams JG (2012) Orbital ephemerides of the Sun, Moon, and Planets. In: Urban SE, Seidelmann PK (eds) Explanatory supplement to the astronomical almanac. University Science Books, Mill Valley, pp 305–346. Chapter 8, 978-1-891389-85–978-1-891389-6. https://www.researchgate.net/publication/232203657
Stebbins J (1927) The light-variations of the satellites of Jupiter and their application to measures of the solar constant. In: Lick Obs Bull, vol 385. University California Press, Berkeley, pp 1–11. https://doi.org/10.5479/ADS/bib/1927LicOB.13.1S

Stebbins J, Jacobsen TS (1928) Further photometric measures of Jupiter's satellites and Uranus, with tests of the solar constant. In: Lick Obs Bull, vol 401. University California Press, Berkeley, pp 180–195. https://doi.org/10.5479/ADS/bib/1928LicOB.13.180S

Stephan K, et al (2021) Regions of interest on Ganymede's and Callisto's surfaces as potential targets for ESA's JUICE mission. Planet Space Sci 208:105324. https://doi.org/10.1016/j.pss.2021.105324

Sykes MV, Nelson B, Cutri RM, Kirkpatrick DJ, Hurt R, Skrutskie MF (2000) Near-infrared observations of the outer Jovian satellites. Icarus 143:371–375

Synnott SP (1980) 1979J2: the discovery of a previously unknown Jovian satellite. Science 210:786–788

Synnott SP (1981) 1979J3: discovery of a previously unknown satellite of Jupiter. Science 212:1392

Synnott SP (1984) Orbits of the small inner satellites of Jupiter. Icarus 58:178–181

Takato N, Bus SJ, Terada H, Pyo TS, Kobayashi N (2004) Detection of a deep 3- μm absorption feature in the spectrum of Amalthea (JV). Science 306:2224–2227. https://doi.org/10.1126/science.1105427

Takir D, Emery JP (2012) Outer main belt asteroids: identification and distribution of four 3- μm spectral groups. Icarus 219:641–654

Tanga P, Pauwels T, Mignard F, Muinonen K, Cellino A, David P, Hestroffer D, Spoto F, Berthier J, Guiraud J, Roux W, Carry B, Delbo M, Dell'Oro A, Fouron C, Galluccio L, Jonckheere A, Klioner SA, Lefustec Y, Liberato L, Ordénovic C, Oreshina-Slezak I, Penttilä A, Pailler F, Ch P, Petit JM, Portell J, Poujoulet E, Thuillot W, Van Hemelryck E, Burlacu A, Lasne Y, Managau S (2023) Gaia data release 3. The Solar System survey. Astron Astrophys 674:A12. https://doi.org/10.1051/0004-6361/202243796

Taylor GE (1972) The determination of the diameter of Io from its occultation of $\beta$-scorpii on may 14. Icarus 17:202–208. https://doi.org/10.1016/0019-1035(72)90056-5. 1971

Thelen AE, de Kleer K, Cordiner MA, de Pater I, Moullet A, Luszcz-Cook S (2025) Io's $SO_2$ and NaCl wind fields from ALMA. Astrophys J Lett 978:L1. https://doi.org/10.3847/2041-8213/ad9bb5

Thomas PC (1993) Gravity, tides, and topography on small satellites and asteroids: application to surface features of the Martian satellites. Icarus 105:326–344. https://doi.org/10.1006/icar.1993.1130

Thomas PC, Burns JA, Rossier L, Simonelli D, Veverka J, Chapman CR, Klaasen K, Johnson TV, Belton MJS (1998) The small inner satellites of Jupiter. Icarus 135:360–371

Thomas PC, Burns JA, Hedman M, Helfenstein P, Morrison S, Tiscareno MS, Veverka J (2013) The inner small satellites of Saturn: a variety of worlds. Icarus 226:999–1019. https://doi.org/10.1016/j.icarus.2013.07.022

Tiscareno MS, Burns JA, Sremčević M, Beurle K, Hedman MM, Cooper NJ, Milano AJ, Evans MW, Porco CC, Spitale JN, Weiss JW (2010) Physical characteristics and non-Keplerian motion of "propeller" moons embedded in Saturn's rings. Astrophys J Lett 718:L92–L96

Tiscareno MS, Nicholson PD, Cuzzi JN, Spilker LJ, Murray CD, Hedman MM, Colwell JE, Burns JA, Brooks SM, Clark RN, Cooper NJ, Déau E, Ferrari C, Filacchione G, Jerousek RG, Le Mouélic S, Morishima R, Pilorz S, Rodriguez S, Showalter MR, Badman SV, Baker EJ, Buratti BJ, Baines KH, Sotin C (2019) Close-range remote sensing of Saturn's rings during Cassini's ring-grazing orbits and grand finale. Science 364:eaau1017. https://doi.org/10.1126/science.aau1017

Tosi F, Turrini D, Coradini A, Filacchione G (2010) Probing the origin of the dark material on Iapetus. Mon Not R Astron Soc 403:1113–1130. https://doi.org/10.1111/j.1365-2966.2010.16044.x

Tosi F, Mura A, Lopes RMC, Filacchione G, Ciarniello M, Zambon F, Adriani A, Bolton SJ, Brooks SM, Noschese R, Sordini R, Turrini D, Altieri F, Cicchetti A, Grassi D, Hansen CJ, Migliorini A, Moriconi ML, Piccioni G, Plainaki C, Sindoni G (2020) Mapping Io's surface composition with Juno/JIRAM. J Geophys Res 125(E11):e06522. https://doi.org/10.1029/2020JE006522

Tosi F, Mura A, Cofano A, Zambon F, Glein CR, Ciarniello M, Lunine JI, Piccioni G, Plainaki C, Sordini R, Adriani A, Bolton SJ, Hansen CJ, Nordheim TA, Moirano A, Agostini L, Altieri F, Brooks SM, Cicchetti A, Dinelli BM, Grassi D, Migliorini A, Moriconi ML, Noschese R, Scarica P, Sindoni G, Stefani S, Turrini D (2024a) Salts and organics on Ganymede's surface from infrared observations by Juno/JIRAM. Nat Astron 8:82–93. https://doi.org/10.1038/s41550-023-02107-5

Tosi F, Roatsch T, et al (2024b) Characterization of the surfaces and near-surface atmospheres of Ganymede, Europa and Callisto by JUICE. Space Sci Rev 220(5):59. https://doi.org/10.1007/s11214-024-01089-8

Trumbo SK, Davis MR, Cassese B, Brown ME (2022) Spectroscopic mapping of Io's surface with HST/STIS: $SO_2$ frost, sulfur allotropes, and large-scale compositional patterns. Planet Sci J 3:272. https://doi.org/10.3847/PSJ/aca46d

Tsang CCC, Spencer JR, Lellouch E, Lopez-Valverde MA, Richter MJ (2016) The collapse of Io's primary atmosphere in Jupiter eclipse. J Geophys Res Planets 121(8):1400–1410. https://doi.org/10.1002/2016JE005025

Turtle EP, Keszthelyi LP, McEwen AS, Radebaugh J, Milazzo M, Simonelli DP, Geissler P, Williams DA, Perry J, Jaeger WL, Klaasen KP, Breneman HH, Denk T, Phillips CB (Galileo SSI Team) (2004) The final Galileo SSI observations of Io: orbits G28-I33. Icarus 169:3–28. https://doi.org/10.1016/j.icarus.2003.10.014

Van Helden A, Zuidervaart H (2018) A word of caution about the "rehabilitation" of Simon Marius. In: Gaab H, Leich P (eds) Simon Marius and his research. Historical & Cultural Astronomy, vol 16. Springer, Cham, pp 413–416. https://doi.org/10.1007/978-3-319-92621-6_16
Van Hoolst T, Tobie G, et al (2024) Geophysical characterization of the interiors of Ganymede, Callisto and Europa by ESA's Jupiter ICy moons Explorer. Space Sci Rev 220(5):54. https://doi.org/10.1007/s11214-024-01085-y
Velez MA, Retherford KD, Hue V, Kammer JA, Becker TM, Gladstone GR, Davis MW, Greathouse TK, Molyneux PM, Brooks SM, Raut U, Versteeg MH (2024) Strategies for UV occultation measurements, planetary illumination modeling, and sky map analyses using hybrid IUE-kurucz spectra. Planet Sci J 5(4):93. https://doi.org/10.3847/PSJ/ad0e70
Veverka J, Thomas PC, Davies ME, Morrison D (1981) Amalthea: Voyager imaging results. J Geophys Res 86(A10):8675–8692
Vilas F, Hendrix AR (2024) Clues to the origin of Jovian outer irregular satellites from reflectance spectra. Planet Sci J 5:34. https://doi.org/10.3847/PSJ/ad150b
Vilas F, Lederer SM, Gill SL, Jarvis KS, Thomas-Osip JE (2006) Aqueous alteration affecting the irregular outer planets satellites: evidence from spectral reflectance. Icarus 180:453–463
Von Oppolzer E (1901) Notiz betr. Planet (433) Eros. Astron Nachr 154:297
Wagner JK, Hapke BW, Wells EN (1987) Atlas of reflectance spectra of terrestrial, lunar and meteoritic powders and frosts from 92 to 1800 nm. Icarus 69:14–28
Wamsteker W, Kroes RL, Fountain JA (1974) On the surface composition of Io. Icarus 23:417–424. https://doi.org/10.1016/0019-1035(74)90059-1
Warner BD (2016) A practical guide to lightcurve photometry and analysis. Springer, Cham. https://doi.org/10.1007/978-3-319-32750-1
Williams DA, Greeley R, Lopes RMC, Davies AG (2001) Evaluation of sulfur flow emplacement on Io from Galileo data and numerical modeling. J Geophys Res 106(E12):33161–33174. https://doi.org/10.1029/2000JE001340
Williams DA, Keszthelyi LP, Crown DA, Yff JA, Jaeger WL, Schenk PM, Geissler PE, Becker TL (2011a) Volcanism on Io: new insights from global geologic mapping. Icarus 214:91–112. https://doi.org/10.1016/j.icarus.2011.05.007
Williams DA, Keszthelyi LP, Crown DA, Yff JA, Jaeger WL, Schenk PM, Geissler PE, Becker TL (2011b) Geologic map of Io. U.S. geological survey scientific investigations map, vol 3168. scale 1:15,000,000. https://pubs.usgs.gov/sim/3168/
Williams DA, Nelson DM, Milazzo MP (2021) The Io GIS database 1.0: a proto-Io planetary spatial data infrastructure. Planet Sci J 2:148. https://doi.org/10.3847/PSJ/ac097f
Wisniewski WZ, McMillan RS (1987) Differential CCD photometry of faint asteroids in crowded star fields and nonphotometric sky conditions. Astron J 93:1264–1267
Witasse O, et al (2026) JUICE Mission Overview. Space Sci Rev in prep.
Wolf M (1901) Über merkwürdige Erscheinungen am Planeten (345) Tercidina. Astron Nachr 155:123–128
Wong MH, de Pater I, Showalter MR, Roe HG, Macintosh B, Verbanac G (2006) Ground-based near infrared spectroscopy of Jupiter's ring and moons. Icarus 185:403–415. https://doi.org/10.1016/j.icarus.2006.07.007
Wurz P (2000) Detection of energetic neutral atoms. In: Scherer K, Fichtner H, Marsch E (eds) The outer heliosphere: beyond the planets. Copernicus Gesellschaft e.V, Katlenburg-Lindau, pp 251–288
Zambon F, Mura A, Lopes RMC, Rathbun J, Tosi F, Sordini R, Noschese R, Ciarniello M, Cicchetti A, Adriani A, Agostini L, Filacchione G, Grassi D, Piccioni G, Plainaki C, Sindoni G, Turrini D, Brooks S, Hansen-Koharcheck C, Bolton S (2023) Io hot spot distribution detected by Juno/JIRAM. Geophys Res Lett 50:e2022GL100597. https://doi.org/10.1029/2022GL100597
Zhang QF, Zhou XM, Tan Y, Lainey V, Cooper NJ, Vienne A, Qin WH, Li Z, Peng QY (2021) A comparison of centring algorithms in the astrometry of Cassini imaging science subsystem images and Anthe's astrometric reduction. Mon Not R Astron Soc 505:5253–5259. https://doi.org/10.1093/mnras/stab1626
Zik Y, Hon G, Manulis I (2020) Did Simon Marius observe Jupiter's satellites on January 8, 1610? An exercise in computation. https://arxiv.org/abs/2002.04643. arXiv:2002.04643 [physics.hist-ph]



## Authors and Affiliations

**Tilmann Denk[1] · David A. Williams[2] · Federico Tosi[3] · James F. Bell III[2] · Stefano Mottola[1] · Imke de Pater[4] · Valéry Lainey[5] · Philippa Molyneux[6] ·**

**Klaus-Dieter Matz[1] · Paul Hartogh[7] · Rosaly M. Lopes[8] · Anezina Solomonidou[9] · Peter C. Thomas[10] · Hans Leo F. Huybrighs[11,12,13] · Leonid I. Gurvits[14,15] · Alessandro Mura[3] · Kurt D. Retherford[6,16] · Ladislav Rezac[7] · Thomas Roatsch[1] · Lorenz Roth[17] · Nico Haslebacher[18] · Cecilia Tubiana[3] · Alice Lucchetti[19] · Yves Langevin[20] · François Poulet[20] · Emmanuel Lellouch[21] · Fuminori Tsuchiya[22] · Claire Vallat[23] · Tim Van Hoolst[24,25] · Audrey Vorburger[18] · Peter Wurz[18] · Emiliano D'Aversa[3] · Randy Gladstone[6,16] · Thomas Greathouse[6] · Nicholas Schneider[26] · Francesca Zambon[3] · Nicolas Altobelli[23] · Pasquale Palumbo[3] · Ganna Portyankina[1] · Oded Aharonson[27] · Lorenzo Bruzzone[28] · John Carter[20] · Baptiste Cecconi[21] · Nick Cooper[29] · Marc Costa Sitjà[23] · Alfredo Escalante López[23] · Yoshifumi Futaana[30] · Elena Mazzotta Epifani[31] · Alessandra Migliorini[3] · William B. Moore[32] · Raphael Moreno[21] · Carl Murray[29] · Luca Penasa[19] · Giuseppe Piccioni[3] · Jürgen Schmidt[33] · Jan-Erik Wahlund[34] · Olivier Witasse[35]**

✉ T. Denk
Tilmann.Denk@dlr.de

1 German Aerospace Center (DLR), Institute of Space Research, Rutherfordstr. 2, 12489 Berlin, Germany

2 Arizona State University, School of Earth and Space Exploration, Box 876004, Tempe, AZ, 85287, USA

3 INAF - IAPS (Istituto Nazionale di Astrofisica – Istituto di Astrofisica e Planetologia Spaziali), Via del Fosso del Cavaliere 100, 00133 Rome, Italy

4 Departments of Astronomy and of Earth and Planetary Science, 501 Campbell Hall, University of California, Berkeley CA 94720, USA

5 LTE, Observatoire de Paris, Université PSL, Sorbonne Université, Univ. Lille, Laboratoire National de Métrologie et d'Essai, CNRS, 77 avenue Denfert Rochereau, 75014, Paris, France

6 Southwest Research Institute, 6220 Culebra Rd, San Antonio, TX 78328, USA

7 Max-Planck-Institut für Sonnensystemforschung, 37077 Göttingen, Germany

8 Jet Propulsion Laboratory, California Institute of Technology, Pasadena, CA 91109, USA

9 Hellenic Space Center, 178 Kifissias Avenue, 15231, Athens, Greece

10 Visiting Scientist, 517 Space Sciences, Cornell University, Ithaca NY 14850, USA

11 Astronomy & Astrophysics Section, School of Cosmic Physics, Dublin Institute for Advanced Studies, DIAS Dunsink Observatory, Dublin D15 XR2R, Ireland

12 Space and Planetary Science Center, Khalifa University, Abu Dhabi, UAE

13 Department of Mathematics, Khalifa University, Abu Dhabi, UAE

14 Joint Institute for VLBI ERIC, Oude Hoogeveensedijk 4, 7991 PD Dwingeloo, The Netherlands

15 Faculty of Aerospace Engineering, Delft Univ. of Technology, Kluyverweg 1, Delft 2629 HS, The Netherlands

16 University of Texas at San Antonio, San Antonio, TX 78249, USA

17 Space and Plasma Physics, KTH Royal Institute of Technology, 100 44 Stockholm, Sweden

[18] Space Research and Planetary Sciences, Physics Institute, University of Bern, Sidlerstrasse 5, 3012 Bern, Switzerland

[19] INAF - OAPd (Istituto Nazionale di Astrofisica – Osservatorio Astronomico di Padova), Vicolo Osservatorio 5, 35122 Padova, Italy

[20] Institut d'Astrophysique Spatiale, Université Paris-Saclay, CNRS, Orsay, 91405, France

[21] LIRA, Observatoire de Paris, Université PSL, Sorbonne Université, Université Paris Cité, CY Cergy Paris Université, CNRS, 5 place Jules Janssen, 92195 Meudon, France

[22] Planetary Plasma & Atmospheric Research Center, Graduate School of Science, Tohoku University, 6-3 Aramaki Aza Aoba, Aoba-ku, Sendai, Miyagi, 980-9578, Japan

[23] European Space Agency- ESA/ESAC, Camino Bajo del Castillo s/n, 28692 Villanueva de la Canada, Madrid, Spain

[24] Royal Observatory of Belgium, Ringlaan 3, 1180 Brussels, Belgium

[25] Institute of Astronomy, KU Leuven, Celestijnenlaan 200B, 3001 Leuven, Belgium

[26] Laboratory for Atmospheric and Space Physics, University of Colorado, Boulder, CO, 80303, USA

[27] Department of Earth & Planetary Sciences, Weizmann Institute of Science, Rehovot, 76100, Israel

[28] University of Trento, Dept. of Information Engineering and Computer Science, Via Sommarive 5, I-38123, Trento, Italy

[29] Astronomy Unit, Queen Mary University of London, Mile End Road, London E1 4NS, UK

[30] Swedish Institute of Space Physics, Bengt Hultqvists väg 1, Kiruna SE-98192, Sweden

[31] INAF - OAR (Istituto Nazionale di Astrofisica – Osservatorio Astronomico di Roma), Via Frascati 33, 00040 Monte Porzio Catone RM, Italy

[32] Hampton University, 200 Wm. R Harvey Way, Hampton, VA 23668, USA

[33] Freie Universität Berlin, UB-Inst. for Geosciences, Malteserstr. 74-100, 12249 Berlin, Germany

[34] Swedish Institute of Space Physics (IRF), Uppsala, Sweden

[35] European Space Agency - ESA/ESTEC, Science Engagement and Oversight Office (SCI-E), Keplerlaan 1, 2201 AZ Noordwijk, The Netherlands